# THE USE OF SIMPLE INERTIAL FORMULATION OF THE SHALLOW WATER EQUATIONS IN 2-D FLOOD INUNDATION MODELING

A THESIS SUBMITTED TO
THE GRADUATE SCHOOL OF NATURAL AND APPLIED SCIENCES
OF
MIDDLE EAST TECHNICAL UNIVERSITY

BY

ARTUR NIMAEV

IN PARTIAL FULFILLMENT OF THE REQUIREMENTS
FOR
THE DEGREE OF MASTER OF SCIENCE
IN
CIVIL ENGINEERING

FEBRUARY 2015

Approval of the thesis:

**THE USE OF SIMPLE INERTIAL FORMULATION OF THE SHALLOW WATER EQUATIONS IN 2-D FLOOD INUNDATION MODELING**

submitted by **ARTUR NIMAEV** in partial fulfillment of the requirements for the degree of **Master of Science in Civil Engineering Department, Middle East Technical University** by,

Prof. Dr. Gülbin Dural Ünver
Dean, Graduate School of **Natural and Applied Sciences** _____

Prof. Dr. Ahmet Cevdet Yalçıner
Head of Department, **Civil Engineering** _____

Prof. Dr. Zuhal Akyürek
Supervisor, **Civil Engineering Dept., METU** _____

**Examining Committee Members:**

Prof. Dr. Melih Yanmaz
Civil Engineering Dept., METU _____

Prof. Dr. Zuhal Akyürek
Civil Engineering Dept., METU _____

Prof. Dr. Zafer Bozkuş
Civil Engineering Dept., METU _____

Assoc. Prof. Dr. Nuri Merzi
Civil Engineering Dept., METU _____

Assoc. Prof. Dr. Uğur Murat Leloğlu
GGIT Dept., METU _____

**Date:** 16.02.2015

**I hereby declare that all information in this document has been obtained and presented in accordance with academic rules and ethical conduct. I also declare that, as required by these rules and conduct, I have fully cited and referenced all material and results that are not original to this work.**

| | | |
|---|---|---|
| Name, Last Name | : | Artur Nimaev |
| Signature | : | |

## ABSTRACT

THE USE OF SIMPLE INERTIAL FORMULATION OF THE SHALLOW WATER EQUATIONS IN 2-D FLOOD INUNDATION MODELING

Artur Nimaev
M.S., Department of Civil Engineering
Supervisor: Prof. Dr. Zuhal Akyürek

February 2015, 125 pages

Hydrodynamic computational modeling plays a vital role in assessment and management of flood risks. In particular, flood modeling in urban environments is especially important due to high damage to infrastructure and property as well as losses of human lives. Many numerical two-dimensional schemes, as a consequence, have been developed to perform simulations of urban flood inundation benefiting from recent technological advancements in topographic surveying techniques. To understand sensitivity of model outputs to different hydraulic modeling approaches; namely, Flow-limited, Adaptive, Acceleration and Roe numerical solvers of varying complexity in terms of representing shallow water equations of Lisflood-FP and 2D full-dynamic Mike 21 models were evaluated in this study. Furthermore, 25 cm, 50 cm and 1 m resolution rasters based on terrestrial LIDAR data of town center of Terme located in Samsun, as well as four different roughness parameters representing urban surface conditions were compared to see how resolution and surface friction may impact simulation results using simplified inertial solver of Lisflood-FP model. The results indicate that among 4 solvers of Lisflood-FP model, only Acceleration numerical scheme provided consistent results to be used in practical applications. Also, compared to the Mike 21 hydraulic

model, Acceleration solver generally predicted similar test results, except for the areas of ponding. Increasing DEM resolution resulted in more rapid flow propagation due to more detailed representation of the topography such as sloping alignment of a road. However, it was shown that the use of LIDAR data in flood modeling studies obtained from high frequency terrestrial laser scanners is limited due to sophisticated processing techniques. Moreover, the Acceleration solver correctly predicted sensitivity to friction as water was conveyed faster in models with lower Manning's coefficients.

Keywords: Terrestrial LIDAR data, urban flood modeling, 2D numerical modeling, resolution and roughness effects, shallow water equations

# ÖZ

2 BOYUTLU TAŞKIN YAYILIMI MODELLEMESİNDE SIĞ SU DENKLEMLERİNİN BASİT EYLEMSİZLİK FORMÜLASYONUNUN KULLANILMASI

Artur Nimaev
Yüksek Lisans, İnşaat Mühendisliği Bölümü
Tez Yöneticisi: Prof. Dr. Zuhal Akyürek

Şubat 2015, 125 sayfa

Hesaplamalı hidrodinamik modelleme, taşkın risk değerlendirmesi ve yönetiminde önemli bir rol oynamaktadır. Özellikle, şehir bölgelerinde taşkın modellemesi altyapı ve mülklerde oluşabilecek yüksek hasar ve insan hayatı kayıpları için oldukça önemlidir. Bunun neticesinde, topografik ölçme tekniklerindeki gelişmelerden faydalanarak şehir taşkın yayılımını simüle eden birçok sayısal iki boyutlu model geliştirilmiştir. Bu çalışmada, farklı hidrolik modelleme yaklaşımlarının sonuçlarının hassasiyetini anlayabilmek adına, 2 Boyutlu Tam-Dinamik Mike 21 modeli ve sığ su denklemleri farklı karmaşıklıktaki Flow-limited, Adaptive, Acceleration ve Roe sayısal çözücülerin kullanıldığı Lisflood-FP modeli değerlendirilmiştir. Aynı zamanda, hücre çözünürlüğü ve yüzey sürtünmesinin simülasyon sonuçlarını nasıl etkilediğini görmek için Lisflood-FP modelinin sadeleştirilmiş eylemsizlik çözücüsü kullanılarak; Samsun iline bağlı Terme ilçe merkezinin karasal LIDAR verilerinden yola çıkılarak, 25 cm, 50 cm ve 1 m çözünürlükteki hücreler ile şehir yüzey durumunu yansıtan dört farklı pürüzlülük parametresi karşılaştırılmıştır. Sonuçlar göstermektedir ki; Lisflood-FP modelindeki dört çözücü arasında yalnızca Accelaration sayısal çözücüsü pratik

uygulamalarda kullanılabilecek tutarlı sonuçları sağlamıştır. Ayrıca, Acceleration çözücüsü genellikle Mike 21 hidrolik modeli ile göllenme bölgeleri dışında benzer test sonuçları vermiştir. Sayısal Yükseklik Modeli (SYM) çözünürlüğünü yükseltmek, cadde eğimi gibi topografik öğeleri daha detaylı ortaya koyduğu için daha ani akım yayılımı ile sonuçlanmıştır. Ancak gösterilmiştir ki; sofistike işleme tekniklerinden dolayı taşkın modelleme çalışmalarında yüksek frekanslı karasal lazer taramalarından elde edilen LIDAR verilerinin kullanımı sınırlıdır. Aynı zamanda Accelaration çözücüsü sürtünme hassasiyetini doğru şekilde tahmin etmiştir; Manning katsayısı daha düşük modellerde su daha hızlı yayılmıştır.

Anahtar Kelimeler: Karasal LIDAR verisi, şehir taşkın modelleme, 2 boyutlu sayısal modelleme, çözünürlük ve pürüzlülük etkisi, sığ su denklemleri

To My Parents and Lena

## ACKNOWLEDGMENTS

First and foremost, I would like to express my gratitude to my supervisor, Prof. Dr. Zuhal Akyürek, for her continuos guidance, invaluable advice, caring and insight throughout the research. Without her patience and encouragement this thesis would not have been completed.

I would also like to express my sincere thanks to Prof. Dr. Melih Yanmaz, Prof. Dr. Zafer Bozkuş, Assoc. Prof. Dr. Nuri Merzi and Assoc. Prof. Dr. Uğur Murat Leloğlu for their suggestions and contributions during my thesis defense.

I owe thanks to DHI Türkiye for providing technical assistance with Mike 21 simulations as well as to Kenan Bolat for the help with processing of raw terrestrial LIDAR point cloud data.

Also, I am also very grateful to my close friends, Zekerya Can Özvarlik and Ahmet Fatih Koç for their endless support and advice during my Masters years.

My sincere thanks also go to my parents for the love, support and care they provided my through my entire life.

Finally, I have special thanks to my little soul-mate, Elena Dambueva for always being there for me through all the good and bad times as well as for her never ending love, encouragement, patience, and trust.

## TABLE OF CONTENTS

## LIST OF TABLES

TABLES

## LIST OF FIGURES

FIGURES

# CHAPTER 1

# INTRODUCTION

Water has been the most important factor for survival providing potable water and food supplies as well as economic and cultural development for humankind. It is well known that great civilizations were built around rivers and other sources of water. On the other hand, floods are the reason for huge economic losses and they have been affecting millions of people worldwide both for developed and underdeveloped nation states. During the last decade, disastrous floods occurred in Bangladesh, China, India, Germany, United States and elsewhere. In particular, it has become obvious that floods result in destruction of infrastructure, decline in economic growth and most importantly lead to human deaths as well as spread of infectious diseases. Therefore, it shall be obvious that these negative impacts shall be avoided and/or minimized by executing adequate management of floodplain development, watershed land use organization, flood forecasting and other response techniques. To achieve these goals, it is important to perform research and implement recent approaches in flood modeling and forecasting as well as employ experience acquired from past flood events (UNISDR, 2002).

One such example is Flood Directive of the European Union Parliament where all member states are required to provide flood risk and hazard maps showing the outcomes of possible flooding using best available industry practice and technology without overpriced expenditures (European Parliament, 2007).

Hydraulic modeling is one of the key elements in accurate prediction of flood inundation, hence authorities and general public can benefit greatly from the computational simulation outputs to produce flood maps (Gilles and Moore, 2010).

Until very recently, implementation of topographic data was limited in flood modeling studies due to labor intensive and financially expensive methods (leading to very small mapping area and poor accuracy) used in data collection such as photogrammetry and ground surveys. However, contemporary developments in LIDAR (Light Detection and Ranging) technology produce digital elevation models of extremely high resolution obtained from three-dimensional point cloud allowing to depict manmade terrain features like kerbs, walls, steps or wall cambers which are very crucial in urban hydraulic modeling (Sampson et al., 2012).

The use of two-dimensional flood modeling was limited due to scarcity of fine scale data. In particular, flood propagation in urban areas requires 1 to 5 m grid resolution to include representative topographical features. For this reason, researchers specializing in this field preferred working with less complicated rural hydraulic modeling. Nonetheless, development of modern topographic digital data collection methods like described above had cleared the way to perform studies on two-dimensional hydraulic models in metropolitan environment. And consequently, within the last decade applicability of numerical models representing various complexity of shallow water equations was analyzed and tested on number of complicated urban problems (Hunter et al., 2008).

The aim of this study is to analyze the use of simple inertial formulation of the shallow water equations in 2-D flood inundation modeling. The comparison is done by using the models – Mike 21 where full momentum equation is solved during the modeling and Lisflood-FP where local acceleration is considered in the solution of dynamic wave equations. Furthermore, the effect of spatial resolution of a DEM

and surface roughness in shallow water equations is analyzed. The use of terrestrial LIDAR data in flood modeling is also discussed.

## 1.1 Project Data

There are various topographic data collection techniques available nowadays. Two types of such methods were used in this work to construct Digital Elevation Model (DEM) of Terme town, Samsun Province located in coastal region of Black Sea, Turkey. Small area of the highly urbanized town center that was chosen to simulate a flood event can be seen in Figure 1-1.

### 1.1.1 DSI DEM

The first type of DEM used in the analysis of flood inundation modeling was obtained from 1/1000 topographic measurements with a resolution of 1 m acquired by Directorate of State Hydraulic Works (DSI) in 2013. The vertical accuracy of the DEM is 10 cm. It is worth noting that elevations of buildings were included in the DEM. Three-dimensional and plan views are shown in Figure 1-2 and Figure 1-3 for better understanding of topographical features of this elevation model. To correctly represent surface topography in three dimensions without any distortions, buildings were only schematically shown in the 3D figure and elevations were magnified twice. It should be mentioned that as can be seen in Figure 1-2, there are two major zones of depression. The low elevations of the first zone are exaggerated and were most probably incorrectly captured during surveying of the area. The second zone has no such issues as the elevations in this area are low.

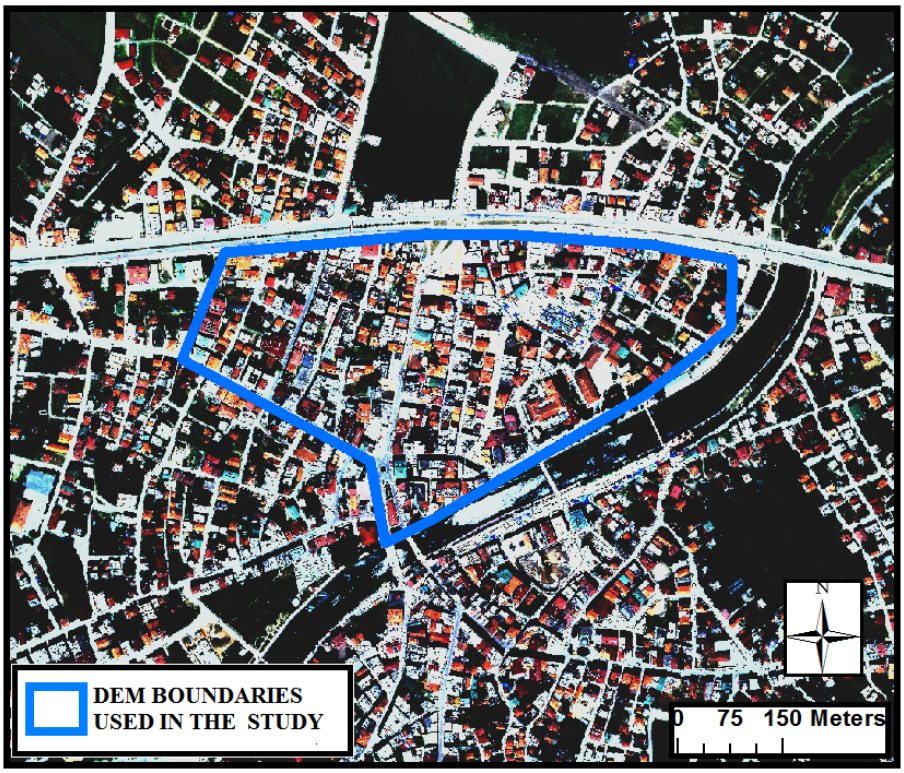


**Figure 1-1** Location of the Study Area

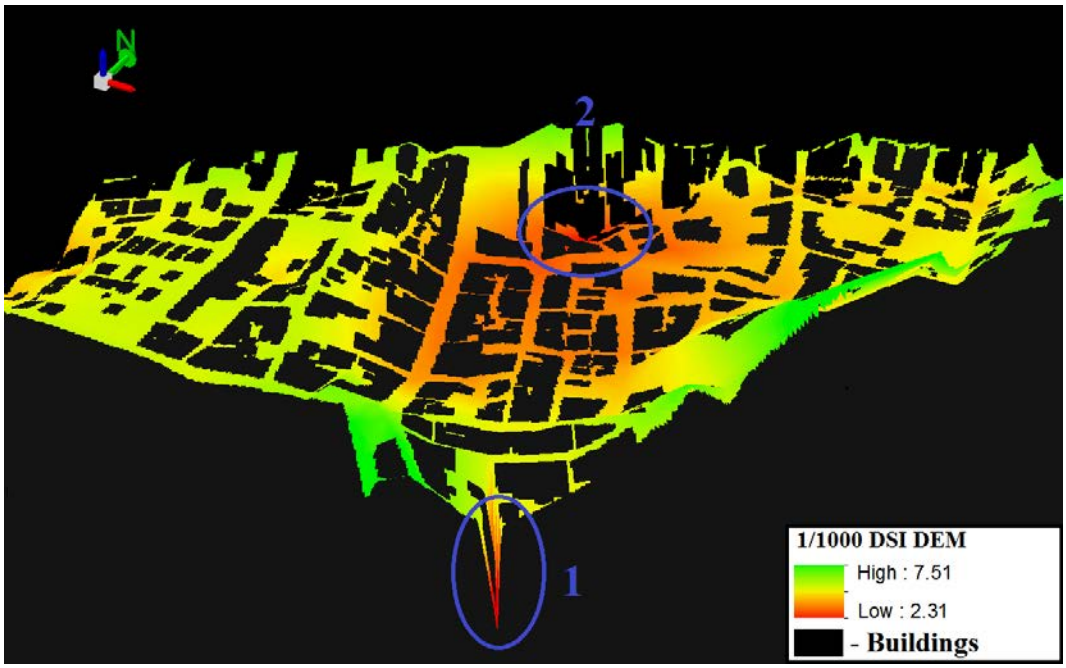


**Figure 1-2** Three-dimensional view of the DSI DEM

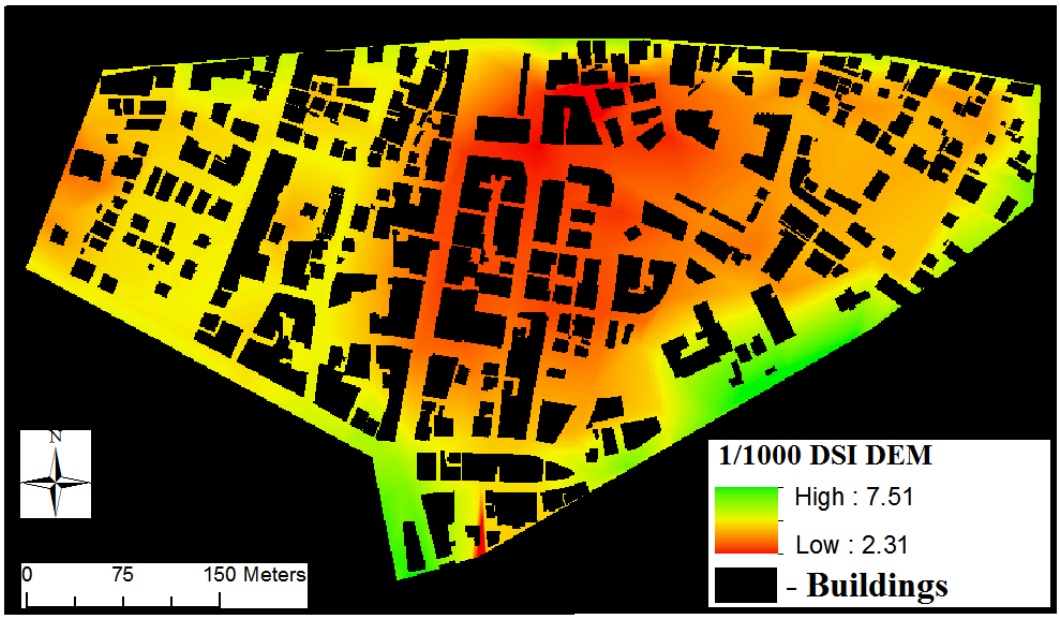


**Figure 1-3** Plan view of the DSI DEM

### 1.1.2 Terrestrial LIDAR DEM

The second type of the DEM was specifically used to evaluate varying resolution in urban flood modeling studies benefitting from LIDAR data of centimetric resolution. The 400 kHz Mobile Laser Scanner system with 360˚ line of sight and GPS receivers employed for positional accuracy was mounted on top of a vehicle (Figure 1-4) to collect three-dimensional point cloud data of the study area displayed in Figure 1-5. To show the features that terrestrial laser scanner is able to capture, detailed view of the raw point cloud and an aerial photograph of the same region in the study area were presented (Figure 1-6 and Figure 1-7).

It is important to process LIDAR raw point cloud data isolating irrelevant features such as buildings, cars or trees to build a DEM to be used in the flood simulation studies. First of all, LIDAR dataset in a LAS format was converted into a raster using the "LAS Dataset to Raster tool" of ArcMap software. Afterwards, filtering of this raster was repeated ten times to exclude unnecessary topographic features and obstacles like cars parked on the sides of roads using the mean statistics type of "Focal Statistics" tool of ArcMap. This tool calculates the value of a target cell according to a mean of all surrounding cells of predefined size by a user. The resulting 1 cm raster was resampled to 10 cm, 50 cm and 1 m resolution DEMs via ArcMap resample method using nearest neighbor assignment which is mainly used for discrete data such as land use classification because values of the cells remain the same. The building were excluded from DEMs and set as "nodata" to avoid possible incorrect detection of buildings by terrestrial laser scanner. Finally, small region in the study area was chosen to compare the resulting 10 cm, 50 cm and 1 m resolution LIDAR models with 1 m resolution DSI DEM (Figure 1-8 and Figure 1-9). It can be seen that topographic features such as trees or vegetation were not completely eliminated in LIDAR DEMs, but they are less distinguishable with decreasing resolution. This will lead to some obstacles in hydraulic modeling and will be discussed later.

**Figure 1-4** Mobile Laser Scanner System mounted on top of a vehicle

**Figure 1-5** 3-D Raw point cloud data of Terme town center

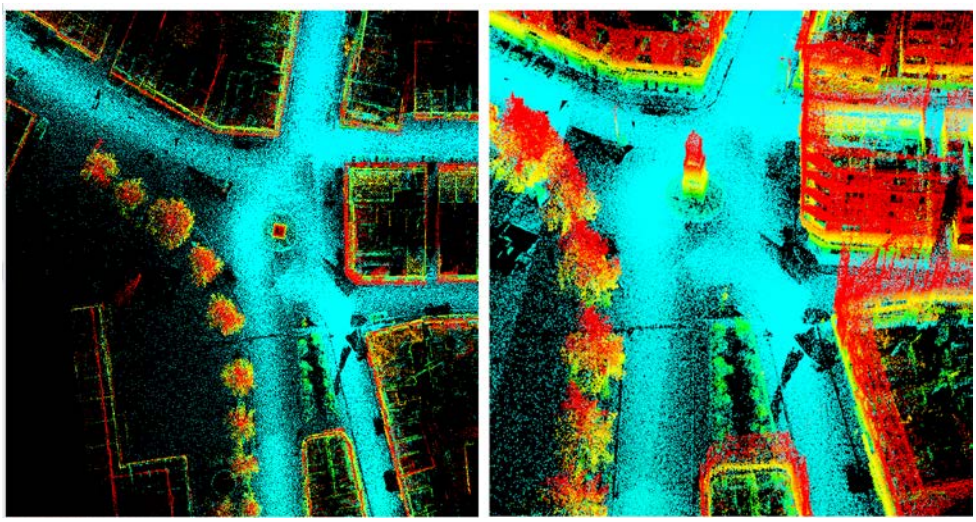

(a) (b)

**Figure 1-6** Region of the study area where (a) Plan View and (b) 3-d View of raw point cloud

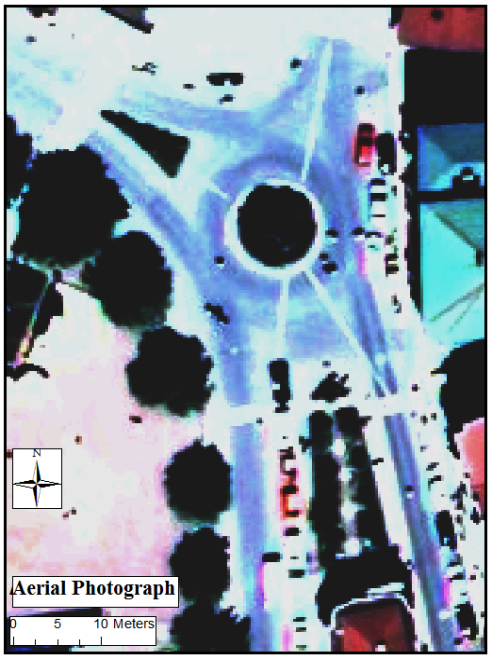


**Figure 1-7** Aerial photograph of a region in the study area

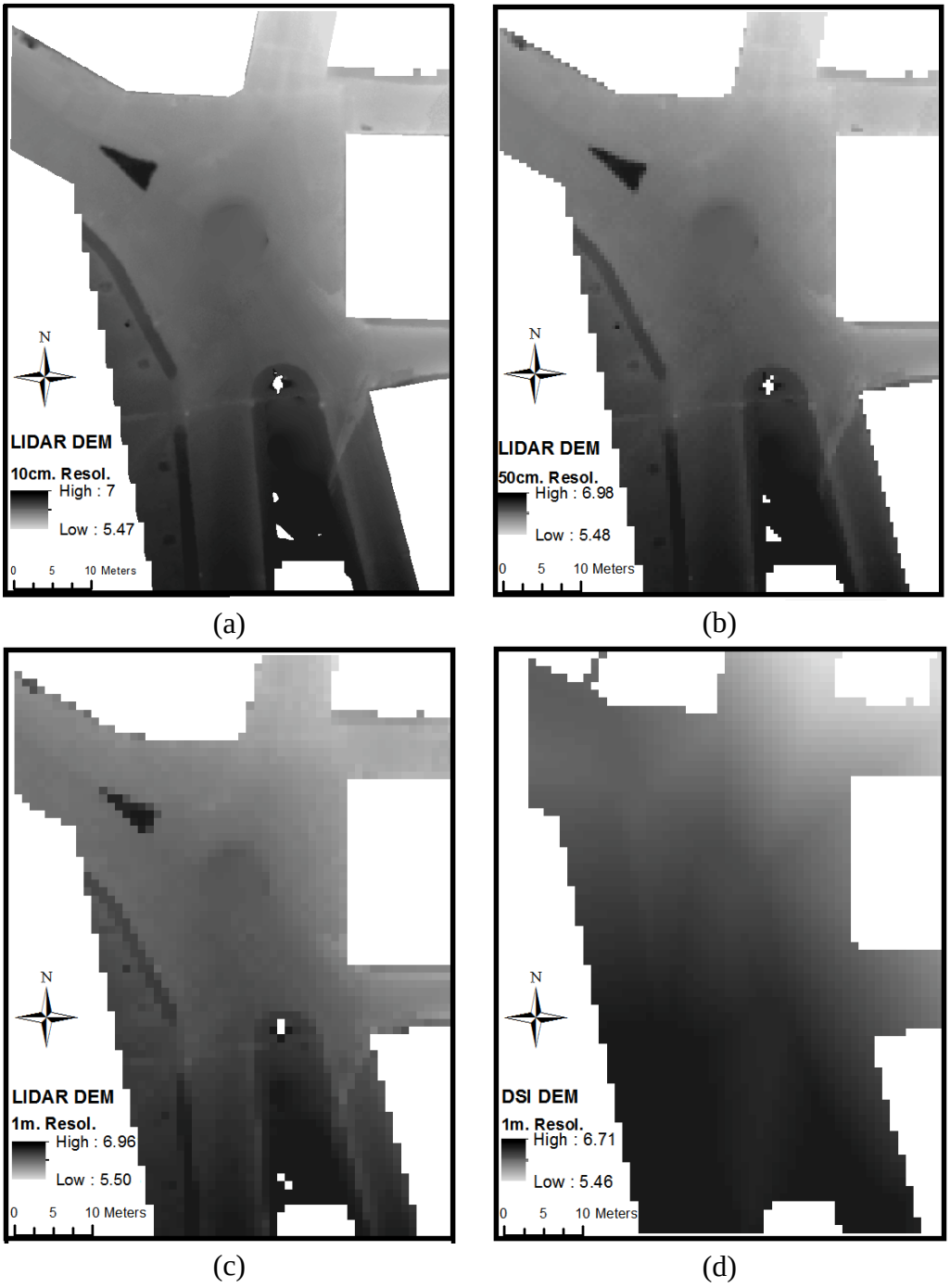


**Figure 1-8** Illustration of a region in the study area where (a) 10 cm resolution LIDAR DEM; (b) 50 cm resolution LIDAR DEM, (c) 1 m resolution LIDAR DEM and (d) 1 m resolution DSI DEM

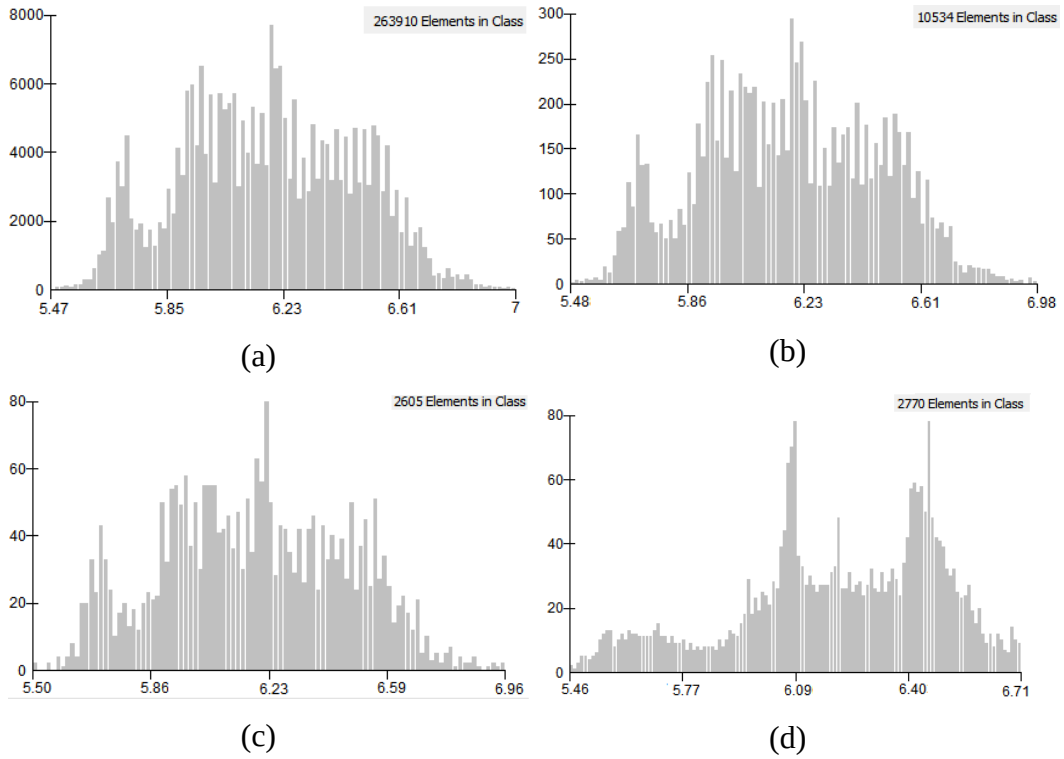


**Figure 1-9** Histogram of the same region in the study area where (a) 10 cm resolution LIDAR DEM; (b) 50 cm resolution LIDAR DEM, (c) 1 m resolution LIDAR DEM and (d) 1 m resolution DSI DEM

## 1.2 Organization of the Thesis

The information regarding the theoretical composition of numerical hydraulic two-dimensional flood models is provided in Chapter 2.

In Chapter 3, four numerical approaches of solving shallow water equations, namely, Flow-limited, Adaptive, Acceleration and Roe solvers implemented in LISFLOOD-FP model were evaluated. In particular, inertial terms are neglected in momentum equation both in Flow-limited and Adaptive solvers representing diffusive wave approach, local acceleration term is omitted in Acceleration solver and all terms are represented in Roe solver.

To further analyze the differences between simplified inertial formulation and full representation of shallow water equations, Lisflood-FP acceleration solver was compared to widely used Mike 21 hydrodynamic model in Chapter 4.

To study the effects of grid resolution and roughness, the investigation of urban flood modeling using the inertial acceleration model of the Lisflood-FP taking advantage of fine spatial LIDAR data was performed in Chapter 5.

Finally, discussion of results and conclusions are provided in Chapter 6.

# CHAPTER 2

# LITERATURE REVIEW

Developments in topographic data collection techniques and computing technologies had cleared the path for more active use of hydrodynamic models in flood simulation studies. Yet, performing such studies at very fine resolution can lead to serious issues such as high computation time, precise field data acquisition and end user qualifications. Therefore, designing computationally efficient numerical codes and obtaining meaningful and accurate input (hydrologic, hydraulic, topographical, etc.) data is very crucial for simulating floods.

Precise representation of the surface topography implemented in numerous applications had led to more extensive exploration of technology in topographic mapping (Gruen et al., 1997). In particular, LIDAR technology is considered as a reliable method for extracting surface information in three dimensions (Priestnall et al., 2000). Development of two-dimensional flood modeling was not possible due to insufficient accuracy and resolution of topographic data. However, advancement of LIDAR data had allowed a wider spreading of such models (Marks and Bates, 2000).

Hydrodynamic models used in practice can be divided into one-dimensional, two-dimensional and three-dimensional models, although the latter one is very rarely implemented due to computational constraints. One-dimensional flow terms implemented in the Saint-Venant equations were widely used until late 1990s. The problem with this type of models was propagation of flood wave only in one spatial dimension, alignment of suitable cross-sections of topographic field data collection

as well as numerical interpolation of model parameters lying between surveyed cross-sections. Two-dimensional models, on the other hand, allowed to resolve these shortcomings by continuous representation of topography within DEM in numerical modeling, although at the price of increased computational efforts. These models are utilized in the numerical formulation by full shallow water equations using finite difference and finite volume methods. However, computational time is drastically increased due to nonlinear and hyperbolic behavior of local and convective acceleration terms within these equations. To overcome this drawback, simplified versions of numerical codes, where some of the terms of Saint-Venant equations are neglected, were used as quite often full representation of shallow water equations is not necessary in flood inundation simulations (Hunter et al., 2007).

## 2.1 Overview of Lisflood-FP Solvers

Lisflood-FP is a software that was developed for research purposes in Bristol University. It is a raster based flood inundation model that simulates propagation of a water body through the river channels and over floodplains based on the simplified versions of shallow water equations by using various numerical solvers described below (Bates et al., 2013). The Saint-Venant equations are as follows:

$$\frac{\partial Q}{\partial x} + \frac{\partial A}{\partial t} = 0 \qquad (2\text{-}1)$$

$$\frac{1}{A}\frac{\partial Q}{\partial t} + \frac{1}{A}\frac{\partial}{\partial x}\left(\frac{Q^2}{A}\right) + g\frac{\partial h}{\partial x} - g\left(S_0 - S_f\right) = 0 \qquad (2\text{-}2)$$

(a) (b) (c) (d) (e)

where

Q – flow discharge in x-direction ($m^3/s$);

A – cross-section flow area ($m^2$);

g – gravitational acceleration ($m/s^2$);

h – cross-section average flow depth (m).

It is also worth noting that numerical solvers were designed based on the idea of inclusion of the following terms within the momentum conservation equation into the programming code:

(a) – local acceleration term;
(b) – convective acceleration term;
(c) – pressure term;
(d) – bed slope term;
(e) – friction slope term;

and Equation (2-1) and Equation (2-2) represent continuity equation and momentum conservation equation, respectively.

Since the aim of this study is to investigate urban flood modeling, only floodplain solvers will be discussed herein. Table 2-1 outlines main characteristics of each numerical solver. These solvers were developed at different stages of time during maturation process of Lisflood-FP program. Therefore, it shall be obvious that with increasing the quality of GIS data and more efficient computational capacity, later solvers perform better than the earlier ones. Nonetheless, for the sake of comparing these models as well as analyzing how different terms within momentum equation affect the flood model outputs Flow-limited, Adaptive, Acceleration and Roe solvers will be discussed herein.

### 2.1.1 Flow-limited Solver

The Lisflood-FP flow-limited diffusive model was designed to perform channel and floodplain hydraulic simulation studies taking advantage of the recent developments in topographic mapping and implementing computationally efficient two-dimensional numerical scheme (Bates and De Roo, 2000). It should be emphasized that this solver is only valid for gradually varied flows excluding inertia

**Table 2-1** Solvers implemented in the study (Bates et al., 2013)

| Solver | Dimensions | Shallow water terms included | Shallow water terms assumed negligible | Time step |
|---|---|---|---|---|
| Flow-Limited | 1D on 2D grid | Friction and water slopes | Local and convective acceleration | Fixed |
| Adaptive | 1D on 2D grid | As above | As above | Adaptive |
| Acceleration | 1D on 2D grid, friction terms in 2D | Friction and water slopes, local acceleration | Convective acceleration | Adaptive |
| Roe | 2D | All terms | None | Adaptive |

terms, thus providing accurate results only for subcritical flows. Formulization of the model was explained by Hunter et al. (2005). In this model, ignoring both local and convective acceleration, continuity equation is solved by considering each cell in DEM as a storage volume and its change in time depends on inflowing and outflowing fluxes:

$$\frac{\partial h^{ij}}{\partial t} = \frac{Q_x^{i-1,j} - Q_x^{i,j} + Q_y^{i,j-1} - Q_y^{i,j}}{\Delta x \Delta y} \tag{2-3}$$

Meanwhile, the flow between each cell is calculated using momentum equation based on Manning's equation (only x-direction is shown):

$$Q_x^{i,j} = \frac{h_{flow}^{\frac{5}{3}}}{n}\left(\frac{h^{i-1,j} - h^{i,j}}{\Delta x}\right)^{1/2} \Delta y \qquad (2\text{-}4)$$

where

$h^{ij}$ – water free surface height at node (i,j) (m);

$\Delta x$, $\Delta y$ – cell dimensions (m);

n – Manning's roughness coefficient;

$Q_x$, $Q_y$ – discharge between cells in x and y directions ($m^3/s$);

$h_{flow}$ – difference between highest water depth and highest bed elevation among two cells (m).

Finally, combining Equations (2-3) and (2-4) flow depths are updated using explicit form of finite difference discretization of the time derivative:

$$h_{i,j}^{t+\Delta t} = h_{i,j}^{t} + \Delta t \frac{Q_{xi-1,j}^{t} - Q_{xi,j}^{t} + Q_{yi,j-1}^{t} - Q_{yi,j}^{t}}{\Delta x^2} \qquad (2\text{-}5)$$

In this solver, a time step is manually chosen by the user and is fixed for duration of simulation time. Due to explicit nature of the numerical model, selection of optimal time step is very important. Choosing a very small time step is computationally intensive while a large time step may produce 'chequerboard oscillations' in the solution (Figure 2-1). As a result, it was necessary to include a flow limiter to restrict maximum flow change between cells, thus avoiding instabilities within the solver. The flow limiter equation is a function of cell resolution, depth of flow and time step and shown below:

$$Q_x^{i,j} = \min(Q_x^{i,j}, \frac{\Delta x \Delta y (h^{ij} - h^{i-1,j})}{4\Delta t}) \qquad (2\text{-}6)$$

Equation (2-6) takes over the formula of calculating the flow between each cell using Manning's equation (Equation (2-4)).

### 2.1.2 Adaptive Solver

The adaptive solver implements the same equations to calculate flow between grid cells as in flow limited model. But instead of using flow limiter, adaptive time step is utilized. The problem with the previous model was – when the equation of a flow limiter is used, flow is dependent on grid cell resolution as well as preselected time step but independent of Manning's roughness coefficient. This means that model outputs are completely insensitive to floodplain friction which might not be advantageous for certain simulations where flow limiter is frequently activated. Also, due to manually chosen time step as well as varying grid resolution, it may be difficult to calibrate parameter set as to provide relatively similar simulation results (Hunter et al., 2005). To overcome this deficiency, a time step similar to Courant-Friedrichs-Levy for advective flows condition was implemented anytime the flow limiter is activated. At each iteration, a single largest stable time step that is fixed in space is found within the domain to update flow depth *h* (Hunter et al., 2005):

$$\Delta t = \frac{\Delta x^2}{4} min\left(\frac{2n}{h_{flow}^{5/3}}\left|\frac{\partial h}{\partial x}\right|^{\frac{1}{2}}, \frac{2n}{h_{flow}^{5/3}}\left|\frac{\partial h}{\partial y}\right|^{\frac{1}{2}}\right) \qquad (2\text{-}7)$$

Looking at Equation (2-7), the time step depends on water surface slope meaning that for flat water surfaces the time step will approach zero drastically increasing computational time. To avoid stalling of the solver, linearization of the time step equation was implemented for grid cells where differences in flow depth are less than a specified $h_{lin}$ threshold (Hunter et al., 2005).

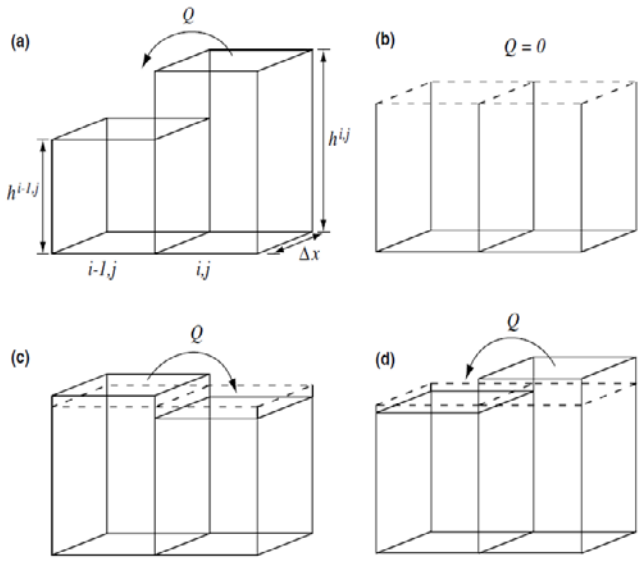


Illustration of chequerboard oscillations between two adjacent cells. (a) At end of time step $t$, the level in cell $i, j$ has for the first time risen above that of cell $i-1, j$. (b) At the end of time step $t+\Delta t$, the discharge from $i, j$ to $i-1, j$ should be equal to zero as the levels in each cell are equal (i.e. $h^{(i-1,j)} = h^{(i,j)}$). (c) However, an oscillation begins develop as a result of the low free surface gradient between the two cells (i.e. $h^{(i-1,j)} \approx h^{(i,j)}$) and, at the end of time step $t+\Delta t$, the discharge from $i, j$ to $i-1, j$ causes the level in $i-1, j$ to jump too high. This will result in an erroneous flow reversal at time step $t+2\Delta t$. (d) At the end of time step $t+2\Delta t$, the level in $i-1, j$ has caused a large discharge toward $i, j$, whose level rises too high and causes a second successive flow reversal. These oscillations develop rapidly and spread, destroying the solution.

**Figure 2-1** Illustration of chequerboard oscillations (Hunter et al., 2005)

### 2.1.3 Acceleration Solver

Adaptive time step solver when compared to analytical solutions of flood wave spreading over inclined surfaces showed better results than flow limited solver regardless of grid resolution or selected time step and also displayed intuitively correct sensitivity to floodplain friction over spatially complex topography (Hunter et al., 2005).

The main reason to use simplified equations of Saint-Venant equations within the numerical scheme was to achieve computational efficiency. Nonetheless, as grid resolution Δx decreases, time step Δt increases quadratically as can be seen in Equation (2-7). For this reason, the studies have indicated that urban flood simulations that were run on high grid resolution (1-10m) performed even slower

than complete two-dimensional shallow water equations leading to a conclusion that adaptive time step numerical scheme is not suitable for such applications. Therefore, it was necessary to develop a new scheme that would accurately represent physical processes of flow dynamics but with computational advantages over full shallow water equations (Bates et al., 2010).

The new numerical model was presented by Bates et al. (2010) where a new set of equations was developed to include local acceleration term within explicit storage cell code of the previous models but ignoring convective acceleration term in Equation (2-2). The new equation in terms of flow between cells per unit width is defined as:

$$\frac{\partial q}{\partial t} + \frac{gh\partial(h+z)}{\partial x} + \frac{gn^2q^2}{R^{4/3}h} = 0 \qquad (2\text{-}8)$$

where

q – discharge per unit width ($m^3/s/m$);

z – bed elevation (m);

g– gravitational acceleration ($m/s^2$);

R– hydraulic radius (m).

Modifying Equation (2-8) to discretize and solve explicitly for $q$ at time $t+\Delta t$:

$$q_{t+\Delta t} = q_t - gh_t\Delta t\left[\frac{\partial(h_t+z)}{\partial x} + \frac{n^2q_t^2}{h_t^{10/3}}\right] \qquad (2\text{-}9)$$

The acceleration term was added into new formulation of flow in Equation (2-9) and thus containing the term with inertial mass which prevents chequerboard oscillations. Still, this equation may still produce instabilities at shallow depths

whenever friction is high. Therefore, Equation (2-9) was further modified to produce the following explicit equation of flow:

$$q_{t+\Delta t} = \frac{q_t - gh_t\Delta t\frac{\partial(h_t + z)}{\partial x}}{(1 + gh_t\Delta t n^2 q_t / h_t^{10/3})} \quad (2\text{-}10)$$

The continuity equation is used to update flow depths inside the grid cells of Equation (2-5). The friction term is located in the denominator in Equation (2-10), hence whenever this term dominates, the equation flow will approach zero as intuitively one might expect (Bates et al., 2010).

To improve stability of explicit numerical solution, Equation (2-10) depends on Courant- Freidrichs-Levy condition:

$$C_r = \frac{V\Delta t}{\Delta x} \quad (2\text{-}11)$$

where

$C_r$ – dimensionless Courant number that should be smaller than one for stability purposes;

V – characteristic velocity (m/s), or else defined as wave celerity $\sqrt{gh}$ ignoring advection.

Equation (2-11) plays an important although not sufficient role in model stability, thus the time step at t+Δt is calculated:

$$\Delta t_{max} = \alpha\frac{\Delta x}{\sqrt{gh_{max}}} \quad (2\text{-}12)$$

where

$h_{max}$ – maximum flow depth in the domain;

$\alpha$ – coefficient employed for providing stable simulations and lies between 0.2 and 0.7 to additionally decrease time step and further improve stability of numerical model (the default value used in the model is 0.7).

It shall be noted that even though a more sophisticated numerical scheme is implemented compared to adaptive solver, a linear relation of $\Delta x$ and $\Delta t$ in Equation (2-12) can lead to considerable reduction of computational time (Bates et al., 2013).

Series of test simulations were analyzed using analytical solutions and real life fine scale topography urban flood models. Acceleration model was favorably compared to benchmark solutions in terms of predicted flow depths and root mean square error did not exceed average vertical error of DEM used for flood inundation studies. Moreover, the new model was much more computationally efficient than diffusive adaptive solver depending on grid cell resolution and water surface gradients (Bates et al., 2010; Fewtrell et al., 2011). However, acceleration solver produced increased flow depth errors and model instabilities at very low friction conditions such as n=0.01 which represents realistic urban surface roughness (Bates et al., 2010).

To overcome this deficiency, a new numerical formulation of local acceleration scheme that solves the system of partial differential equations and increases model stability at low friction without significant computational effort was presented by de Almeida et al. (2012). The unit discharge originating from simplified momentum equation of Equation (2-2) neglecting convective acceleration is solved explicitly between cells:

$$q_{i-1/2}^{n+1} = \frac{\theta q_{i-1/2}^{n} + \frac{(1-\theta)}{2}\left(q_{i-3/2}^{n} + q_{i+1/2}^{n}\right) - g h_f \frac{\Delta t}{\Delta x}\left(y_i^n - y_{i-1}^n\right)}{1 + g\Delta t n^2 q_{i-1/2}^{n}} h_f^{7/3} \qquad (2\text{-}13)$$

where

y – water surface elevation;

$h_f$ – difference between max.($y_i$, $y_{i-1}$) and max.($z_i$, $z_{i-1}$);

θ – weighting factor that regulates quantity of artificial numerical diffusion added to the numerical scheme to control numerical oscillations.

The subscript “i”, “i-1” in Equation (2-13) stands for center of grid cell while “i-1/2”, “i-3/2”, “i+1/2” indicate cell interfaces shown in Figure 2-2. It should also be emphasized that subscripts “i” and “n” represent space and time variables, respectively.

The values of θ can be manually adjusted between 0 and 1 such that if θ=1 is chosen, then no artificial diffusion is added and the numerical scheme of Bates et al. (2010) is maintained. But as coefficient of θ is decreased, artificial diffusion is added to balance discontinuities that may emerge due to nonlinear behavior in the solution such as shock waves. Consequently, the use of θ varying between 0.7 and 1 provided good results for low friction simulations as well as cases with rapid changes of flow (de Almeida and Bates, 2013).

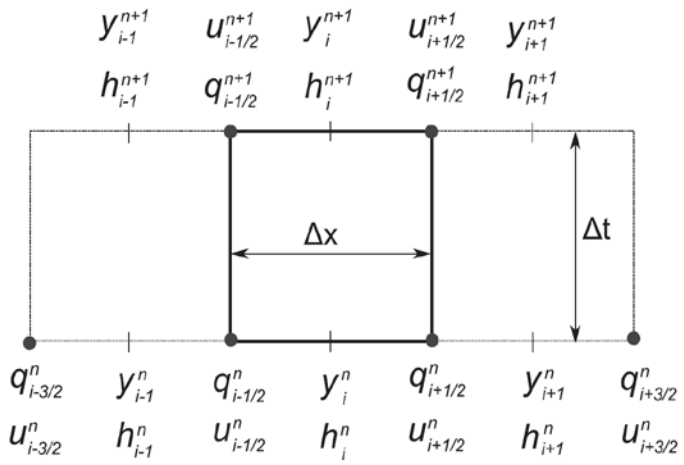


**Figure 2-2** Location of grid and variables implemented in the numerical scheme (only x direction is shown).

It should be noted that *y* and *h* variables are calculated at cell center but *q* and *u* variables at cell interfaces (de Almeida et al., 2012).

Afterwards, flow discharges calculated at four faces of a grid cell are used to update flow depths inside cells according to discretized form of continuity equation:

$$y_{i,j}^{n+1} = y_{i,j}^{n} + \frac{\Delta t}{\Delta x}\left(q_{i-\frac{1}{2}}^{n+1} - q_{i+\frac{1}{2}}^{n+1} + q_{j-\frac{1}{2}}^{n+1} - q_{j-\frac{1}{2}}^{n+1}\right) \qquad (2\text{-}14)$$

The subscript "j" in Equation (2-14) defines second horizontal dimension. The time step is calculated in the same way as in Equations (2-11) and (2-12).

### 2.1.4 Roe Solver

Some of the problems in two-dimensional flood modeling may necessitate inclusion of supercritical flows as well as shock capturing capabilities which the previous solvers are unable to handle. The last solver presented herein is Roe solver formulated in the work of Villanueva and Wright (2006), representing fully-

dynamic shallow water numerical model containing all terms in momentum conservation of Equation (2-2). This solver is based on finite volume method of Godunov approach and approximate Riemann solver by Roe where explicit discretization is first order in space and time on a rectangular and rectilinear raster grids implementing shock capturing scheme.

Roe's solver is considered as one of the most frequently used Riemann solver being a crucial component of Godunov-type schemes implemented within two-dimensional shallow water flows. Roe's solver basically transforms hyperbolic system into linear system of conservation laws that is much more manageable to deal with (Guinot, 2003).

The main idea behind this scheme is that assuming hydrostatic distribution of a long wave and vertical direction of a fluid flow being much less than horizontal direction, three-dimensional Navier-Stokes system of equations can be reduced to two-dimensional shallow water model. Furthermore, ignoring effects due to viscosity, turbulence, wind and Coriolis term, a new system of partial derivatives representing mass and momentum conservation can be expressed in mathematical form (Brufau et al., 2004).

The two-dimensional mass conservation is as follows (Villanueva and Wright, 2006):

$$\frac{\partial h}{\partial t} + \frac{\partial h\boldsymbol{u}}{\partial x} + \frac{\partial h\boldsymbol{v}}{\partial y} = \boldsymbol{Q}_l \tag{2-15}$$

Two-dimensional momentum conservation in two spatial dimensions is as follows:

$$\frac{\partial h\boldsymbol{u}}{\partial t} + \frac{\partial h\boldsymbol{u}^2}{\partial x} + \frac{\partial h\boldsymbol{uv}}{\partial y} + gh\frac{\partial h}{\partial x} = gh(S_{0x} - S_{fx}) \tag{2-16}$$

$$\frac{\partial h\boldsymbol{v}}{\partial t}+\frac{\partial h\boldsymbol{uv}}{\partial x}+\frac{\partial h\boldsymbol{v}^2}{\partial y}+gh\frac{\partial h}{\partial x}=gh(S_{0y}-S_{fy}) \qquad (2\text{-}17)$$

where

**u**, **v** – x and y depth averaged components of velocity, respectively (m/s);

$\mathbf{Q_l}$ – transfer of mass to a two-dimensional cell ($m^3/s/m^2$) (used for transferring one dimensional discharge into two-dimensional cells).

The terms $S_{0x}$ and $S_{0y}$ represent bed slopes in two spatial dimensions (only x-direction shown):

$$S_{0x}=-\frac{\partial z}{\partial x} \qquad (2\text{-}18)$$

The terms $S_{fx}$ and $S_{fy}$ represent friction losses in two spatial dimensions (only x-direction shown):

$$S_{fx}=\frac{n^2u\sqrt{u^2+v^2}}{h^{4/3}} \qquad (2\text{-}19)$$

The stability of the numerical scheme is controlled by Courant- Freidrichs-Levy condition for shallow water models as follows (Neal et al., 2011):

$$\Delta t_{max}=\alpha\frac{\Delta x}{|v|_{max}+\sqrt{gh_{max}}} \qquad (2\text{-}20)$$

where

$|v|_{max}$ – maximum normal velocity component in the domain.

## 2.2 Overview of Mike 21 model

The Mike 21 flow model includes a hydrodynamic model that is a numerical modelling system to simulate unsteady two-dimensional flows of vertically uniform fluids based on hyperbolic partial differential equations to produce computer model outputs of flow extents, flow depths and velocities in estuaries, bays and coastal areas (DHI, 2007).

The equations based on mass and momentum conservation principles that describe water flows can be outlined as follows:

$$\frac{\partial \zeta}{\partial t} + \frac{\partial p}{\partial x} + \frac{\partial q}{\partial y} = \frac{\partial d}{\partial t} \tag{2-21}$$

$$\frac{\partial p}{\partial t} + \frac{\partial}{\partial x}\left(\frac{p^2}{h}\right) + \frac{\partial}{\partial y}\left(\frac{pq}{h}\right) + gh\frac{\partial \zeta}{\partial x} + \frac{gp\sqrt{p^2+q^2}}{C^2 \times h^2} - \frac{1}{\rho_w}\left[\frac{\partial}{\partial x}(h\tau_{xx}) + \frac{\partial}{\partial y}\left(h\tau_{xy}\right)\right] - \Omega_p - fVV_x + \frac{h}{\rho_w}\frac{\partial}{\partial x}(p_a) = 0 \tag{2-22}$$

$$\frac{\partial q}{\partial t} + \frac{\partial}{\partial y}\left(\frac{q^2}{h}\right) + \frac{\partial}{\partial x}\left(\frac{pq}{h}\right) + gh\frac{\partial \zeta}{\partial y} + \frac{gq\sqrt{p^2+q^2}}{C^2 \times h^2} - \frac{1}{\rho_w}\left[\frac{\partial}{\partial y}\left(h\tau_{yy}\right) + \frac{\partial}{\partial x}\left(h\tau_{xy}\right)\right] + \Omega_p - fVV_y + \frac{h}{\rho_w}\frac{\partial}{\partial xy}(p_a) = 0 \tag{2-23}$$

where

h (x, y, t) – flow depth (h=$\zeta$-d, m);

d (x, y, t) – ground surface elevation (bathymetry, m);

$\zeta$ (x, y, t) – surface elevation (m);

p, q (x, y, t) – flux densities in x and y directions ($m^3/s/m$) - depth averaged velocity multiplied by flow depth h;

C (x,y) – Chezy roughness coefficient ($m^{1/2}/s$);

f (V) – wind resistance coefficient;

$V$, $V_x$, $V_y$ $(x, y, t)$ – wind velocities and its components in x and y directions(m/s);

$\Omega$ – Coriolis coefficient, latitude controlled ($s^{-1}$);

$p_a$ – atmospheric pressure ($kg/m/s^2$);

$\tau_{xx}$, $\tau_{xx}$ , $\tau_{xx}$ – effective shear stress components;

x, y – Cartesian coordinates (m);

t – time (s);

Coriolis terms are not usually included as far as flood modeling is concerned. Also, wind resistance effects on water elevations in urban flood modeling may also be neglected, although this still may depend on wind severity and its direction. Moreover, wall friction terms can be neglected due to the fact that they are applicable when the resolution of a flood model is very high (Néelz and Pender, 2009).

The shallow water equations are represented in numerical modeling by a technique called discretization which is a way to convert these differential equations into a set of algebraic equations that couple variables calculated at a finite set of points in a space and time domain. The numerical method used in Mike 21, in particular, is called Alternating Direction Implicit method (Néelz and Pender, 2009).

The Alternating Direction Implicit method (ADI) is a finite difference method that was implemented to integrate shallow water equations derived from continuity and momentum conservation equations in a time domain for one row or column at a time, in an alternating order on a staggered grid. To discretize time, ADI divides the equations used within finite difference method into two parts (called x- and y-sweeps) at each time step. These equations are calculated in both of the sweeps to update flows and depths by solving x-derivative implicitly during one sweep (and y-derivative explicitly) as well as solving y-derivative implicitly (and x-derivative explicitly) during another sweep (DHI, 2007).

# CHAPTER 3

# EVALUATION OF LISFLOOD-FP SOLVERS

## 3.1 General Information

There are numerous flood simulation models in the industry that offer numerical schemes of varying complexity representing natural phenomena. Commonly, benchmarking tests are performed to analyze how different models behave in terms of flood propagation, computation time, etc. However, a problem with model setup formulation of the same flood event may arise when benchmarking different numerical codes due to the way each computational model may deal with topography, wetting and drying of a wave front, treatment of friction, inflow and outflow boundaries. Consequently, all these can significantly impact model outputs further reducing ability to adequately compare models without even considering complexity of a numerical scheme, or any other uncertainty parameter. One way to avoid such an ambiguity is to benchmark models implemented within a single framework of a numerical code to study model results of different complexity in terms of representation of shallow water equations (Neal et al., 2011).

The first part of the thesis study performs the analysis of 4 numerical schemes within a single framework of the numerical code implemented in LISFLOOD-FP raster flood inundation model (version 5.9.5). The big benefit of these solvers is that they all use the same input data for simulations such as Digital Elevation Model (DEM), domain boundary or roughness conditions.

All the models implemented in this study differ from each other according to the numerical formulation of momentum conservation equation. For instance, inertial terms are neglected both in Flow-limited and Adaptive solvers representing diffusive wave approach, local acceleration term is omitted in Acceleration solver and all terms are represented in Roe solver. More detailed information regarding these differences can be seen in Table 2-1.

### 3.2 Model Simulation Setup

The DEM used in this study is 1 m resolution model in a form of ASCII file format collected by State Hydraulic Works (DSI) in 2013 (Figure 3-1).

Since the main reason for conducting this study is to analyze the performance of the four solvers rather than simulating a real flood event, a hypothetical 30 min duration hydrograph was constructed to simulate inflow boundary conditions of a flood event (Figure 3-2). The source point of inflow boundary condition and four control points located in the DEM are shown in Figure 3-3 (Buildings are represented by white polygons).

Uniform Manning's roughness coefficient of n=0.035 was used in all models representing cumulative roughness of urbanized area surface friction.

The duration for both simulations was set for two hours with 30 min inflow of water to the domain and 90 min time for water to propagate on the DEM. It should be mentioned that the outflow boundaries of the DEM are closed, hence the entire volume of water from inflow hydrograph stays in the domain.

The minimum default depth threshold value (depth of a cell considered wet) of all solvers within Lisflood-FP model was set as 1 mm (Bates et al., 2013).

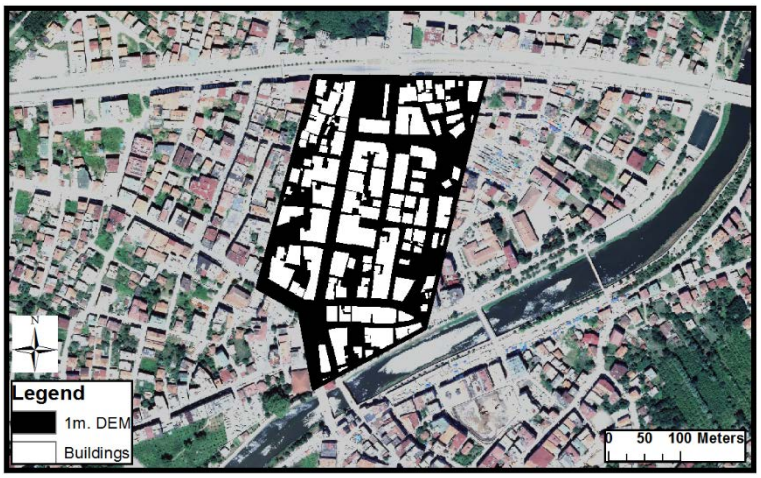


**Figure 3-1** The DEM used in the benchmark tests of four Lisflood-FP solvers

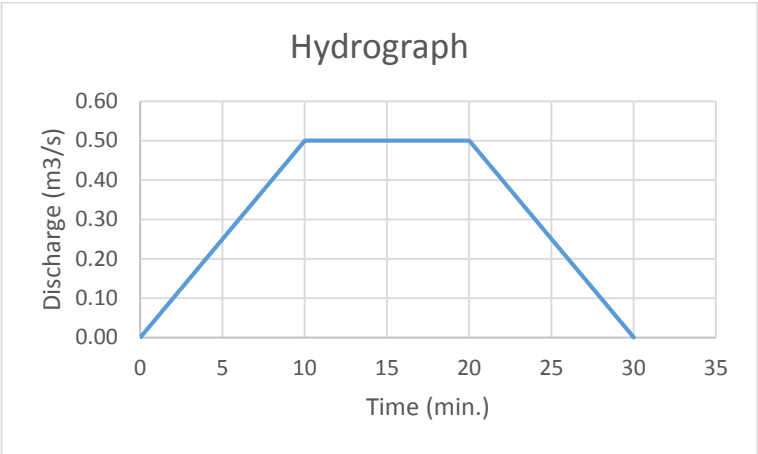


**Figure 3-2** Inflow Hydrograph

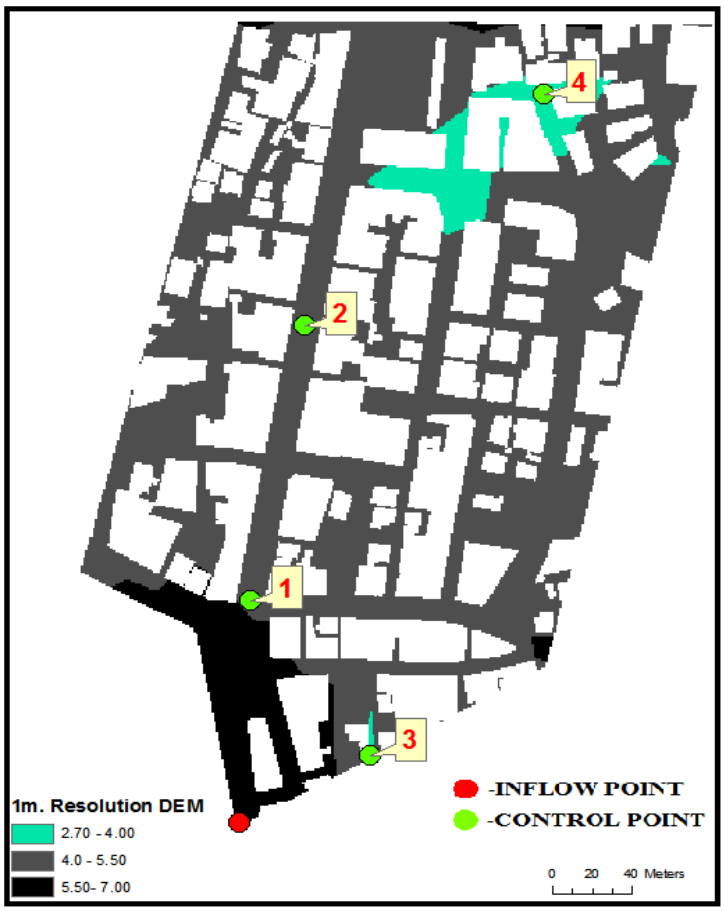


**Figure 3-3** Inflow and Control points location in the DEM

## 3.3 Comparison of the solvers

Before starting the comparison of four hydraulic models, a small discussion regarding Flow-limited solver should be made. As it was described in the previous sections, time step for simulations is chosen manually by a user, thus this parameter was calibrated to approximate the results to Adaptive solver. Simulations of three time steps were run – $\Delta t$=1 sec, $\Delta t$=0.1 sec and $\Delta t$=0.01 sec to see the differences in terms of flood extents and flow depths, the results of last time interval t=120 min can be seen in Figure 3-4. It can be seen that when bigger time steps are chosen, the solver underpredicts flow propagation, leading to a conclusion that large time steps provide very unreliable results compared to lower ones and that the choice of a time step has to be done extremely carefully. The Flow-limited, Adaptive, Acceleration and Roe solvers were all studied to compare the results of simulations in terms of their respective flow inundation extents, flow depth and velocities as well as statistical measures such as Root Mean Square Difference (RMSD) and Fit Statistic ($F^2$).

Herein, RMSD represents difference between values of flow depths or velocities at a particular time step as follows:

$$RMSD = \sqrt{\frac{\sum_{i=1}^{n}(x_i - y_i)^2}{n}} \tag{3-1}$$

where

$x_i$, $y_i$ – values of flow depths or velocities to be compared;

n – sample size or number of cells occupied by water.

As the difference between two compared data sets decreases, RMSD value will decrease meaning that two identical data sets will result in RMSD value of zero.

The Fit Statistic ($F^2$) can be described as a method that compares two models in terms of their inundation extents. One of the models is considered as a benchmark (frequently observed in nature) and the other one is quantitatively compared to that "correct" model by the following formula (Werner et al., 2005):

$$F^2 = \frac{\sum_{i=1}^{n} {P_i}^{D_1 M_1}}{\sum_{i=1}^{n} {P_i}^{D_1 M_1} + \sum_{i=1}^{n} {P_i}^{D_1 M_0} + \sum_{i=1}^{n} {P_i}^{D_0 M_1}} \qquad (3\text{-}2)$$

where

${P_i}^{D_1 M_1}$ – value of 1 for cells classified as inundated both in benchmark and comparative models;

${P_i}^{D_0 M_1}$ – value of 1 for cells observed dry in benchmark model but predicted wet in comparative model;

${P_i}^{D_1 M_0}$ – value of 1 for cells observed wet in benchmark model but predicted dry in comparative model.

It should be mentioned that the range of $F^2$ values varies between zero to one, and complete correlation is represented by a value of one.

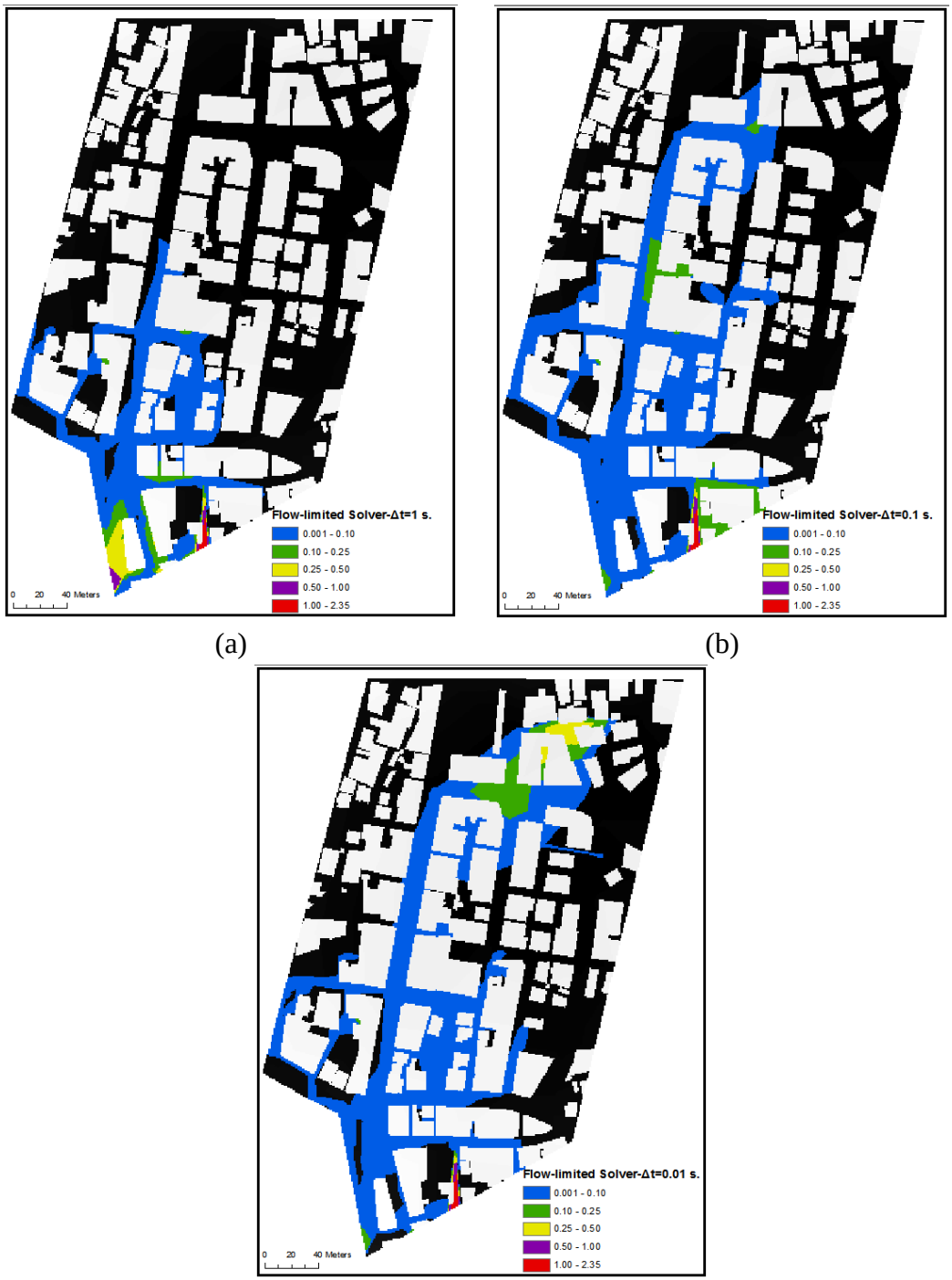


**Figure 3-4** Comparison of Flow-limited solver simulations results at t=120 min run at time steps (a) t=1 s, (b) t=0.1 s and (c) t=0.01 s.

Figure 3-5 to Figure 3-9 show flow propagation within the domain at time intervals t=6, 18, 30, 60 and 120 minutes. At the start of the simulation (t=0 min), map area is empty and water just started to fill the domain at inflow control point in southern corner of the DEM. Just as the water had started to fill the domain at t=6 min, flow is heading to lower elevations in the northern direction toward intersection of the three streets. At time t=18 min, after reaching the intersection flow propagation is divided - one fraction of water continues heading north down the main street, the other one is flowing in the eastern direction and flooding adjacent streets on the right. Meanwhile, it can be seen that water pond is developed just a couple blocks away to the right of the inflow source point due to depression in elevation that can be observed in Figure 3-3. At time t=30 min, no more water is being added into the domain and flood in all models continues flowing within the main street toward lower elevations. As simulation time progresses, at time t=60 min the portion of water body passing through the main street has reached another depression flooding second ponding area. The flow is also propagating toward north-west reaching a closed outflow boundary as well as north-east flooding surrounding streets. Finally, at time t=120 min all numerical schemes except Roe solver have reached a point where no major flow propagation can be observed anymore.

To graphically represent the differences between four hydraulic models, five sections were taken to analyze the behavior of flow depths with respect to DEM elevation at time t=120 min that can be seen in Figure 3-10. The first section (Figure 3-11) represents the variation of flow depth within the main street of the DEM whereas all other sections (Figure 3-12, Figure 3-13 and Figure 3-14) show how water depth may change with respect to two depressions in the DEM demonstrated in Figure 3-3.


**Figure 3-5** Results of Inundation Extents of (a) Flow-limited, (b) Adaptive, (c) Acceleration and (d) Roe solvers at t=6 min.

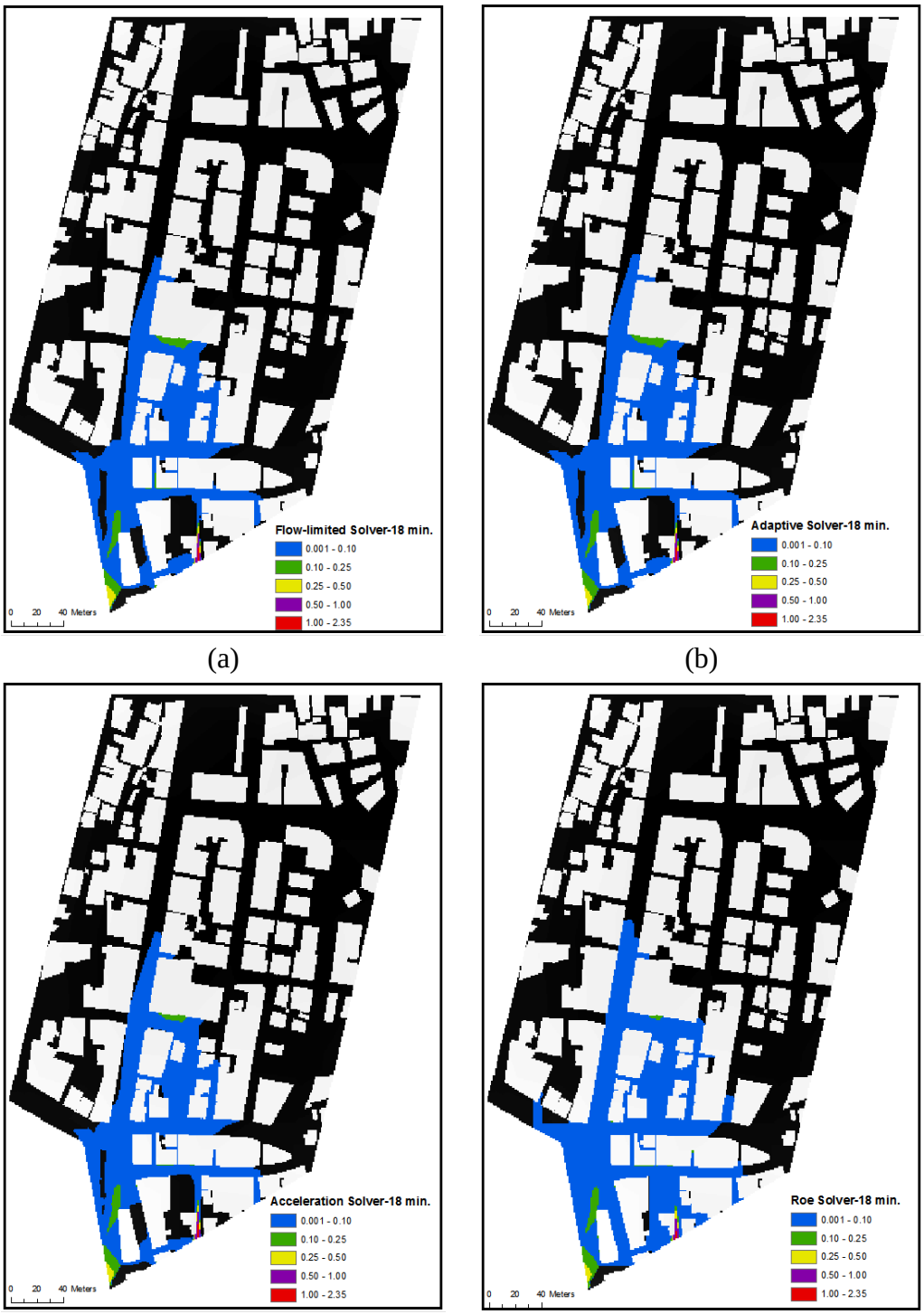


**Figure 3-6** Results of Inundation Extents of (a) Flow-limited, (b) Adaptive, (c) Acceleration and (d) Roe solvers at t=18 min.

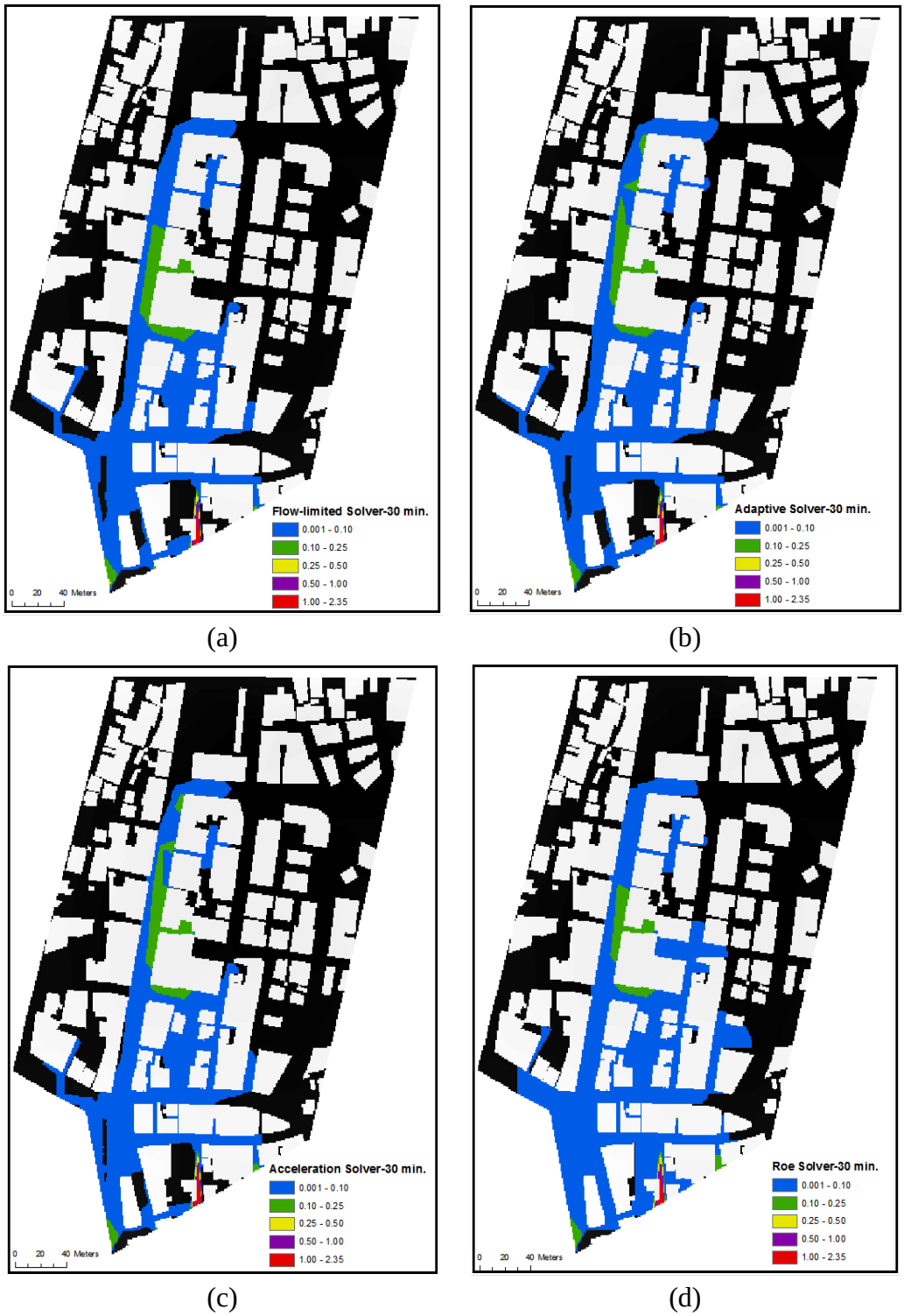


**Figure 3-7** Results of Inundation Extents of (a) Flow-limited, (b) Adaptive, (c) Acceleration and (d) Roe solvers at t=30 min.


**Figure 3-8** Results of Inundation Extents of (a) Flow-limited, (b) Adaptive, (c) Acceleration and (d) Roe solvers at t=60 min.

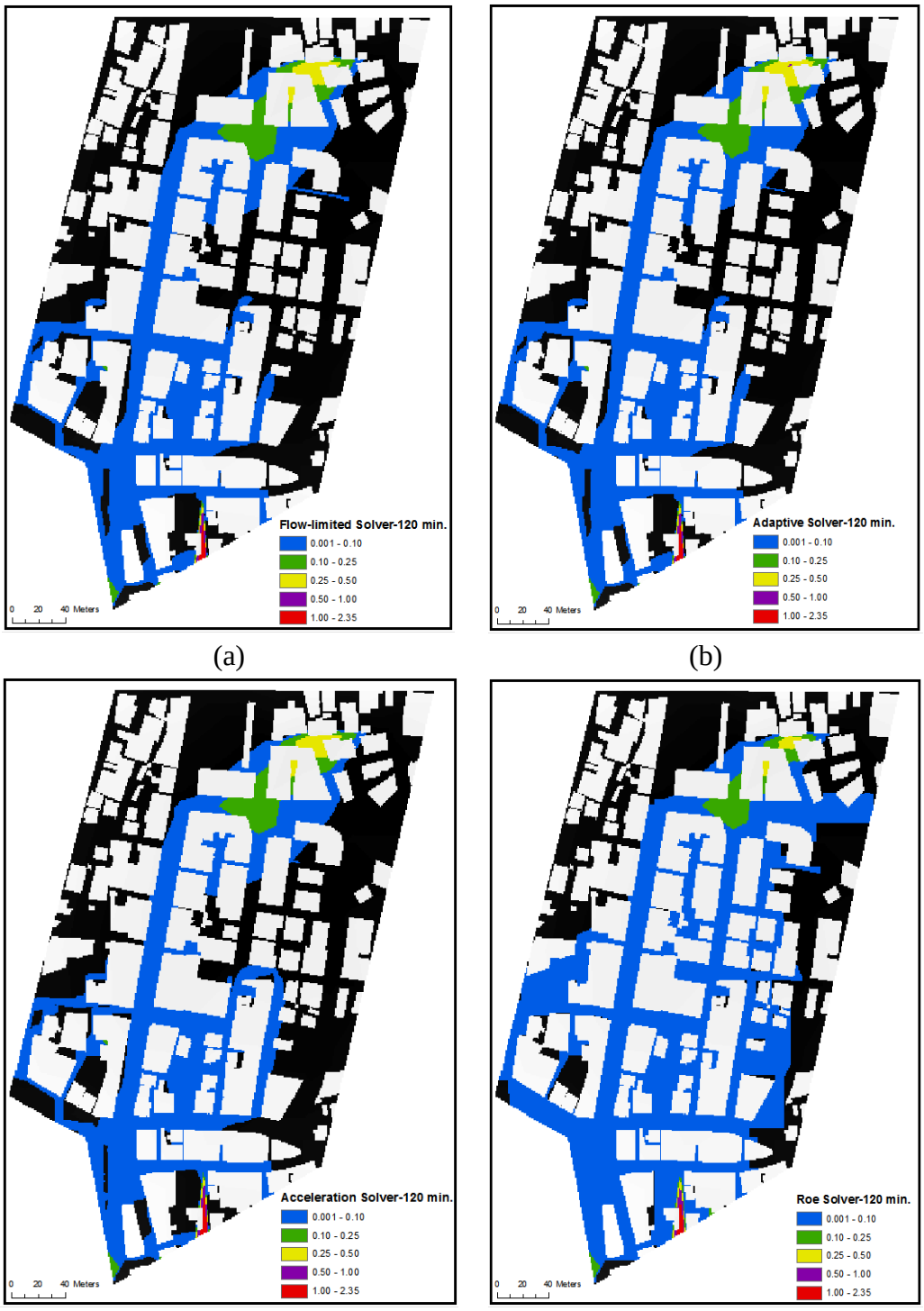


**Figure 3-9** Results of Inundation Extents of (a) Flow-limited, (b) Adaptive, (c) Acceleration and (d) Roe solvers at t=120 min.

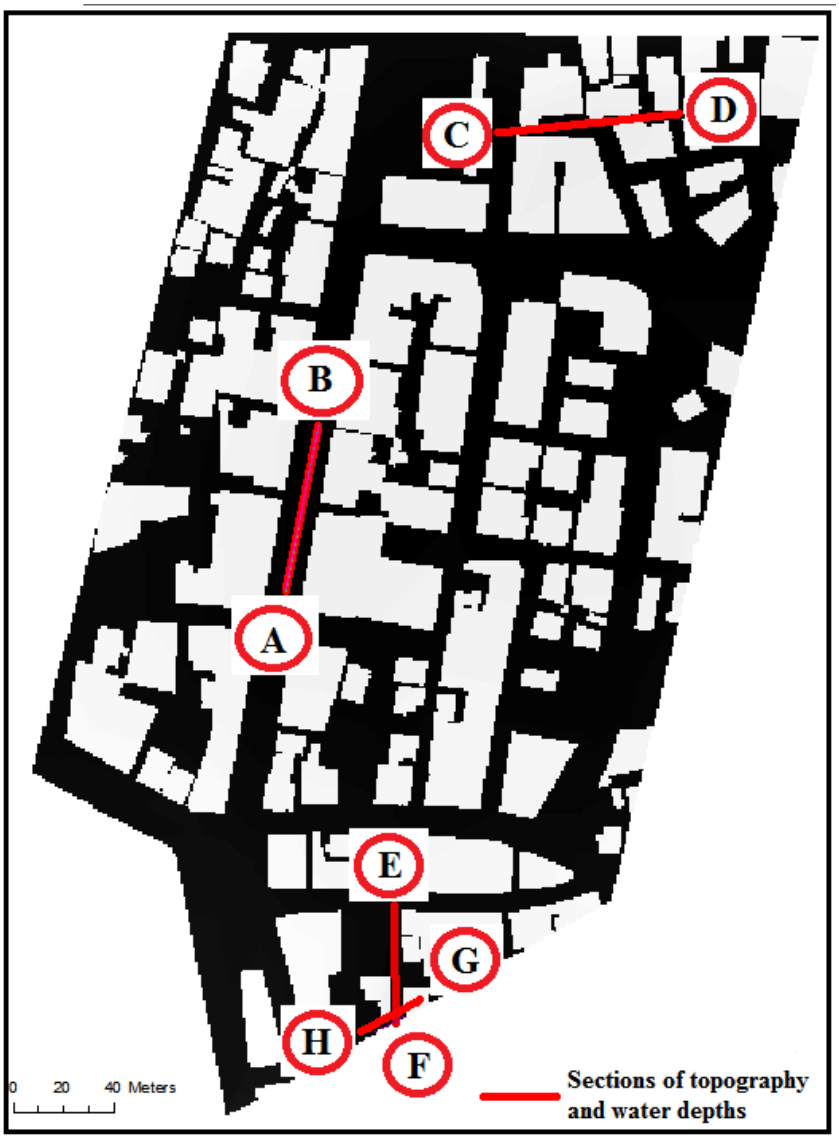


**Figure 3-10** Location of sections to analyze behavior of flow depths with respect to DEM elevation at time t=120 min.

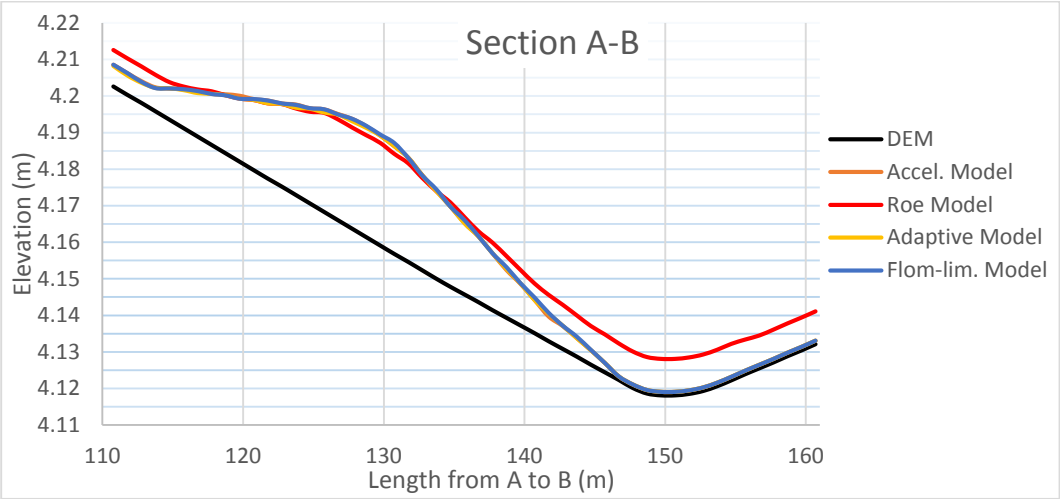


**Figure 3-11** Water Elevations Profile of Section A-B comparing 4 hydraulic models at t=120 min.

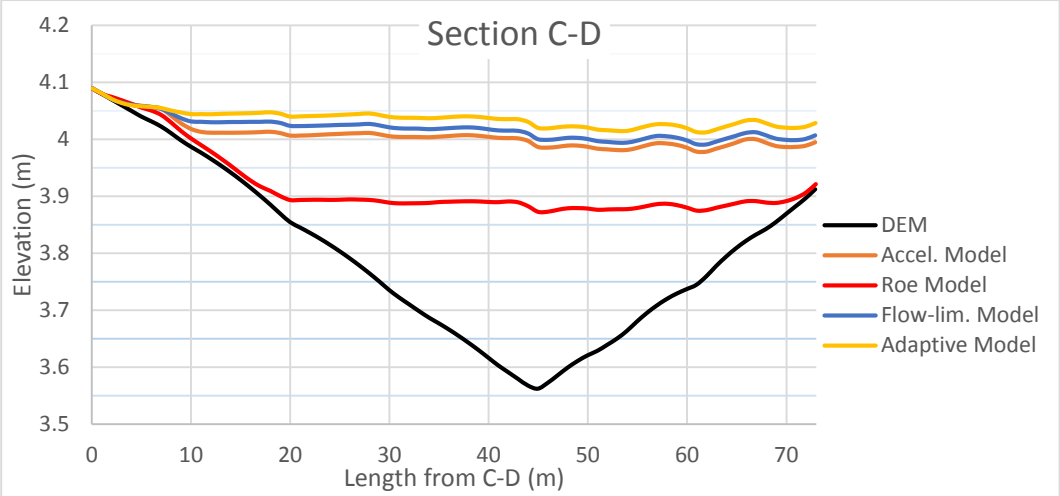


**Figure 3-12** Water Elevations Profile of Section C-D comparing 4 hydraulic models at t=120 min.

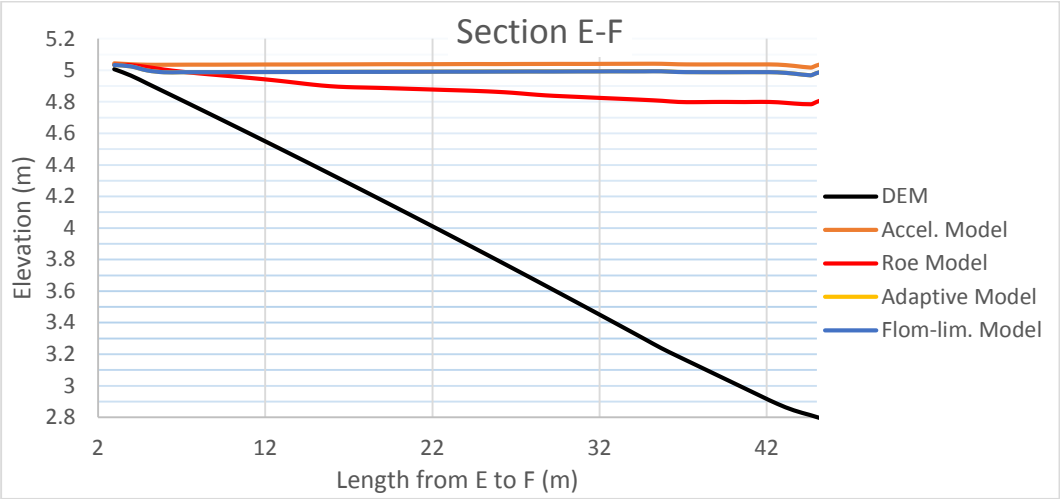


**Figure 3-13** Water Elevations Profile of Section E-F comparing 4 hydraulic models at t=120 min.

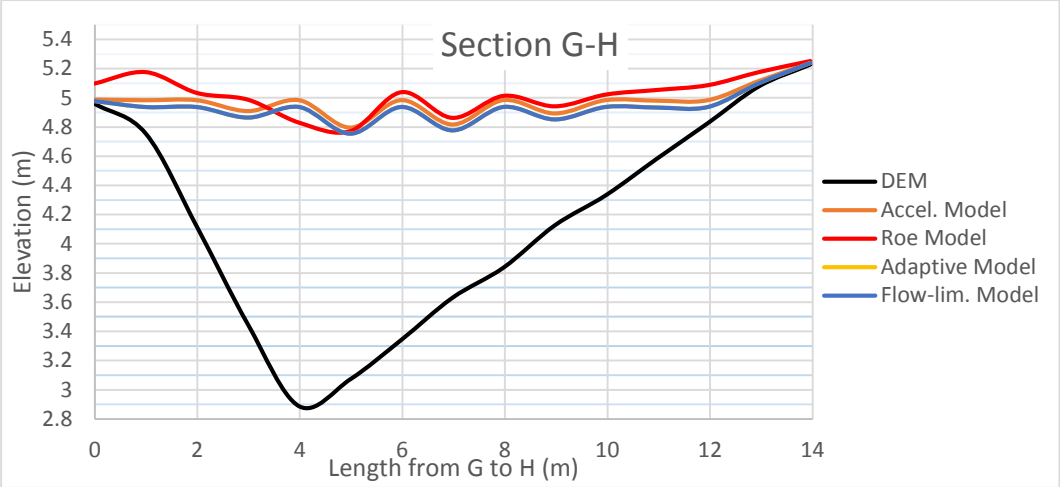


**Figure 3-14** Water Elevations Profile of Section G-H comparing 4 hydraulic models at t=120 min.

Comparing the models in terms of inundation extents, one may distinguish considerable differences developing from time interval t=30 min – in general Flow-limited, Adaptive and Acceleration solvers predict similar flow propagation whereas Roe solver overinundates eastern part of the domain in comparison to the other numerical models. As simulation progresses, the same tendency can be observed as Roe solver continues flooding the domain both in eastern and western directions while three other numerical schemes propagate toward the northern depression zone accumulating water as can be noticed both in time t=60 min and t=120 min (Figure 3-8 and Figure 3-9).

To understand the differences between the models more thoroughly, numerical and graphical variation of four compared models in terms of their respective flow depths and inundation extents for time t=120 min are presented in Figure 3-15 and Figure 3-16, respectively. It should be mentioned that Acceleration solver was chosen as a reference model and all other models were compared accordingly – Figure 3-15 shows numerical subtraction of flow depths of Acceleration solver from Flow-limited solver, Adaptive and Roe solvers separately.

As it was explained in the previous chapter, the main difference between Flow-limited and Adaptive solvers in terms of numerical formulation within code is that, as the names imply, the former implements flow limiter to avoid chequerboard oscillations whenever a large time step is chosen which may lead to poor model outputs, while the latter uses adaptive time step instead of manually arranging time step. Since in this simulation time step for Flow-limited solver was calibrated to resemble the results to Adaptive solver (Figure 3-4), hence similarities between the two numerical models may be observed.

The Acceleration and Diffusive solvers displayed identical behavior, although small differences are still present, in terms of both flood inundation and flow depth prediction. As can be seen in Figure 3-15, the difference of depth between the

models at time interval t=120 min exceeding 1 cm can only be observed in two locations – diffusive solvers accumulate higher depths in northern depression zone while deeper ponding can be observed for Acceleration solver. Diffusive solvers are more susceptible to changes in elevation of topography and it was found out that depth of a wave front for these models is higher because water body should overcome inertia to propagate in acceleration numerical scheme (Fewtrell et al., 2011). The assumption here is that the flow in diffusive solvers propagates more easily toward lower elevations in the northern direction while acceleration solver being unable to flow in that direction in the same way, instead moves in the lateral direction toward the south-east. That way, the wave front of diffusive solvers reach northern depression zone more easily and flood that area when the acceleration solver ponds the southern depression zone. Nonetheless, such differences may not be considered very significant because the maximum flow depth difference in these two ponding areas does not exceed 7 cm.

Comparing Acceleration and Roe solvers, significant variations are evident at time interval t=120 min. In terms of inundation extents, Roe solver floods much higher area of the DEM and that difference cannot be ignored (Figure 3-16). Furthermore, there is also considerable discrepancy between two models in terms of flow depths within two depression zones with maximum difference reaching up to 25 cm. Looking at Figure 3-12 and Figure 3-15, the average depth is higher (~10 cm) in the northern depression zone for Acceleration solver. Meanwhile, in the southern depression zone, Roe solver in general accumulates higher depths averaging 5 to 10 cm. However, it is interesting to note that there is a small area within that zone where a section was taken (Figure 3-13) and Acceleration solver displays higher depths averaging 15 cm. It is not clear what may be causing such deviation but possibly Roe solver distributes water more uniformly within the depression zone and thus lower depths are observed in that particular area.

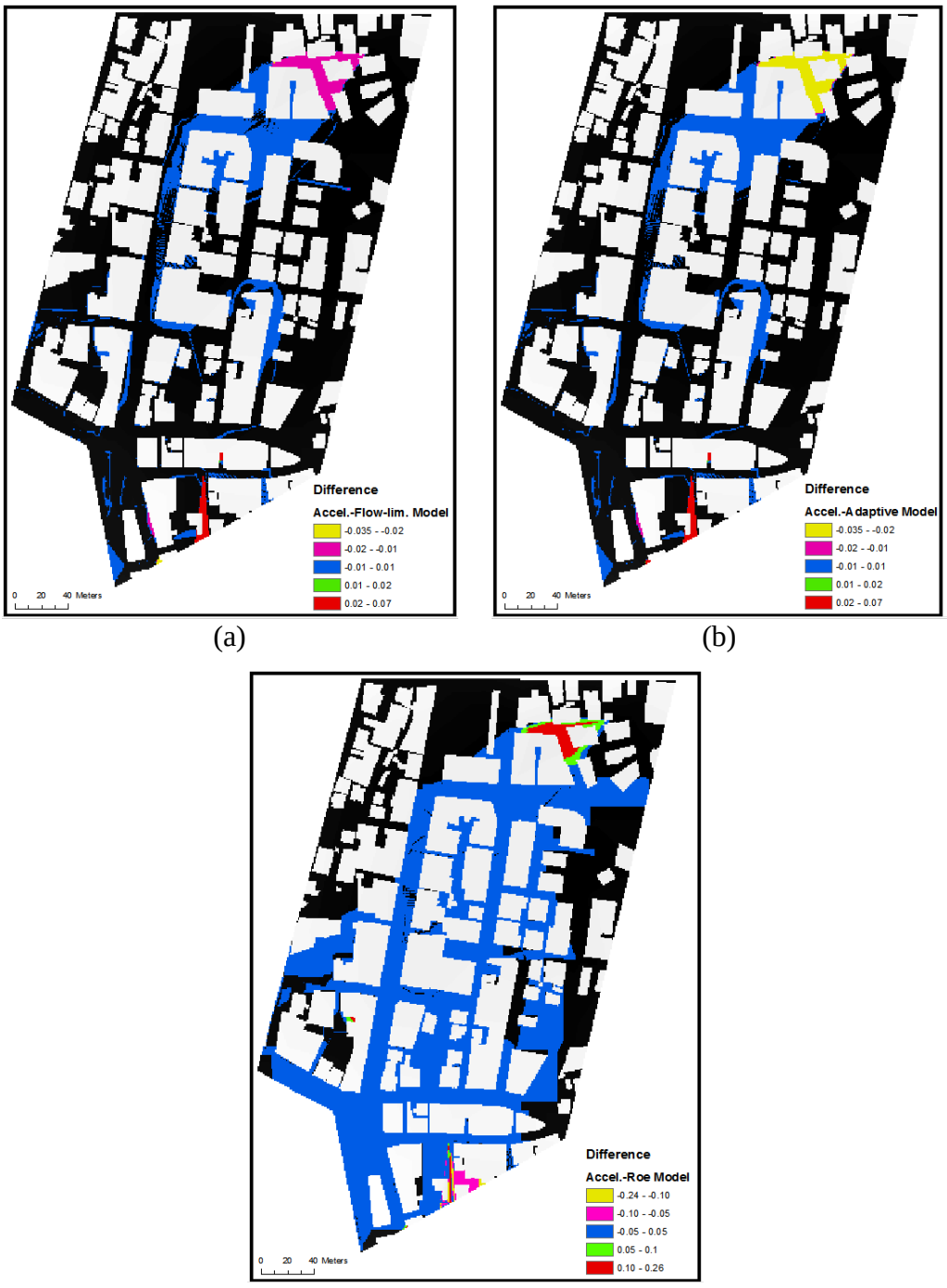


**Figure 3-15** Numerical subtraction of flow depths of (a) Acceleration - Flow-limited, (b) Acceleration-Adaptive, and (c) Acceleration - Roe solvers at time t=120 min.

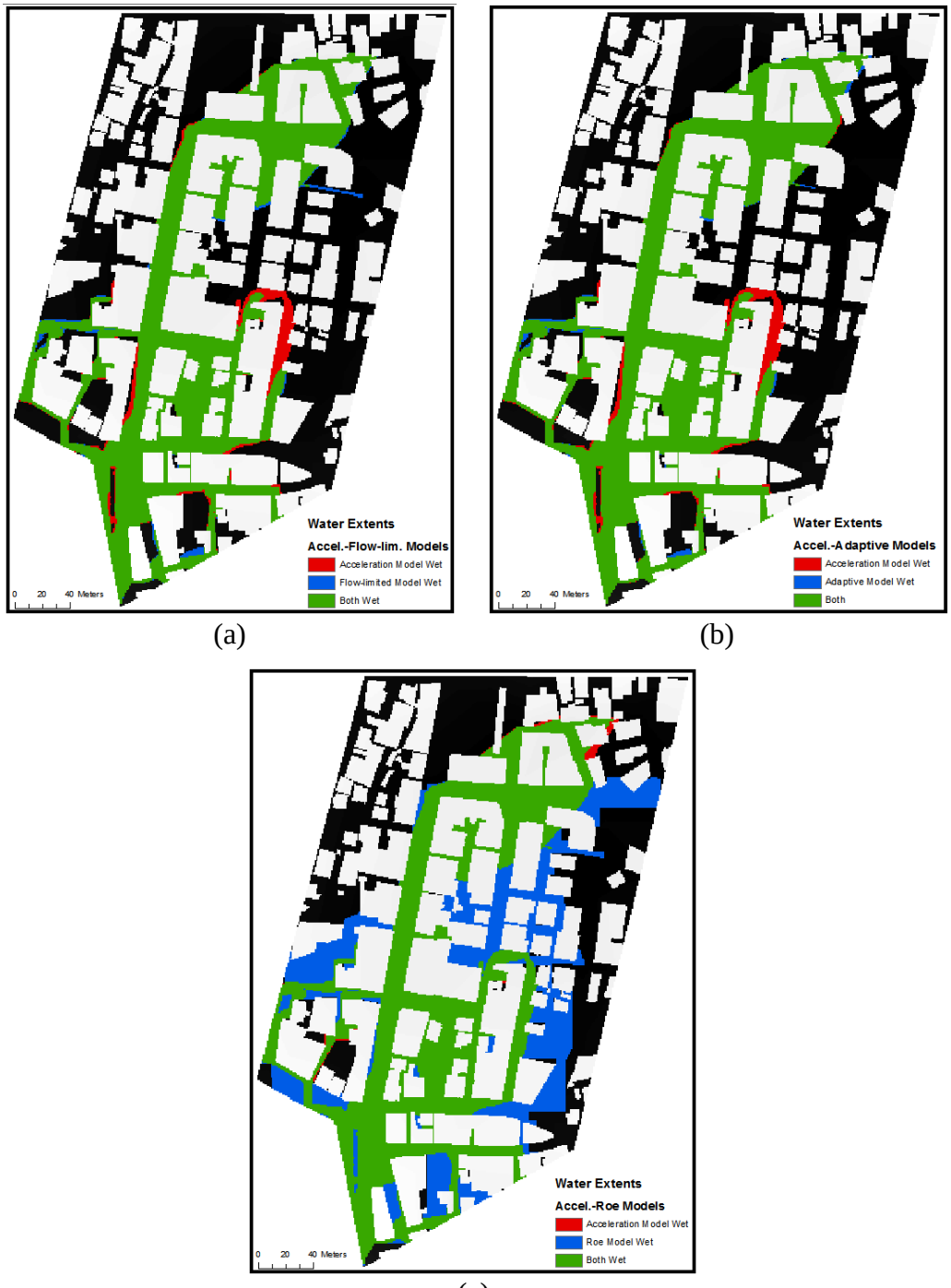


**Figure 3-16** Graphical representation of differences in terms of flow extents between (a) Acceleration and Flow-limited, (b) Acceleration and Adaptive, (c) Acceleration and Roe solvers at time t=120 min.

Nonetheless, considering another ponding area by the same analogy with the previous paragraph it may be assumed that omitting convection acceleration term, Acceleration solver is more prone to elevation differences and therefore the flow propagates toward and floods northern depression zone. Also, Roe solver represents full shallow water equations in the numerical scheme, thus even higher inertia is required to overcome to start the flow and consequently water is propagating in both lateral directions (eastern and western). It is important to emphasize that a total of V=600 $m^3$ of water was inserted into the model. However, looking at Table 3-1 one can notice that Roe solver being affected by numerical instability, over predicts the total amount of water in the model by 29.25 $m^3$. That, in turn, to a certain extent may be the cause of inundation extents over predicting in comparison to other solvers (Figure 3-16).

It should be emphasized that, the slope gradients exceeding 10% in shallow water equations may cause numerical instabilities within the hydraulic models (Sampson et al., 2012). The DEM used in these simulations includes an area where the gradients are above 10% (Figure 3-17). Therefore, it can be concluded that all numerical solvers may not correctly predict simulation outputs at southern depression zone where slope gradients exceed 10%. The slope gradients were calculated taking advantage of slope function of special analysis tool of ArcMap software. The slope function calculates a maximum rate of change of depth values from each cell on a raster grid.

Four numerical schemes used in this study were also analyzed at four control points shown in Figure 3-3. Point 1 symbolizes variation of flow during simulation time nearby inflow source point at the beginning of a main street where elevations are high. Point 2 is located further down on the main street and it is possible to trace behavior of flow as it propagates forward. Points 3 and 4 were chosen because they represent areas of ponding.

**Table 3-1** Volume of water in the domain at different time intervals.

| Time (min) | Acceleration Model ($m^3$) | Flow-limited Model ($m^3$) | Adaptive Model ($m^3$) | Roe Model ($m^3$) |
|---|---|---|---|---|
| 0 | 0.00 | 0.00 | 0.00 | 0.00 |
| 6 | 54.01 | 54.00 | 53.98 | 55.21 |
| 12 | 210.05 | 210.00 | 209.98 | 217.83 |
| 18 | 390.00 | 390.00 | 389.98 | 402.04 |
| 24 | 545.97 | 546.00 | 545.98 | 559.79 |
| 30 | 599.98 | 600.00 | 599.98 | 616.68 |
| 36 | 599.98 | 600.00 | 599.98 | 620.12 |
| 42 | 599.98 | 600.00 | 599.98 | 622.62 |
| 48 | 599.98 | 600.00 | 599.98 | 623.81 |
| 54 | 599.98 | 600.00 | 599.98 | 624.61 |
| 60 | 599.98 | 600.00 | 599.98 | 625.18 |
| 66 | 599.98 | 600.00 | 599.98 | 625.65 |
| 72 | 599.98 | 600.00 | 599.98 | 626.34 |
| 78 | 599.98 | 600.00 | 599.98 | 627.17 |
| 84 | 599.98 | 600.00 | 599.98 | 627.64 |
| 90 | 599.98 | 600.00 | 599.98 | 627.96 |
| 96 | 599.98 | 600.00 | 599.98 | 628.72 |
| 102 | 599.98 | 600.00 | 599.98 | 629.01 |
| 108 | 599.98 | 600.00 | 599.98 | 629.13 |
| 114 | 599.98 | 600.00 | 599.98 | 629.21 |
| 120 | 599.98 | 600.00 | 599.98 | **629.25** |

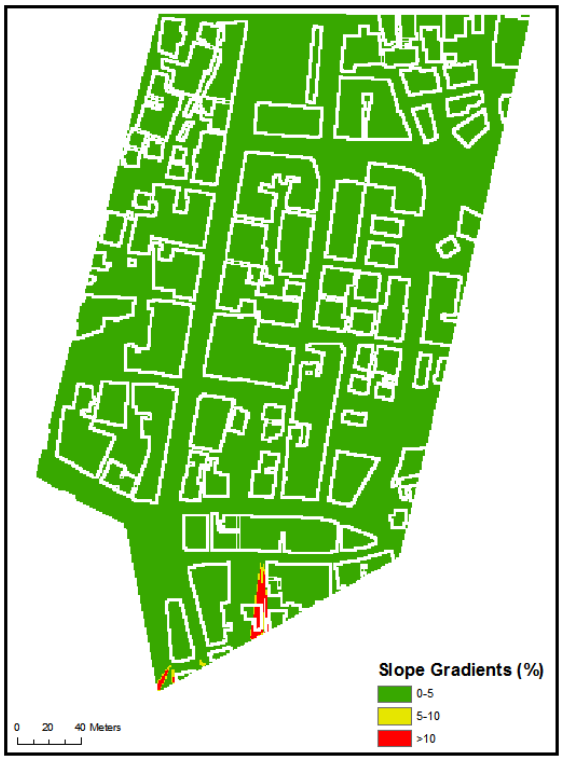


**Figure 3-17 .** Slope gradient variation within DEM (%)

Flow depth variation among the models through simulation time at four control points is displayed in Figure 3-18. The control points 1 and 2 display very similar behavior in terms of flow depths. The arrival times are t=12 min and t=24 min for the first and the second control points, respectively. It should also be mentioned that difference of peak flow depths for both of the control points do not exceed 1 cm. All solvers reach point 3 at t=12 min but as it was mentioned earlier, Roe solver over estimates depths in the southern depression zone which is also the case in control point 3 where average difference is 10 to 15 cm compared to other models. It was also stated that diffusive solvers accumulate higher flow depths in the northern depression zone and looking at control point 4, it can be seen that maximum difference between depths are 4 and 15 cm for Acceleration and Roe

solvers, respectively. Nonetheless, water first appears at t=48 min in all hydraulic models.

The differences between model flow velocities are shown in Figure 3-19. Not surprisingly, velocities at control points 1 and 2 show the similar behavior as in the case of flow depths – arrival times are the same and the peak velocities do not exceed 15% or 0.06 m/s for both points. However, the control point 3 reveals that there is a two and three-fold increase of peak velocity in Roe solver compared to Acceleration and diffusive hydraulic models, respectively. As it was previously described, this may be due to the inability of numerical models to resolve the area where slope gradients exceed 10%. At control point 4, even though in relative terms the maximum difference of peak velocity between diffusive and Roe solvers is about 65%, in absolute terms this difference is only 0.03 m/s.

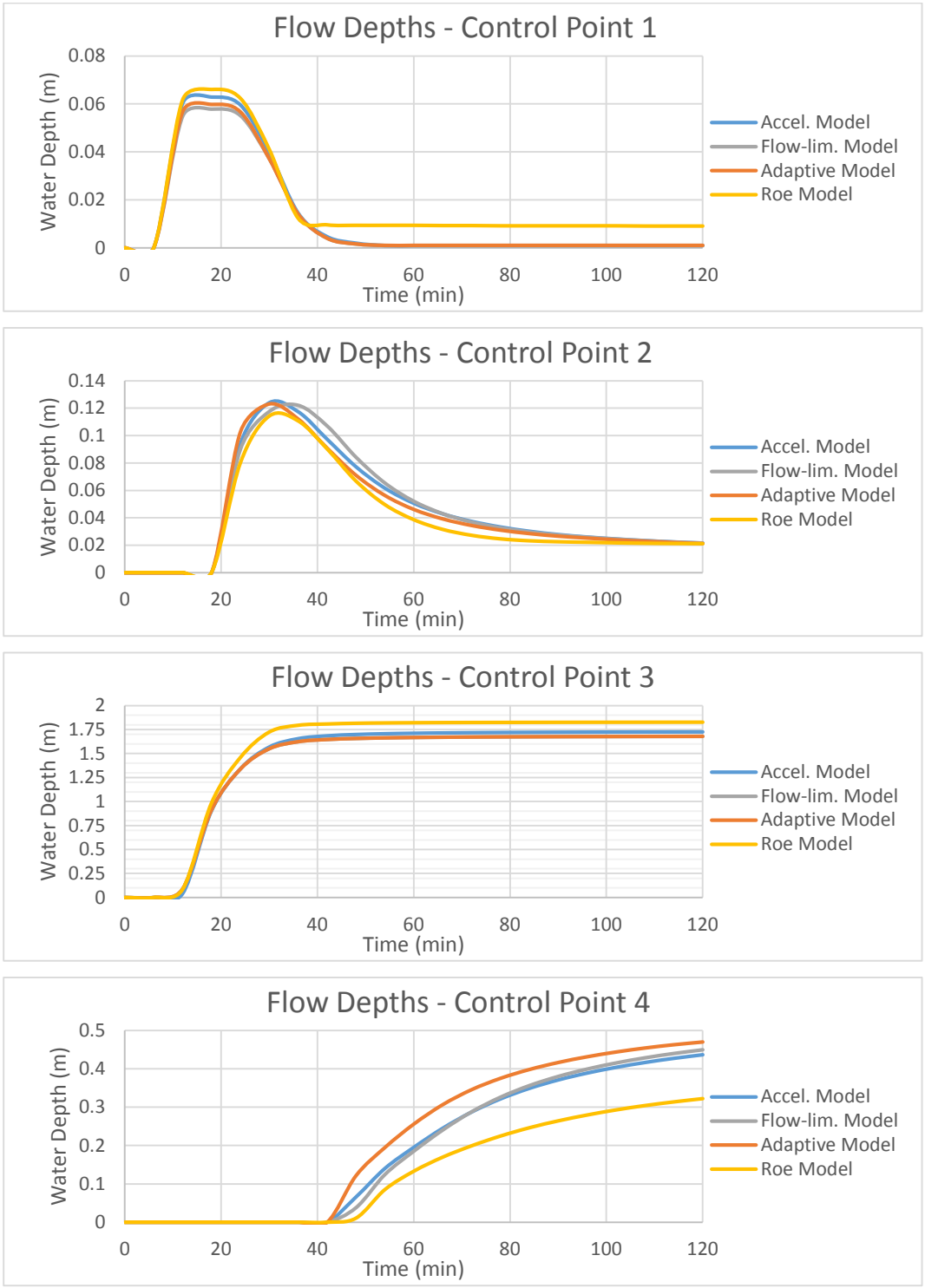


**Figure 3-18** Flow Depth Outputs at 4 control points through simulation time of 4 hydraulic solvers

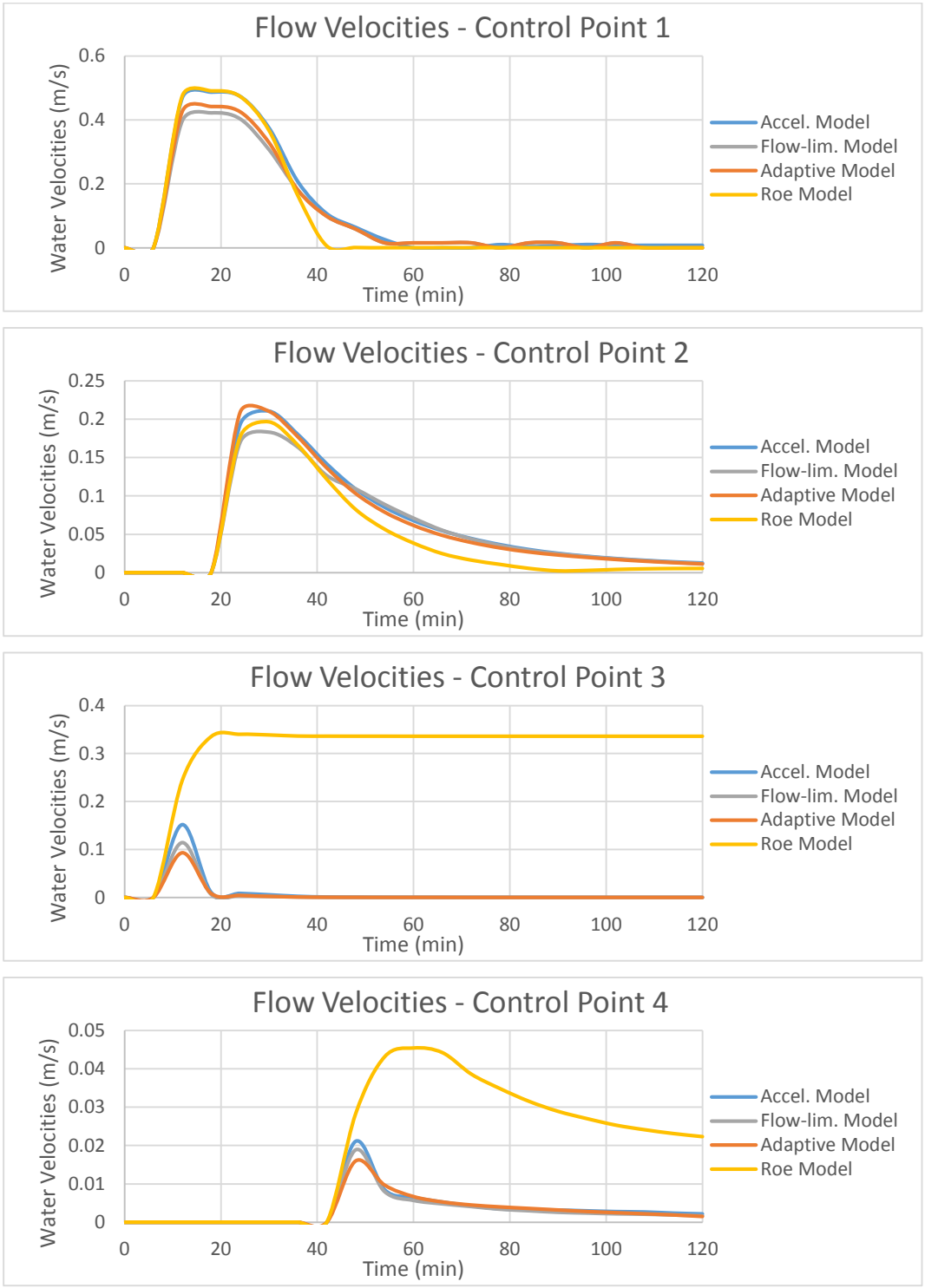


**Figure 3-19** Flow Velocity Outputs at 4 control points through simulation time of 4 hydraulic solvers

The inundated areas were also compared numerically as shown in Figure 3-20 and Figure 3-21. Figure 3-21 defines the numerical subtraction of flooded area obtained by Acceleration solver and flooded areas obtained by the other three codes. Clearly, the flow in Roe solver inundates much higher area reaching up to almost 35% in comparison to Acceleration solver. Meanwhile, between diffusive and Acceleration numerical schemes this difference does not exceed 5%.

Four hydraulic models were also analyzed using statistical measures. Firstly, RMSD of flow depths and velocities (Acceleration model was considered as a benchmark) was studied (Figure 3-22). Again, the significant decrease in Roe model performance can be observed - the maximum difference approaches 9 cm for flow depths in final time interval. Conversely, diffusive solvers show only minor variation of 2 cm maximum value of RMSD across simulation time. Secondly, Fit Statistic was compared for both of the models in terms of inundation extents (Figure 3-23). Likewise, as it was expected Roe solver evidently predicted lower $F^2$ compared to the diffusive solvers providing worse prediction of flow inundation.

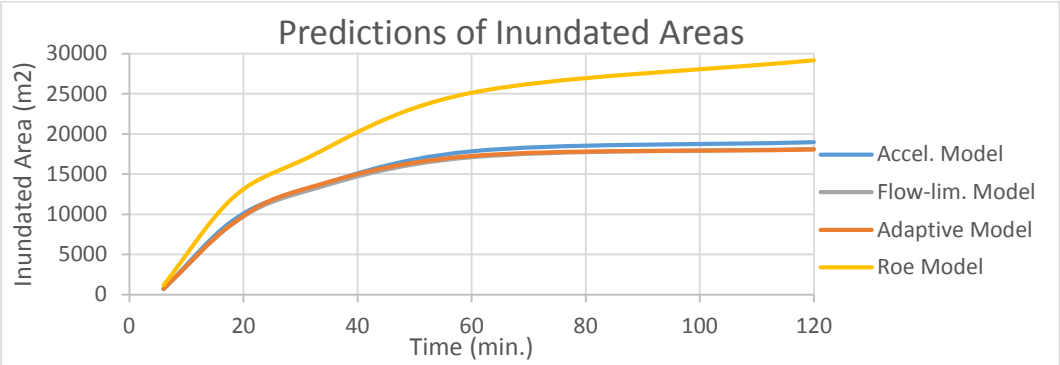


**Figure 3-20** Prediction of Flood Inundation Areas through simulation time of 4 hydraulic solvers

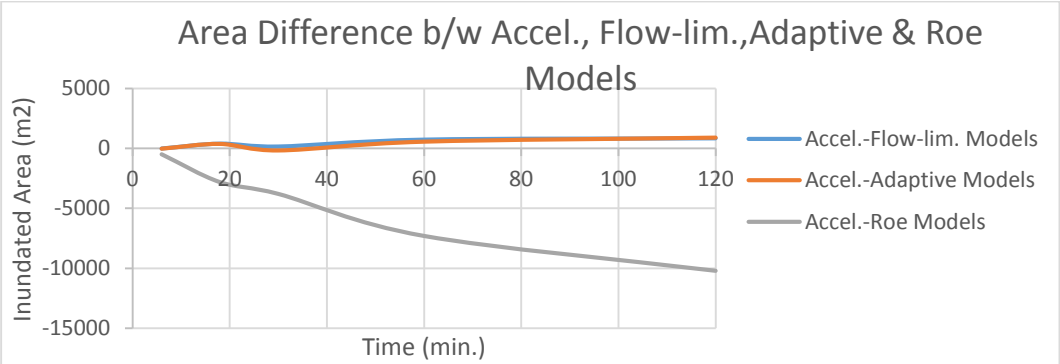


**Figure 3-21** Numerical difference of Flood Inundation Areas through simulation time of 4 hydraulic solvers

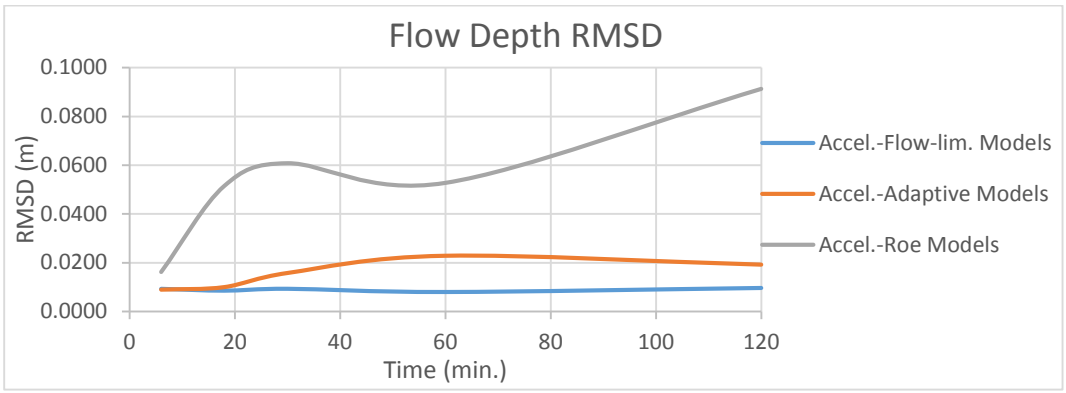


(a)

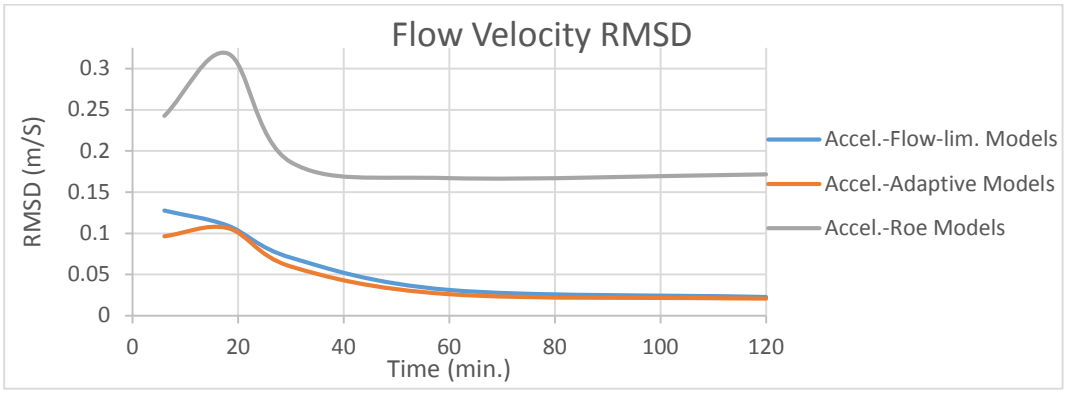


(b)

**Figure 3-22** RMSD of (a) Flow Depths and (b) Velocities through simulation time of 4 hydraulic solvers

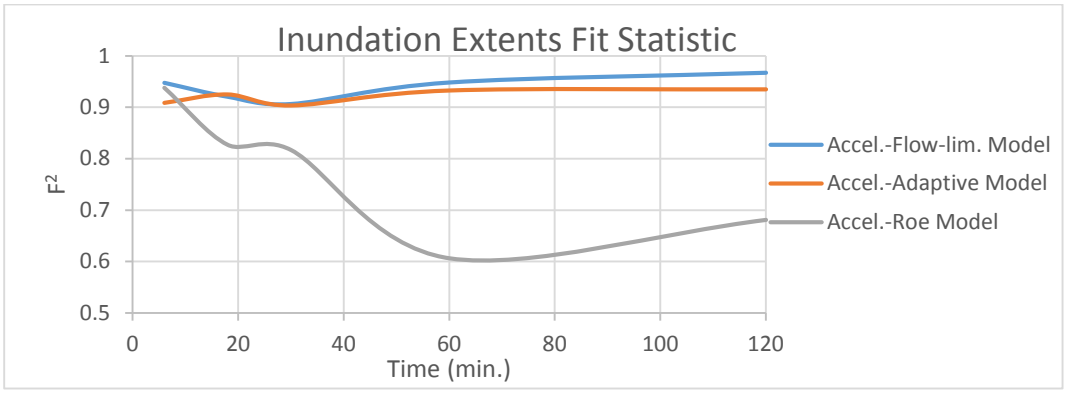


**Figure 3-23** Fit Statistic for Inundation extents through simulation time of 4 hydraulic solvers

Finally, it is necessary to discuss computational efficiency of all solvers examined in this part of study. Table 3-2 shows the simulation run times for the models. Decreasing time step naturally leads to an increase in number of total time steps as simulation progresses affecting computational times (Table 3-3). For Flow-limited solver, time step was chosen manually to improve accuracy of the model. In case of Adaptive scheme, time step depends on quadratic scale of grid resolution as well as small water surface slopes, possibly leading to infinitesimal time step at each iteration. Meanwhile, both Acceleration and Roe solvers depend on CFL condition which assures numerical stability and provides stable time step. To conclude, one may expect increase in computational time with more complex numerical schemes representing shallow water equations. However, in this study the least complex models, namely Flow-limited and Adaptive solvers, performed very poorly leading to a conclusion that it is almost impossible to conduct simulations at this resolution for these models. Instead, Acceleration and Roe solvers provide a good alternative for performing such studies in terms of computational time.

**Table 3-2** Simulation Run times

| Acceleration Model (min) | Flow-limited Model (min) | Adaptive Model (min) | Roe Model (min) |
|---|---|---|---|
| 3.70 | 23.00 | 4511.22 | 4.68 |

All simulations were run using workstation Xeon 2x X5650-2.67 GHz. One of the key model assumptions of Acceleration solver is that the flow is assumed to be gradually varied. In this study, despite the fact that Manning's roughness coefficient is relatively high (n=0.035) compared to surface friction used in urban flood studies such as n=0.013 (asphalt), due to reasonably smooth topographical features of DEM, the Froude number in all time intervals of simulations for Acceleration model

(and consequently both of the diffusive solvers) was predominantly smaller than Fr < 1 within the domain. This means that primarily subcritical flow is observed during simulation which verifies that minimal errors are expected due to model assumptions (de Almeida and Bates, 2013).

**Table 3-3** Number of time steps at each interval

| Time (min) | Acceleration Model (no.) | Flow-limited Model (no.) | Adaptive Model (no.) | Roe Model (no.) |
|---|---|---|---|---|
| 0 | 1 | 1 | 1 | 1 |
| 6 | 739 | 36,001 | 204,464 | 1,164 |
| 12 | 1,726 | 72,001 | 728,408 | 2,895 |
| 18 | 3,396 | 108,001 | 4,278,785 | 4,803 |
| 24 | 5,482 | 144,001 | 11,200,839 | 7,041 |
| 30 | 7,765 | 180,001 | 20,333,953 | 9,485 |
| 36 | 10,131 | 216,000 | 30,416,529 | 12,014 |
| 42 | 12,526 | 252,000 | 40,801,389 | 14,559 |
| 48 | 14,932 | 288,000 | 51,299,918 | 17,109 |
| 54 | 17,344 | 324,000 | 61,858,780 | 19,662 |
| 60 | 19,759 | 360,000 | 72,455,700 | 22,217 |
| 66 | 22,176 | 396,000 | 83,078,554 | 24,772 |
| 72 | 24,595 | 432,000 | 93,720,138 | 27,328 |
| 78 | 27,015 | 468,000 | 104,375,793 | 29,885 |
| 84 | 29,436 | 504,000 | 115,042,352 | 32,442 |
| 90 | 31,858 | 540,000 | 125,717,531 | 34,999 |
| 96 | 34,280 | 576,000 | 136,399,677 | 37,556 |
| 102 | 36,702 | 612,000 | 147,087,569 | 40,113 |
| 108 | 39,125 | 648,000 | 157,780,309 | 42,671 |
| 114 | 41,549 | 684,000 | 168,477,194 | 45,229 |
| 120 | 43,972 | 720,000 | 179,177,657 | 47,787 |

# CHAPTER 4

# EVALUATION OF LISFLOOD-FP SIMPLIFIED INERTIAL SOLVER AND MIKE 21 MODEL

## 4.1 General Information

In this part of the thesis study, a comparative test of an urban flood modeling was performed to evaluate Acceleration solver within Lisflood-FP model and Mike 21 hydrodynamic model to determine whether and/or to what extent numerical methodology of shallow water equations might affect overall performance of simulation outputs such as flow inundation, flow depth and velocity gradients. The main difference between the two models is that, as it was described earlier, Lisflood-FP does not include convective acceleration terms whereas Mike 21 solves complete two-dimensional shallow water equations conserving both mass and momentum.

## 4.2 Model Simulation Setup

The same DEM in ASCII file format that was presented in Figure 1-3 was used in this analysis.

Due to the fact that sensitivity analysis was to be performed in this part of the study, a 30 min duration hypothetical hydrograph was created to simulate inflow boundary conditions of a flood event (Figure 3-2). A point source that represents inflow boundary condition and four control points can be seen in Figure 4-1 (Buildings are represented by white polygons).

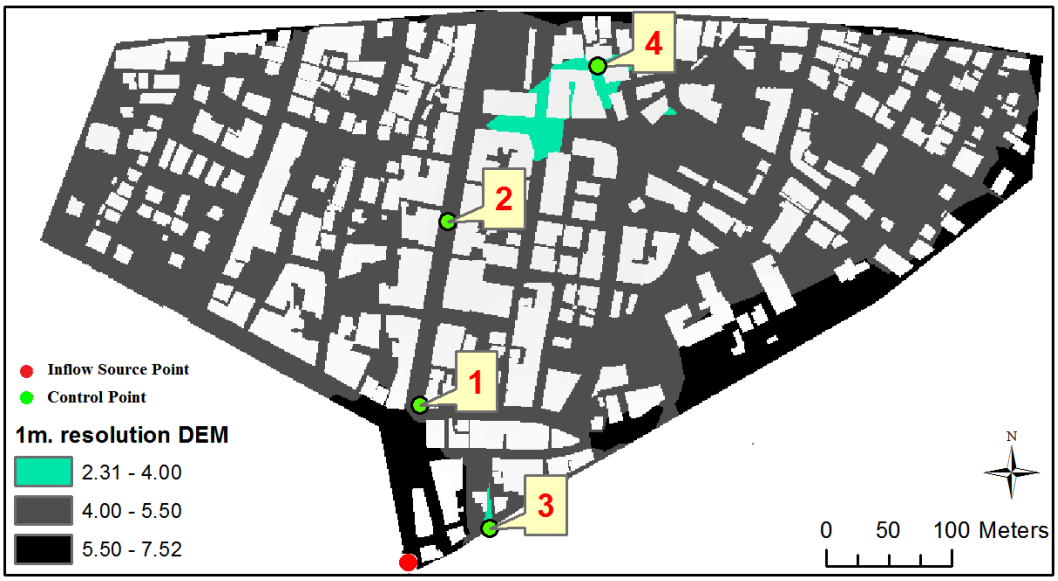


**Figure 4-1** Inflow and Control source points

Uniform Manning's roughness coefficient of n=0.035 was used in both of the models representing cumulative roughness of urbanized area surface friction. Even though it may be argued that this value of n may be higher than the usual roughness used for urban flood studies, n=0.035 was chosen for the sole purpose of sensitivity analysis of two flood modeling programs.

The duration for both simulations was set for two hours with 30 min inflow of water to the domain and 90 min time for water to settle down reaching near steady state. A standard depth threshold value of 1 mm was taken for Lisflood-FP flood model but since 2 cm depth threshold was used in Mike 21 model, a common value of 2 cm was implemented during comparison of inundation areas among these two model outputs.

## 4.3 Comparison of Mike 21 and Lisflood-FP simulation results

The results of Lisflood-FP and Mike 21 simulations were compared in terms of their respective flow inundation extents, flow depths and flow velocities. Figure 4-2 to Figure 4-6 show propagation of flood within the domain at time t=12, 18, 36, 60 and 120 minutes. At t=0 min, the map area is empty and water has just started to fill the domain at the southern corner of DEM. In the beginning of the simulation at t=12 min, the flow propagates in the northern direction while some portion of the flow heads towards east due to a depression in DEM. At time interval t=18 min, the main body of water is divided into 2 parts - one flows down on a main street in the northern direction while some portion of it floods adjacent street on the right. At the same time, the rest of the incoming water has reached first ponding area just a couple blocks away to the right of the inflow source point which is quite intuitive since a depression in that area can be seen in Figure 4-1. As simulation time progresses, at t=36 min the main body of water continues propagating down the main street toward lower elevations. At time interval t=60 min, the main body of water reaches second ponding area in the northern part of the map while flow in the first ponding area is settled and no significant movement is observed at the latter time intervals. In the final time interval t=120 min, flow movement across the domain is not observed anymore and water has reached near steady state.


(a)


(b)

**Figure 4-2** Inundation Extents of (a) Lisflood-FP and (b) Mike 21 models at t=12 min.


(a)


(b)

**Figure 4-3** Inundation Extents of (a) Lisflood-FP and (b) Mike 21 models at t=18 min.


(a)


(b)

**Figure 4-4** Inundation Extents of (a) Lisflood-FP and (b) Mike 21 models at t=36 min.


(a)


(b)

**Figure 4-5** Inundation Extents of (a) Lisflood-FP and (b) Mike 21 models at t=60 min.


(a)


(b)

**Figure 4-6** Inundation Extents of (a) Lisflood-FP and (b) Mike 21 models at t=120 min.

A few sections within three segments were taken to study the behavior of flow depths of Lisflood-FP and Mike 21 models at time interval t=120 min depending on elevations within DEM (Figure 4-7). The first segment includes one longitudinal and three transverse sections in the main street (Figure 4-8). The second (two sections) and third segments (one section) are located in the depression zones of the DEM (Figure 4-9 and Figure 4-10). Consequently, profiles of sections are shown in Figure 4-11, Figure 4-12 and Figure 4-13.

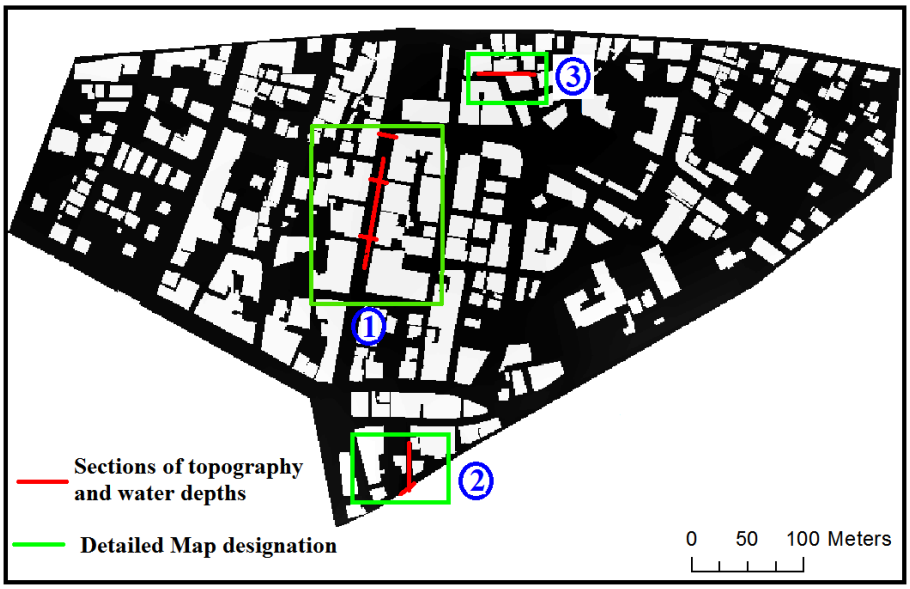


**Figure 4-7** Location of the three segments on the DEM

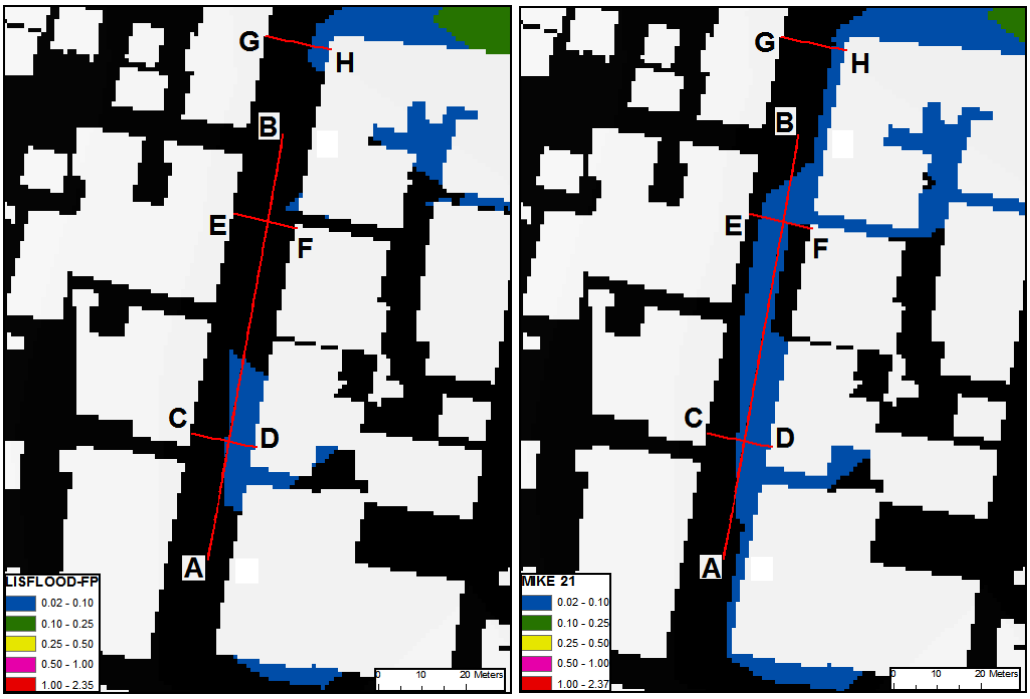


(a) (b)

**Figure 4-8** Sections from A-B to G-H taken in the first segment of (a) Lisflood and (b) Mike 21 models

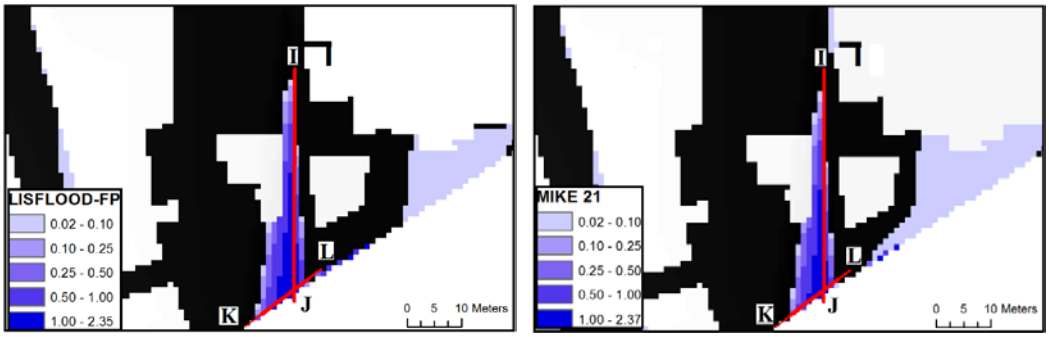


(a) (b)

**Figure 4-9** Sections I-J and K-L taken in the second segment of (a) Lisflood and (b) Mike 21 models

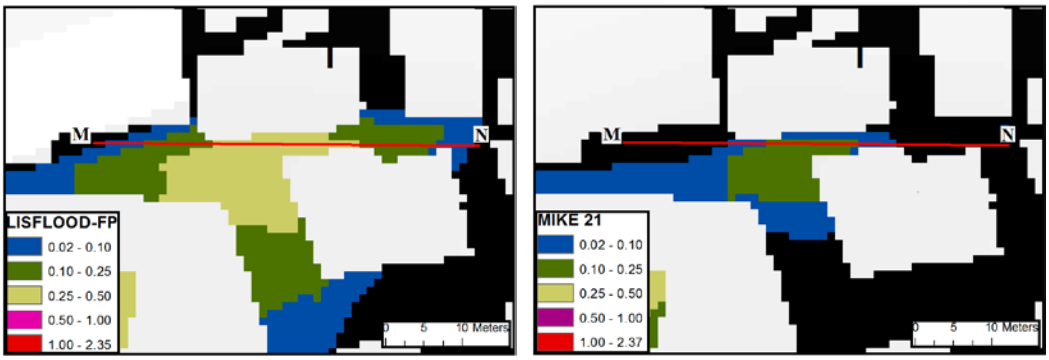


(a) (b)

**Figure 4-10** Section M-N taken in the third segment of (a) Lisflood and (b) Mike 21 models

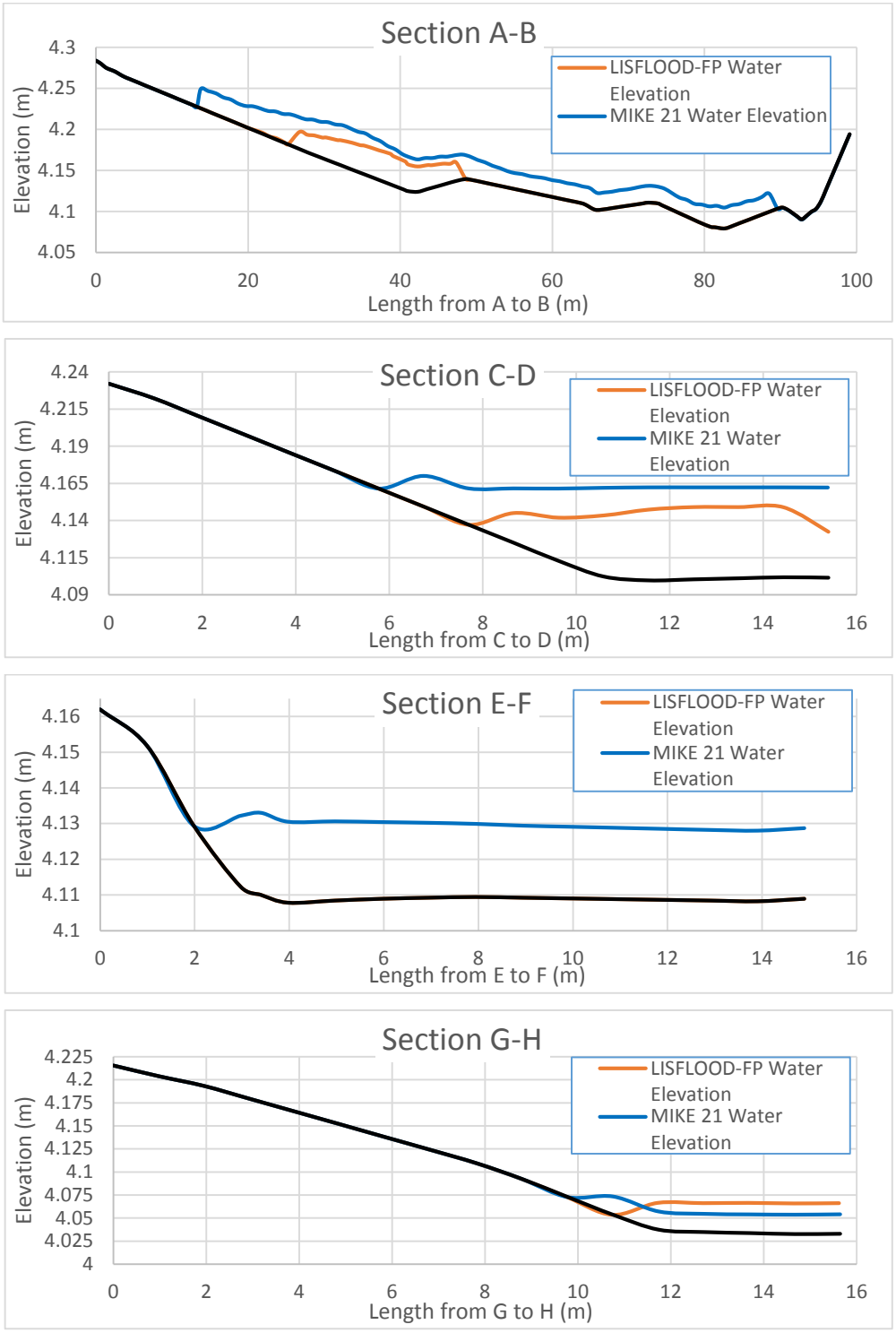


**Figure 4-11** Water Elevations Profiles of Sections (a) A-B, (b) C-D, (c) E-F and (d) G-H at t=120 min.

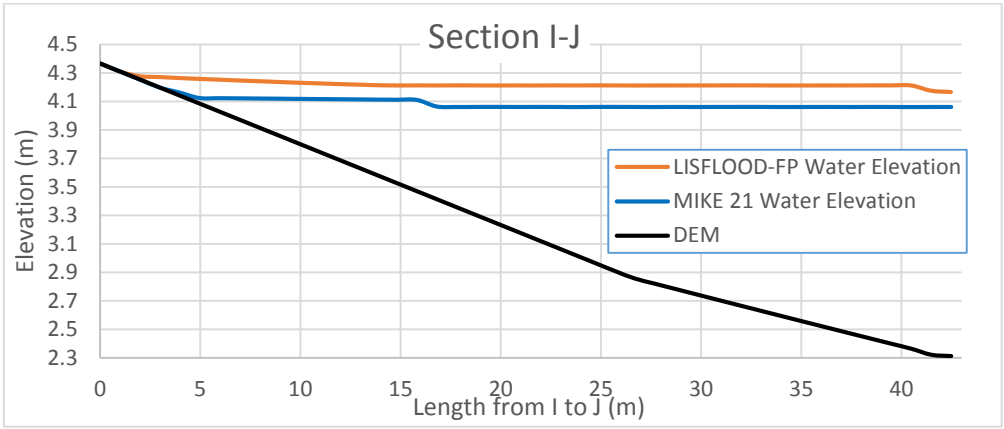


(a)

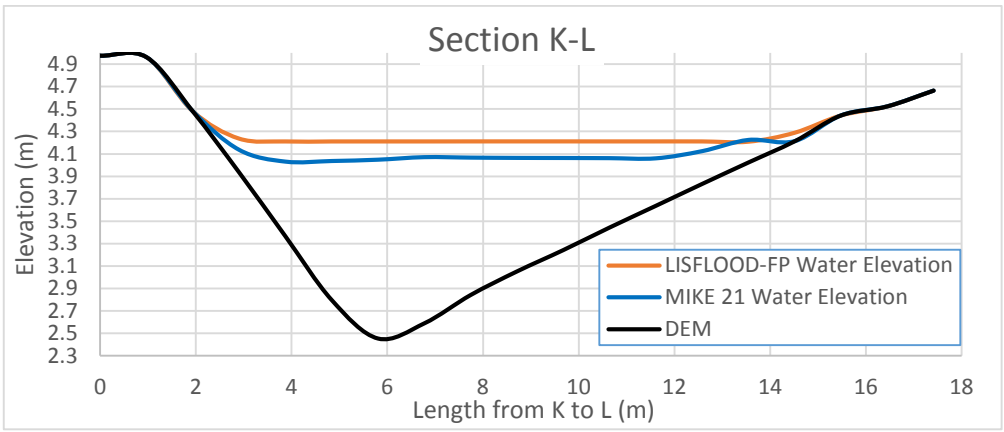


(b)

**Figure 4-12** Water Elevations Profiles of Sections (a) I-J and (b) K-L t=120 min.

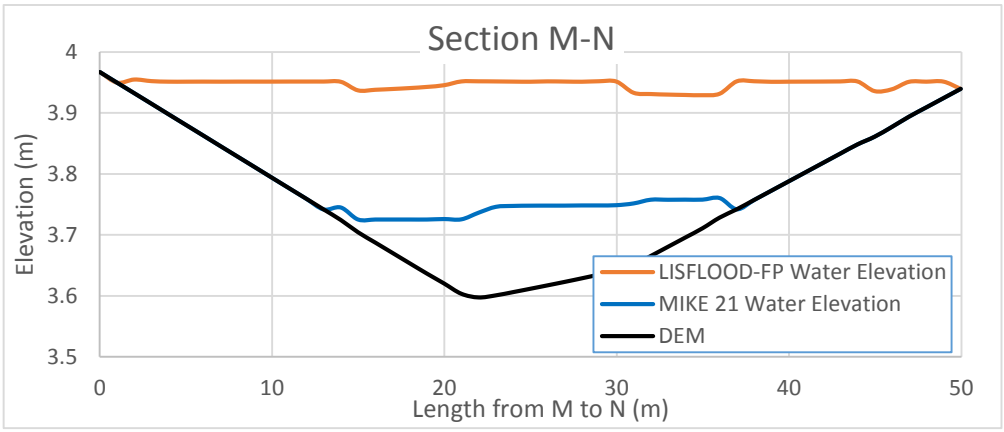


**Figure 4-13** Water Elevations Profiles of Section M-N at t=120 min.

Comparing results of two flood models in terms of inundation extents, noticeable differences can be observed starting from the time interval t=36 min. It can be seen that main body of water propagates faster in Lisflood-FP, however Mike 21 inundates higher area. In the same way, at t=90 min the one can see that higher flow depths are concentrated in second ponding area as the segment 3 in for Lisflood-FP. In the last time interval t=120 min, significant variation can be observed between two models - Lisflood-FP having higher depths in the second ponding area whereas Mike 21 has main water body staying intact along the main street. In particular, it is interesting to see that a disconnected water body right in the middle of the main street for Lisflood-FP model whereas in Mike 21, water is hydraulically connected and generally occupies higher depths displayed in Figure 4-8.

To get a clearer picture of variations between these two models, Figure 4-14 and Figure 4-15 show graphical and numerical difference of inundation extents and flow depths at time t=120 min (Figure 4-15 shows numerical subtraction of flow depths of Lisflood-FP and Mike 21 models). There are basically two significant differences that can be distinguished, namely two areas of ponding designated as segments 2 and 3 in Figure 4-7.

For the first ponding area, two sections were taken to study this region in more detail (Figure 4-9). It can be seen that considerably high flow depths are located in this area. This is attributed to the noticeable depression in DEM (Figure 4-1) as well as the fact that outflow boundaries for both models are closed and naturally water bounces back into that area. Consequently, Lisflood-FP simulates higher flow depths within that region averaging 10 to 15 cm (Figure 4-12). This may be attributed to higher variation of slope gradients (>10%) within DEM for that area as can be seen in Figure 4-16 which may result in local numerical instabilities of hydraulic models *(*Ozdemir et al., 2013).


**Figure 4-14** Graphical representation of differences between Lisflood-FP and Mike 21 models in terms of inundation extents at t=120 min.

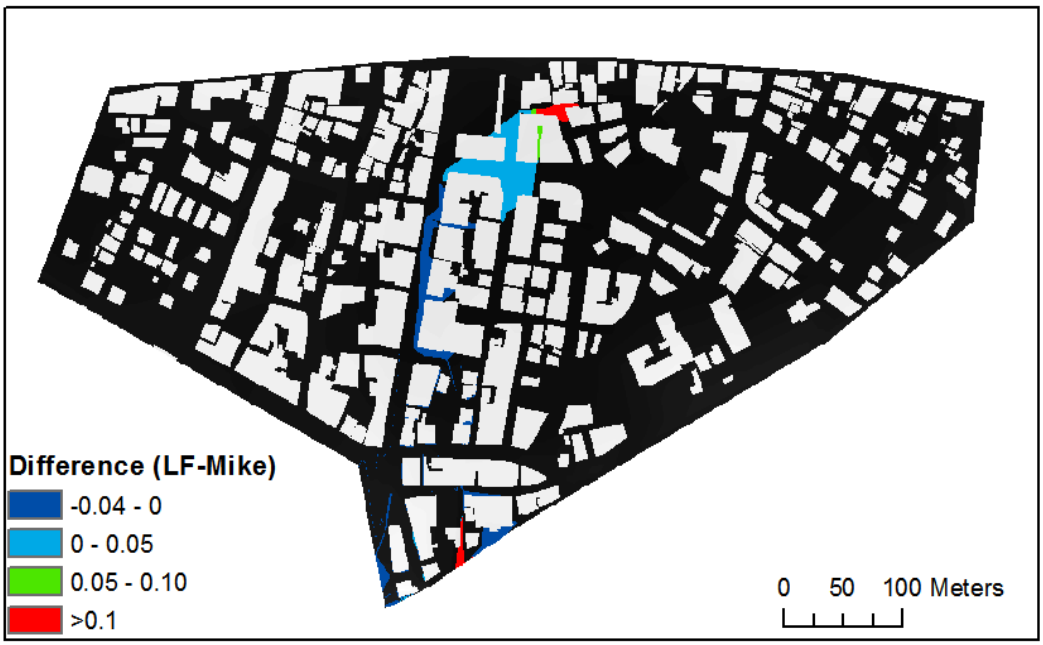


**Figure 4-15** Numerical subtraction of flow depths of Lisflood-FP and Mike 21 models at t=120 min.

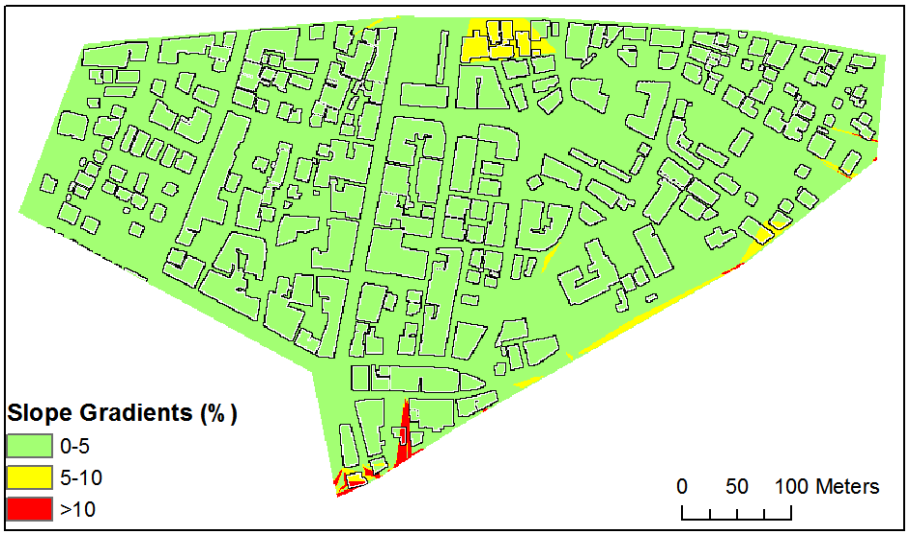


**Figure 4-16** Slope gradient variation within DEM (%)

Comparing depths in the second ponding area where a section shown in Figure 4-10 was taken, Lisflood-FP distributes higher amount of water in this region resulting in a difference of flow depths reaching up to 20 cm (Figure 4-13). Meanwhile, Mike 21 distributes water more evenly within the main body of water without forming hydraulic disconnection in the middle of main street. It was reported that in gradually varied flows, inertial terms in Saint-Venant equations decrease fluxes between cells (Bates et al., 2010). Therefore, it may be possible that such differences between two models are because of convective acceleration term within shallow water equations of Mike 21 does not allow water to propagate more rapidly as Lisflood-FP (missing that term) does. As a consequence, due to lower inertial effects there is a higher dependence of Lisflood-FP on elevation difference within DEM as both ponding areas display higher depths in this model.

To further analyze performance of two models, numerical comparison of flow depths and velocities was performed at four predetermined control points shown in Figure 4-1. Point 1 symbolizes variation of flow during simulation time nearby

inflow source point at the beginning of a main street where elevations are high. Point 2 is located further down the main street and it is possible to trace behavior of flow as it propagates forward. Points 3 and 4 were chosen because they represent areas of ponding.

Flow depth output results through simulation time at four control points can be seen in Figure 4-17. At points 1 and 2, hydraulic models show similarities both in depth values, with maximum differences not exceeding 10%, and arrival times. It takes 12 min for both models to reach point 1. Also, it should be noted that both models reach point 2 at 24 min. Meanwhile, as mentioned before, points 3 and 4 show that Lisflood-FP predicts higher flow depths in the areas of ponding with values reaching up to 15 and 20 cm, respectively. It is worth mentioning that flow in Mike 21 reaches point 3 faster at 12 min while Lisflood-FP - at 18 min. Conversely, water in Lisflood-FP arrives point 4 earlier at 54 min whereas in Mike 21 - at 60 min. Differences in velocities outputs were also studied as shown in Figure 4-18.

As in the case of flow depths, points 1 and 2 show almost identical behavior in terms of velocities (peak velocities not exceeding ~10%) and time to peak. As for point 3, there is a considerable difference in peak velocities. As mentioned before, this may be due to inability of Lisflood-FP to handle slope gradients higher than 10%. It should be noted that oscillations in velocities, although very small, occur on the falling limb of Mike 21 model. This may be explained by the occurrence of grid scale oscillations arising from numerical treatment of advective acceleration term (Hunter et al., 2008). It is interesting to see that although there are some variations within flow depths, in terms of velocities both models display similar results at control point 4.

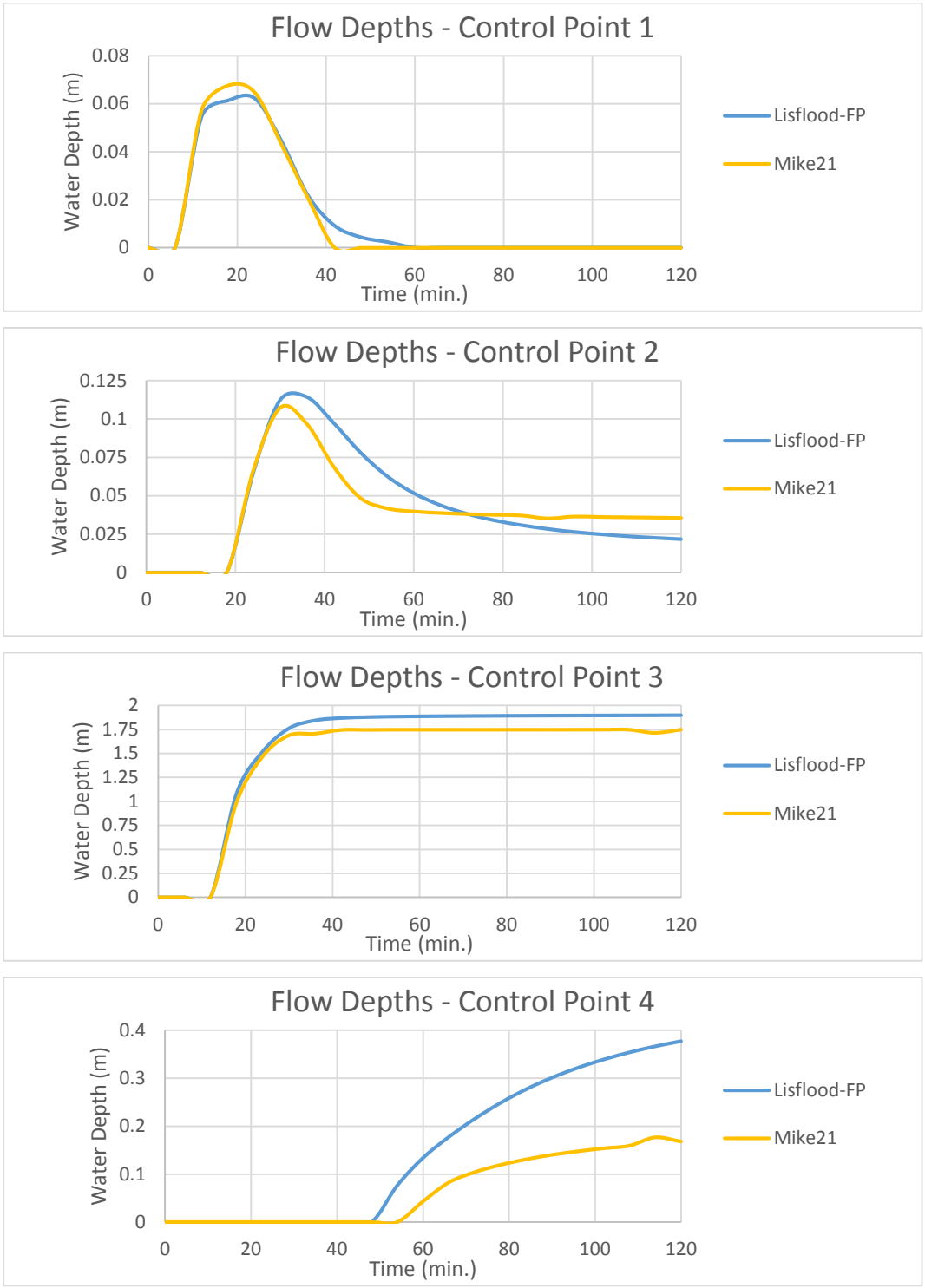


**Figure 4-17** Flow Depth Outputs at 4 control points of Lisflood-FP and Mike 21 models through simulation time

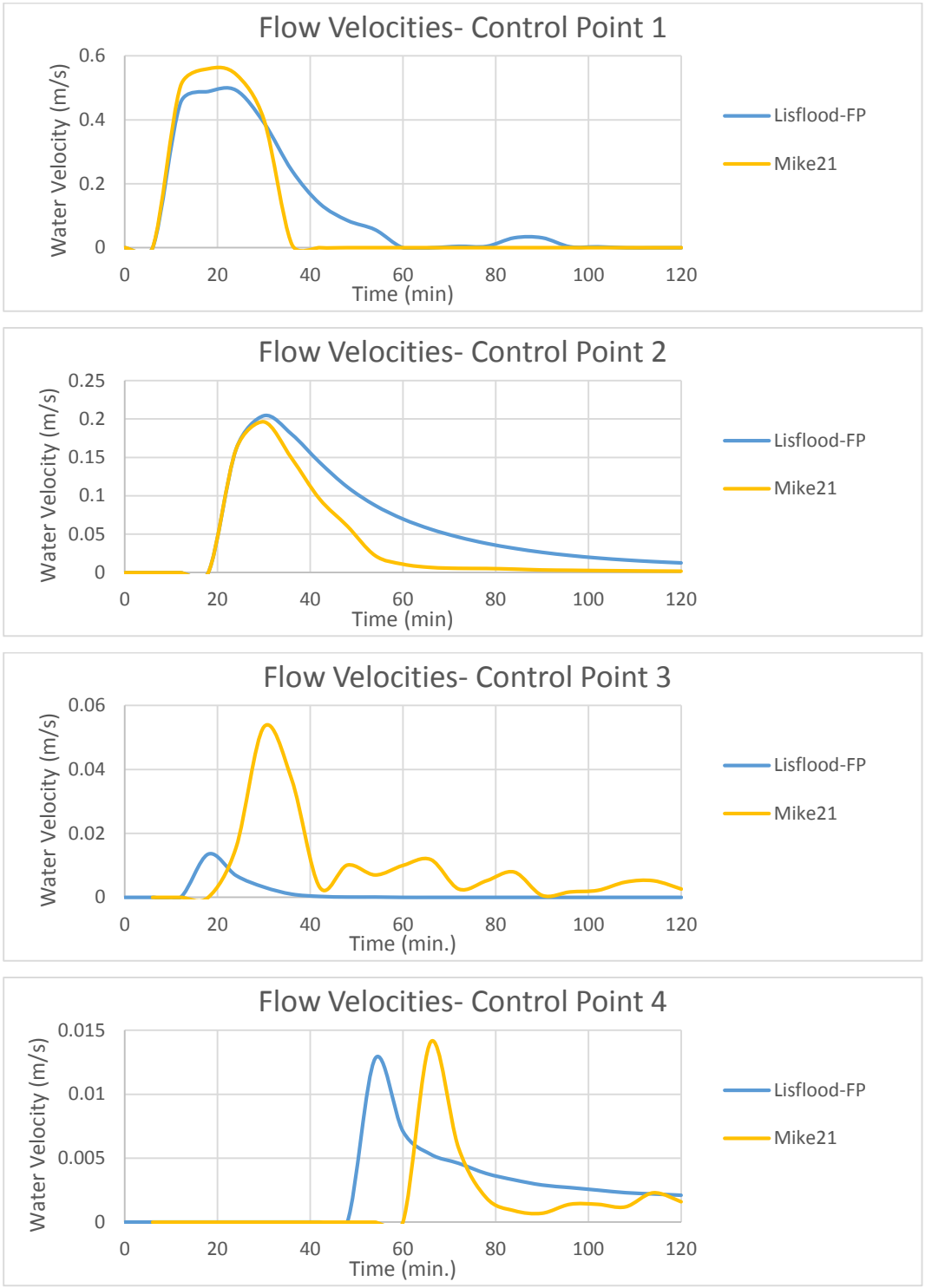


**Figure 4-18** Flow Velocity Outputs at 4 control points of Lisflood-FP and Mike 21 models through simulation time

The variation of two models in terms of predicted inundated areas was also evaluated numerically as shown in Figure 4-19 and Figure 4-20 (area in Mike 21 model was subtracted from Lisflood-FP). The difference reaches its peak within 40 min of simulation but gradually decreases afterwards.

The performance of the two models was also compared in terms of Root Mean Square Difference of flow depths and velocities considering simplified inertial model as a benchmark. In Figure 4-21 and Figure 4-22, the one can be see that that the maximum RMSD of depths and velocities does not exceed 4 cm and 0.12 m/s, respectively showing good correlation between two numerical schemes.

To assure model stability, the Froude number of Lisflood-FP model was checked and it was determined that subcritical flows were dominant in all time intervals of simulations minimizing possible numerical instabilities of the model. In terms of computational time, it was not possible to directly compare two models since the simulations were performed on different workstations. However, to give a general idea it took 3.73 min for Lisflood-FP to finish simulation using Xeon 2x X5650-2.67 GHz while Mike 21 completed simulation in 15.15 min using more powerful Xeon 2x E5-2665 CPU hardware. Consequently, it is evidently clear that numerical formulation of simplified momentum terms of Lisflood-FP significantly reduces computational cost.

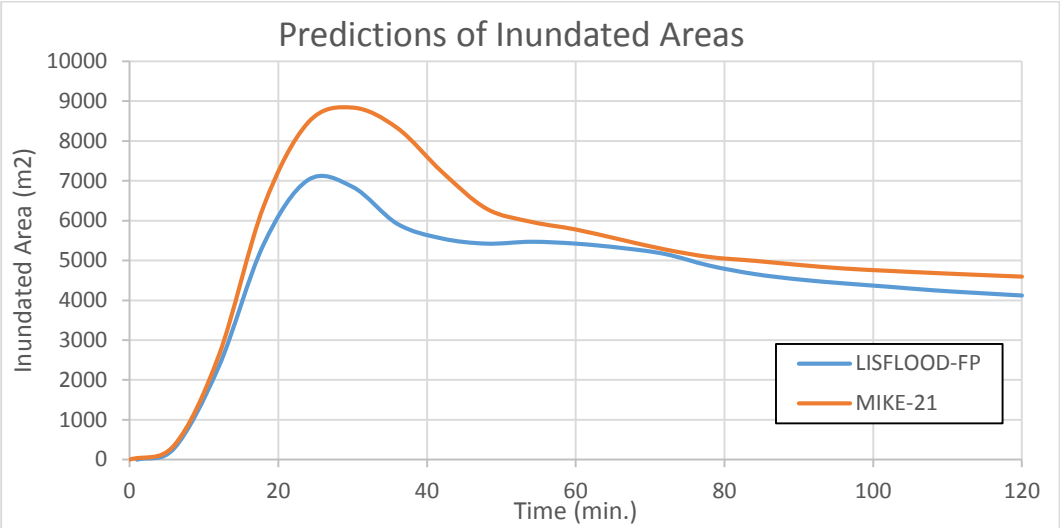


**Figure 4-19** Prediction of Flood Inundation Areas of Lisflood-FP and Mike 21 models through simulation time

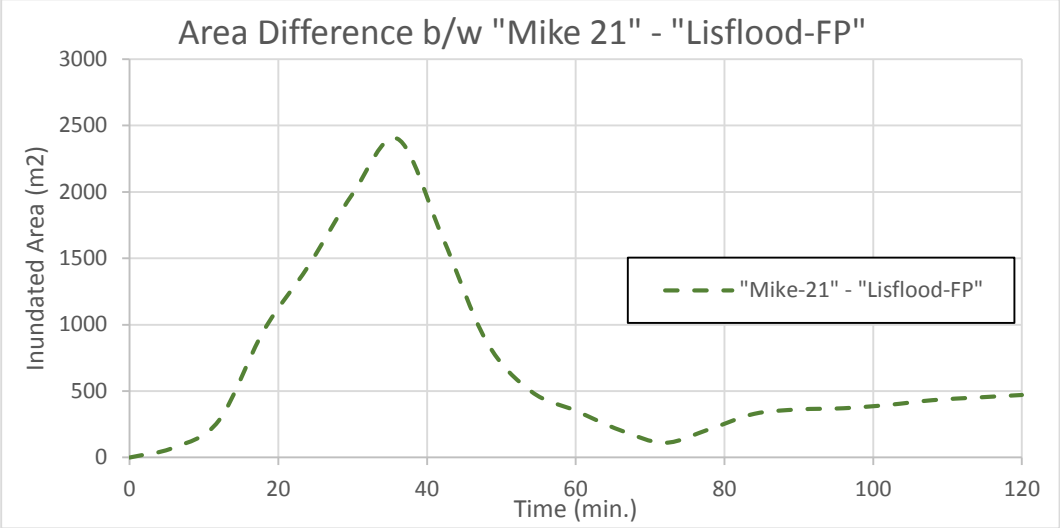


**Figure 4-20** Numerical difference of Flood Inundation Areas of Lisflood-FP and Mike 21 models through simulation time

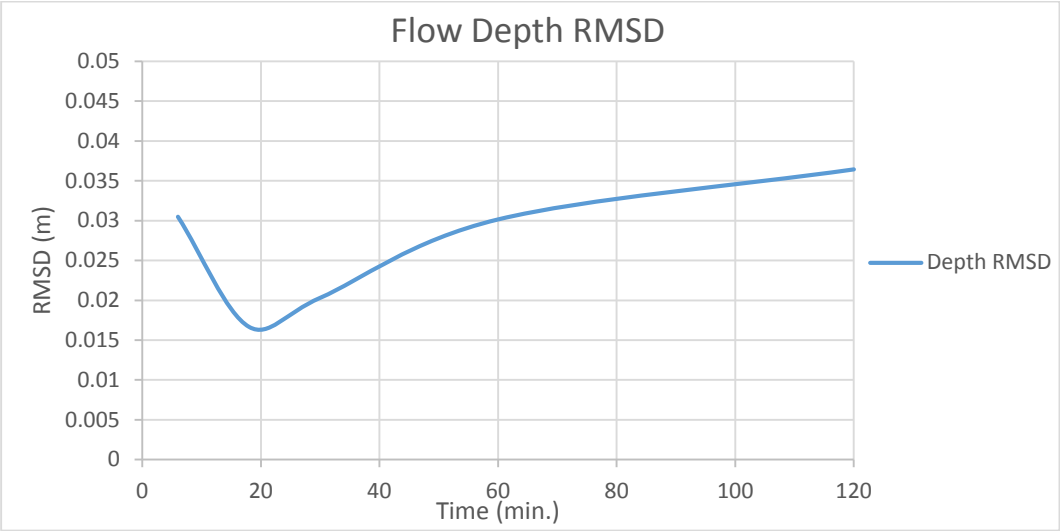


**Figure 4-21** RMSD of Flow Depths between Lisflood-FP and Mike 21 models through simulation time

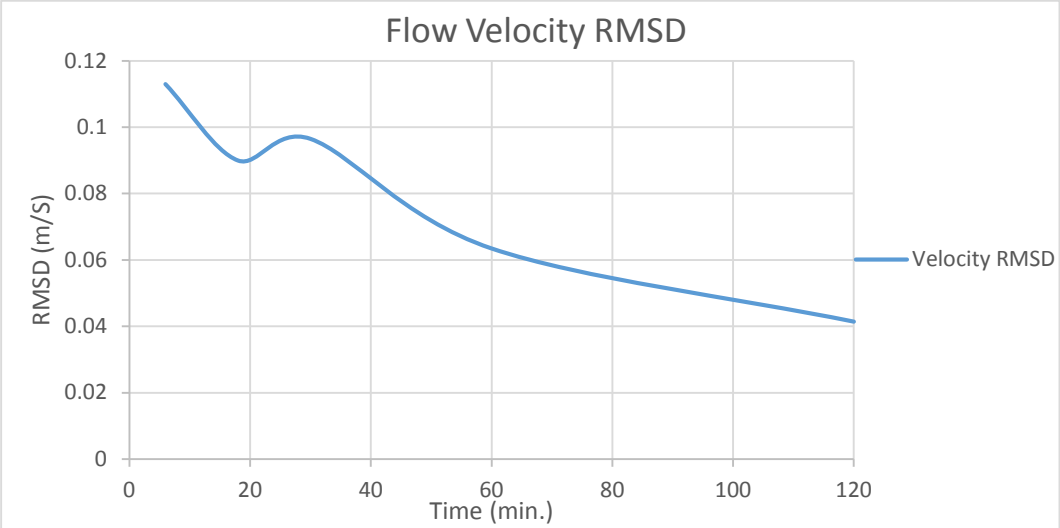


**Figure 4-22** RMSD of Flow Velocities between Lisflood-FP and Mike 21 models through simulation time

# CHAPTER 5

## EVALUATION OF SCALE AND ROUGHNESS EFFECTS USING LISFLOOD-FP SIMPLIFIED INERTIAL SOLVER

This part of the thesis performs the analysis of urban flood modeling using the inertial acceleration module of the Lisflood-FP software comparing the results of varying resolution and roughness of DEM. To evaluate the differences of model outputs in terms of resolution, 25 cm, 50 cm, and 1 m Digital Elevation Models (DEM) with closed boundaries were constructed based on 1 cm terrestrial LIDAR data of highly urbanized area of Terme town, Samsun. Also, flood flow was studied based on the assumption that 4 different roughness conditions may represent dry surface land within the area. To quantitatively compare varying resolution and roughness, output results of flow depths, flow velocities and inundation extents were studied in the following sections.

Previous research in that area (Fewtrell et al., 2011; Sampson et al., 2012; Ozdemir et al., 2013) has indicated that the curved shape of the road and road curbs within the domain are better reproduced at terrestrial LIDAR DEMs at finer scales, thus remarkably affecting results of urban flood simulation. Therefore, since such features are only present in sub 1 meter digital elevation models, the main intension for performing such an analysis was to see how the flow propagation responds to increased DEM resolution and varying roughness conditions using simplified inertial solver of Lisflood-FP.

## 5.1 Model Simulation Setup

A 1 cm Terrestrial LIDAR Raster was obtained for the town center of Terme, Samsun as shown in Figure 5-1 (referred to as Old DEM Boundaries). This raster was then degraded to 10 cm, 50 cm and 1 m resolution DEMs via ArcMap resample method to conduct flood modeling studies. However, a new study area was selected because DEM obtained from LIDAR data has too many artificial depressions which may cause instabilities in hydraulic computations. New area is represented in red in Figure 5-1.

Initially, it was intended to perform analysis of the abovementioned degraded DEMs applying uniform roughness of n=0.013 and the hydrograph previously used that is shown in Figure 3-2. However, it can be seen that there are numerous depressions and altitude differentials that result in slope gradients being higher than %10 in DEMs (Figure 5-2). Section within the three DEMs was taken where depressions are present (Figure 5-3) and plotted on the same graph (Figure 5-4). It should be noted that with decreasing resolution, the regions of abnormal slope gradients decrease as DEMs are degraded to coarser resolutions.

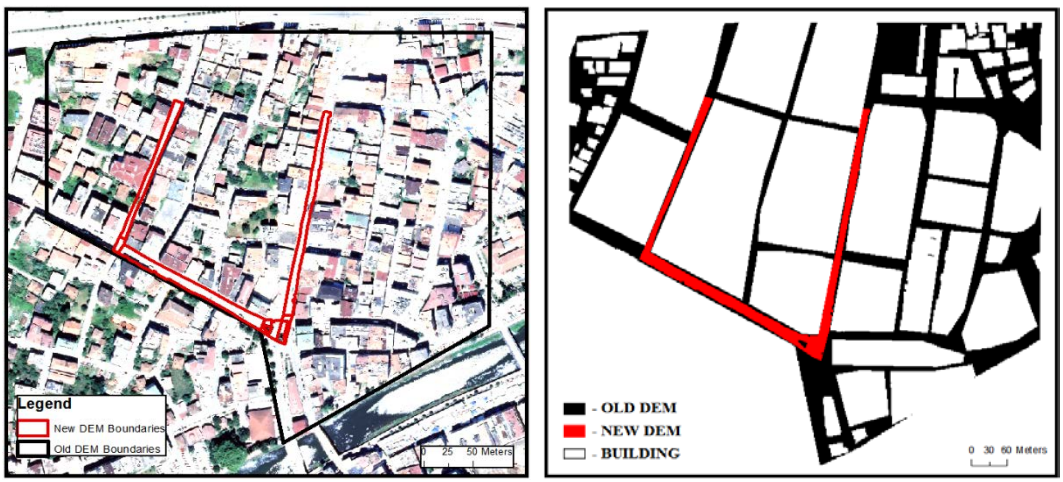


**Figure 5-1** Intended area for simulation studies (Terme, Samsun)

To minimize inaccuracies within the topography, filtering techniques were applied but it was not possible to completely get rid of them without losing vertical accuracy of the entire map. Nonetheless, a series of tests were run to see how the hydraulic model responds to adverse slope gradients and very fine roughness n=0.013. According to Figure 3-2, a total of V=600 $m^3/s$ of water was inserted into the model. The results show that 1 m resolution model at n=0.013 correctly predicts total volume in the domain (Table 5-1). However, due to increase in resolution to 0.5 m


**Figure 5-2** Slope Gradients of the DEMs

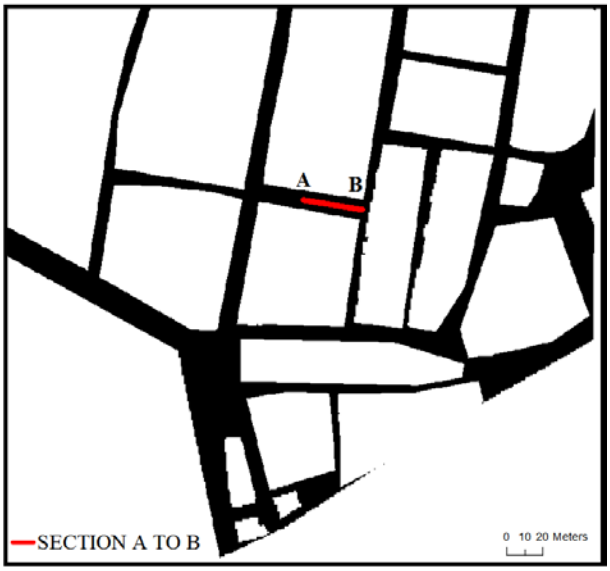


**Figure 5-3** Section taken to show depressions in DEMs

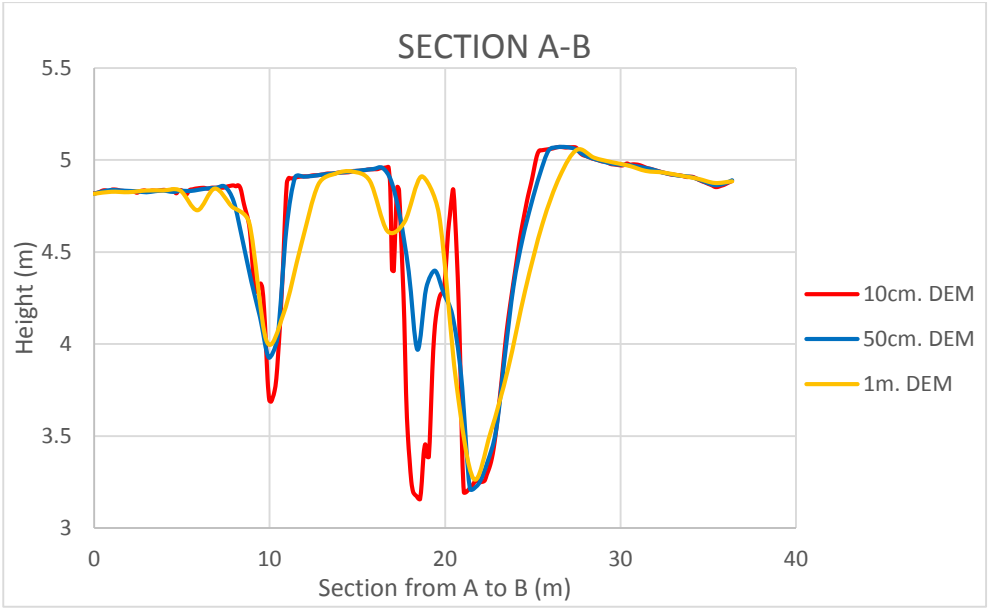


**Figure 5-4** Plot showing depressions in the DEMs

**Table 5-1** Tests simulations that were run using varying resolution and roughness

| Resolution (m) | Roughness coefficient | Volume ($m^3$) |
|---|---|---|
| 1x1 | 0.013 | 600.00 |
| 0.5x0.5 | 0.035 | 600.00 |
| 0.5x0.5 | 0.025 | 600.00 |
| 0.5x0.5 | 0.015 | 628.32 |
| 0.5x0.5 | 0.014 | 769.16 |
| 0.5x0.5 | 0.013 | 1085.6 |

and roughness n=0.013, the mass balance is increased drastically to V=1035.6 $m^3$ which at that point shows instability of the hydraulic model to correctly predict model outputs (10 cm resolution simulation was not run for the same reason). Confirming these findings, it was reported that very high resolution DEMs below 1 m as well as Manning roughness coefficient values below n=0.020 may lead to numerical instabilities in flow models due to high slope gradients (>10%) (Ozdemir et al., 2013). All simulation were run including numerical diffusion ($\theta$=0.8) due to very low roughness conditions. Figure 5-5 shows inundation extent differences of the three models in Table 5-1 where volume of water in the domain is preserved.

It was then decided to find a relatively smooth (without adverse slope gradients exceeding 10%) region in the original DEM to continue comparative study avoiding numerical instability of hydraulic modeling. Such region is shown in Figure 5-1 (referred to as New DEM Boundaries) and Figure 5-6 – it consists of three streets covered in asphalt with uniform slope gradients not exceeding 10%. Since the main goal of this study was to compare the results of varying roughness and scale rather than simulate a real flood event, a hypothetical steady discharge of 0.028 $m^3/s$ (100 $m^3$ of water in total for duration of simulation) was used as an inflow boundary condition with an inflow point displayed in Figure 5-7. Also, uniform Manning roughness n=0.013 representing smooth asphalt was used and simulations were run for one hour.

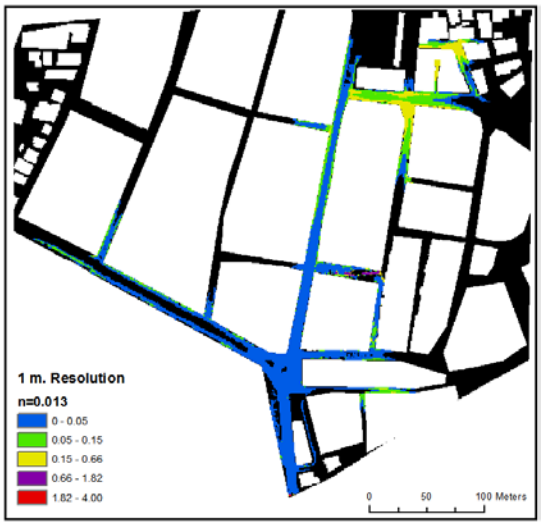


(a)

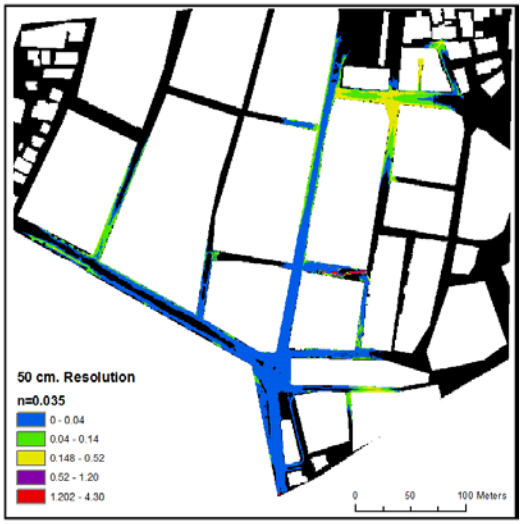


(b)

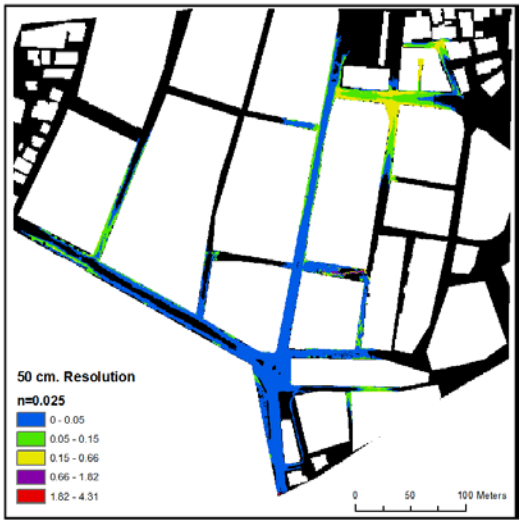


(c)

**Figure 5-5** Inundation Extents of (a) 1 m resolution and n=0.013, (b) 0.5 m resolution and n=0.035, (c) 0.5 m resolution and n=0.025.

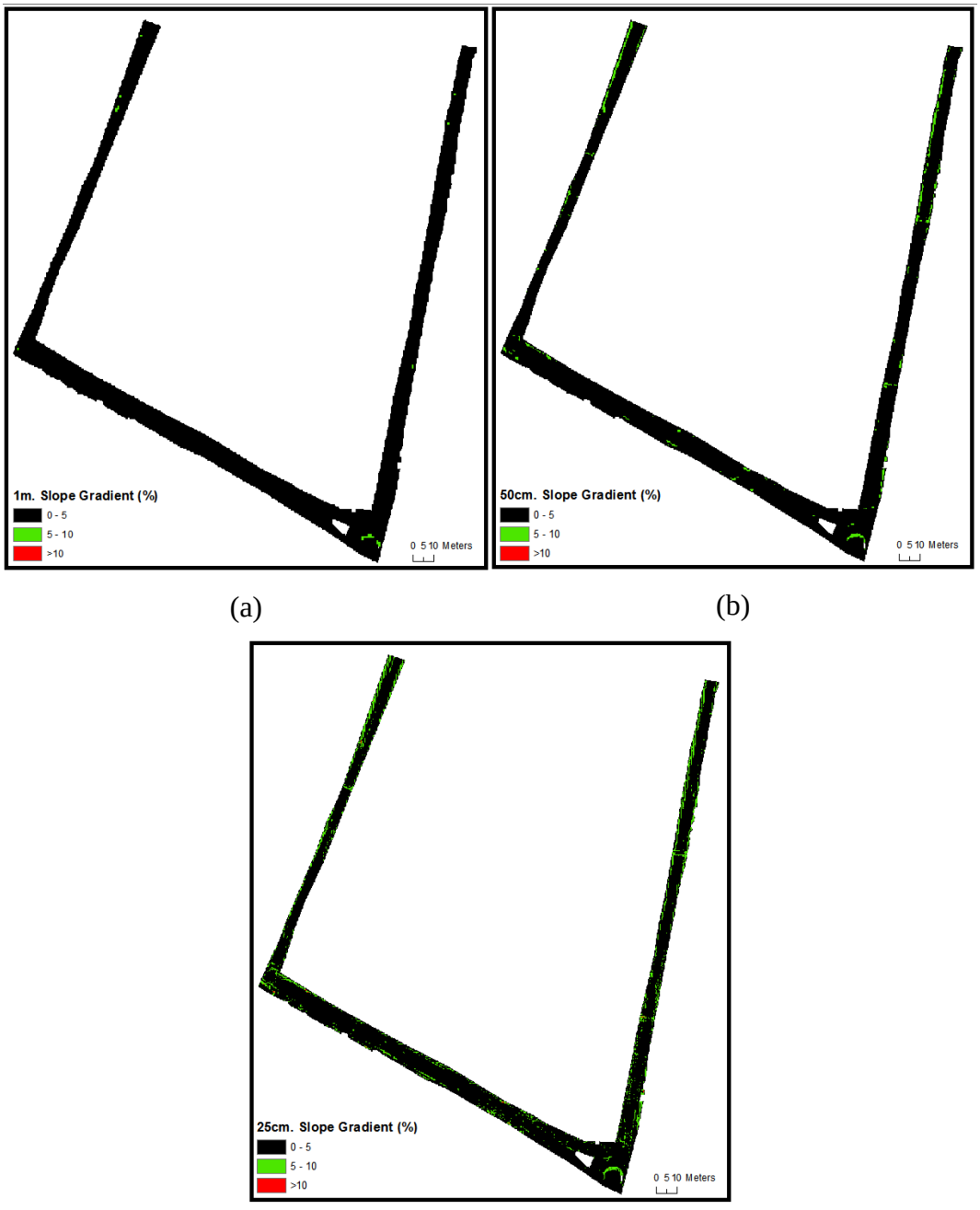


**Figure 5-6** New simulation DEM having (a) 1 m spatial resolution, (b) 50 cm spatial resolution and (c) 25 cm spatial resolution

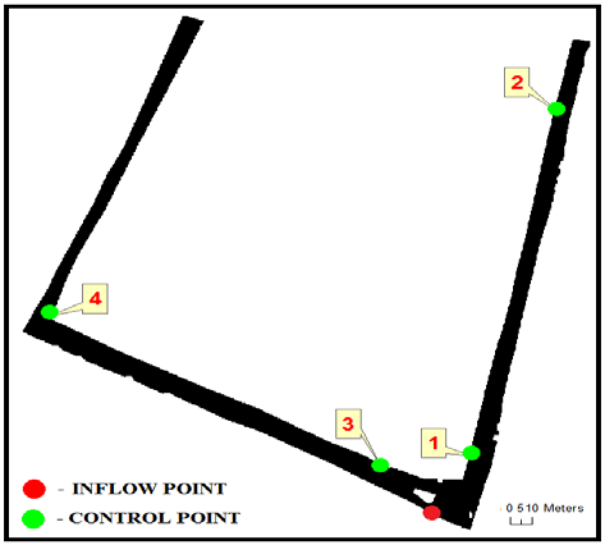


**Figure 5-7** Inflow and Control points of the simulation DEM

To test varying resolution and avoid possible numerical instability, simulations were run on 25 cm, 50 cm and 1 m resolution DEMs. Furthermore, to see how surface roughness affects the flow, 25 cm model was used in simulations that were run applying four different roughness coefficients that were chosen based on Ven Te Chow's table for values of coefficient n (1959) representing smooth asphalt (n=0.013), cemented rubble masonry (n=0.020), earth with no vegetation (n=0.030) and short grass (n=0.035).

## 5.2 Model Comparison of varying resolution and roughness

### 5.2.1 Varying Resolution Study

First of all, results of 25 cm, 50 cm and 1 m resolution DEM models were compared in terms of their respective flow inundation extents, flow depth and velocities as well as statistical measures such as Root Mean Square Difference (RMSD) and Fit Statistic ($F^2$). Figure 5-8 to Figure 5-12 show flow propagation within the domain at time intervals t=6, 18, 30, 48 and 60 minutes.

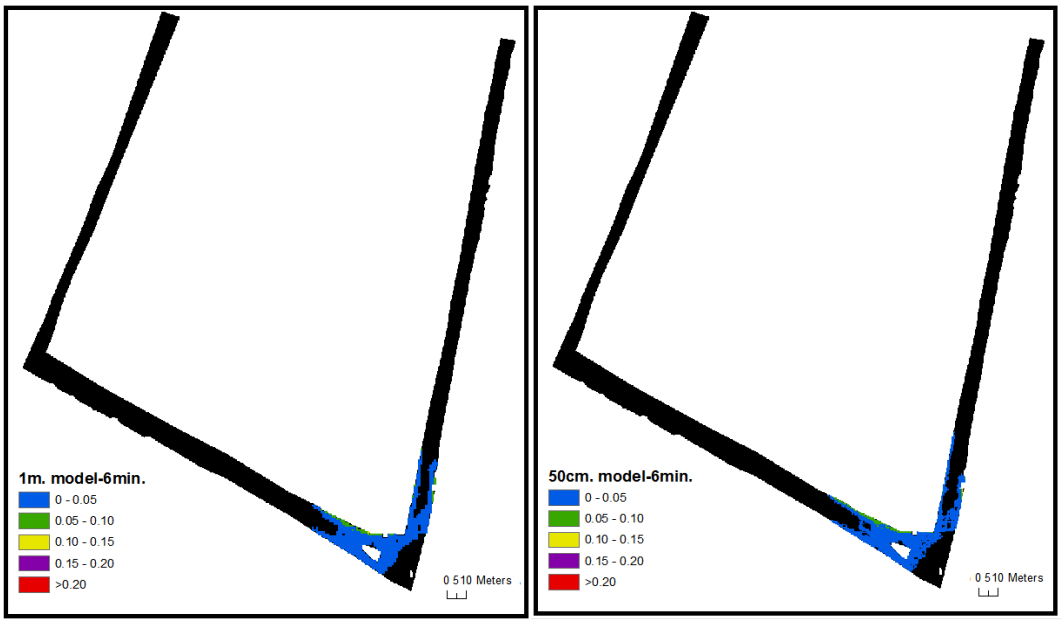


(a) (b)


(c)

**Figure 5-8** Inundation Extents of models having (a) 1 m spatial resolution, (b) 50 cm spatial resolution and (c) 25 cm spatial resolution at t=6 min.

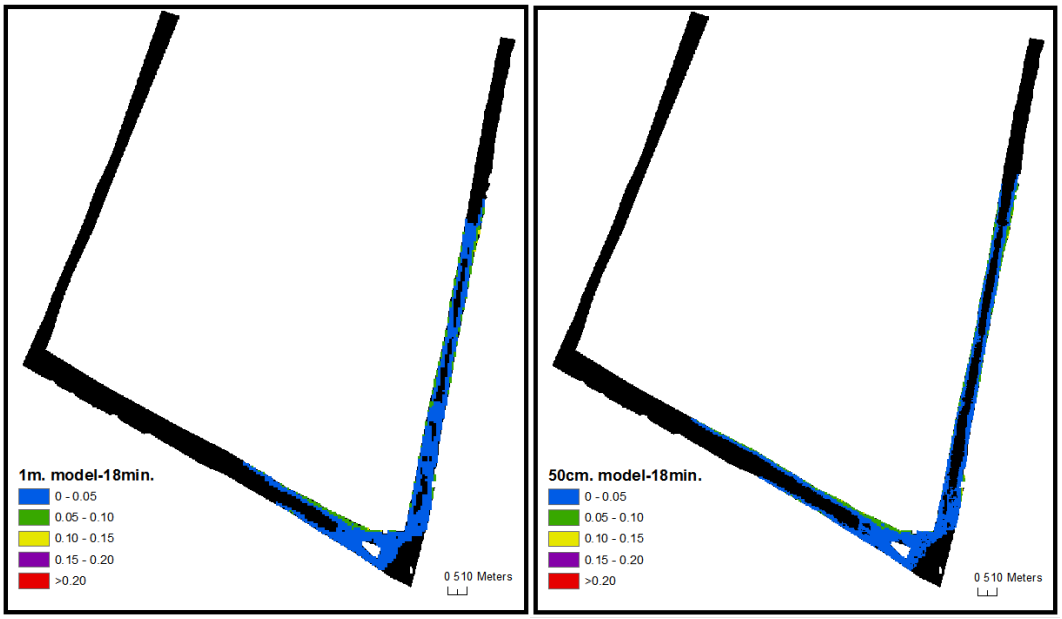


(a) (b)

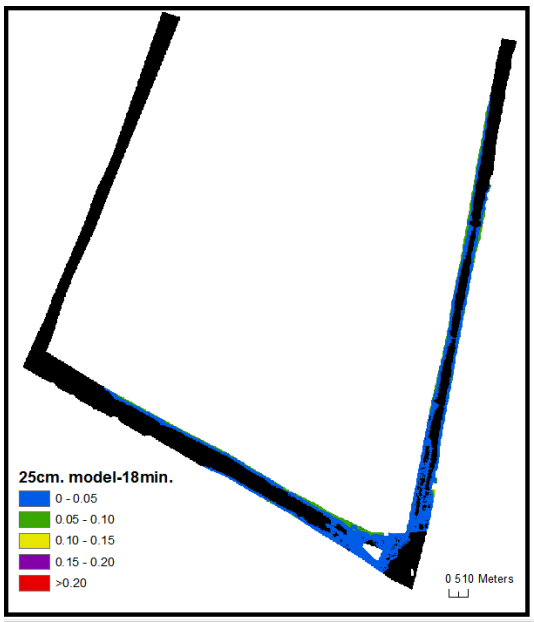


(c)

**Figure 5-9** Inundation Extents of models having (a) 1 m spatial resolution, (b) 50 cm spatial resolution and (c) 25 cm spatial resolution at t=18 min.

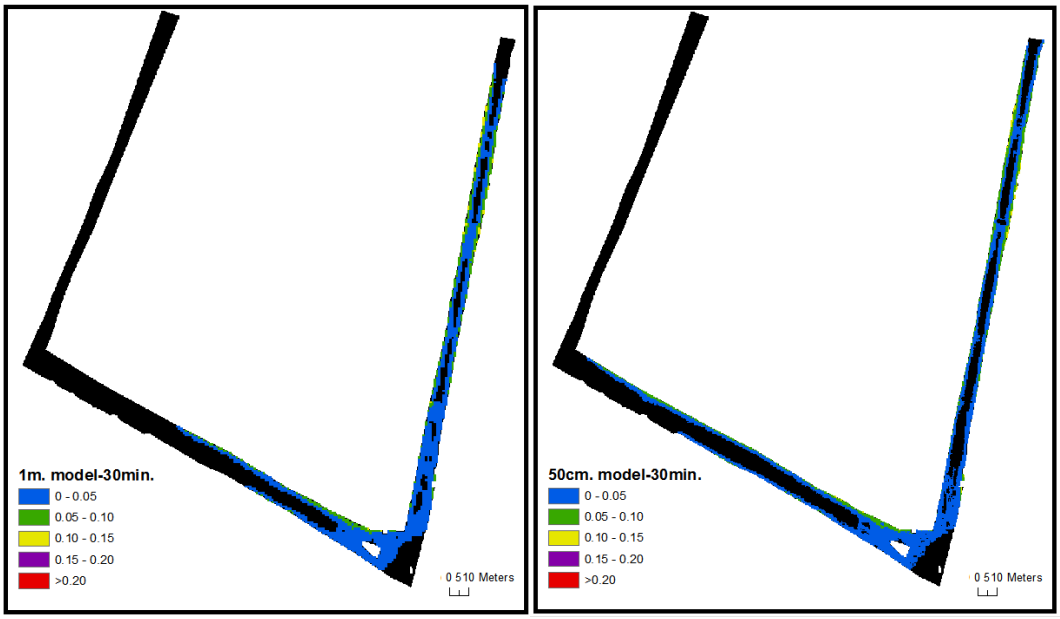


(a) (b)

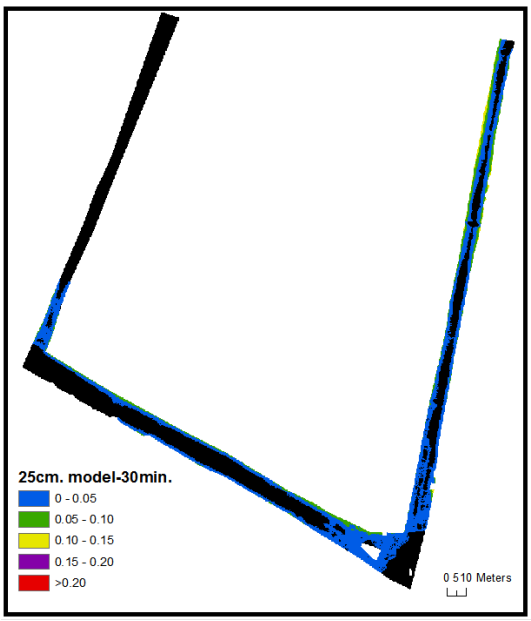


(c)

**Figure 5-10** Inundation Extents of models having (a) 1 m spatial resolution, (b) 50 cm spatial resolution and (c) 25 cm spatial resolution at t=30 min.

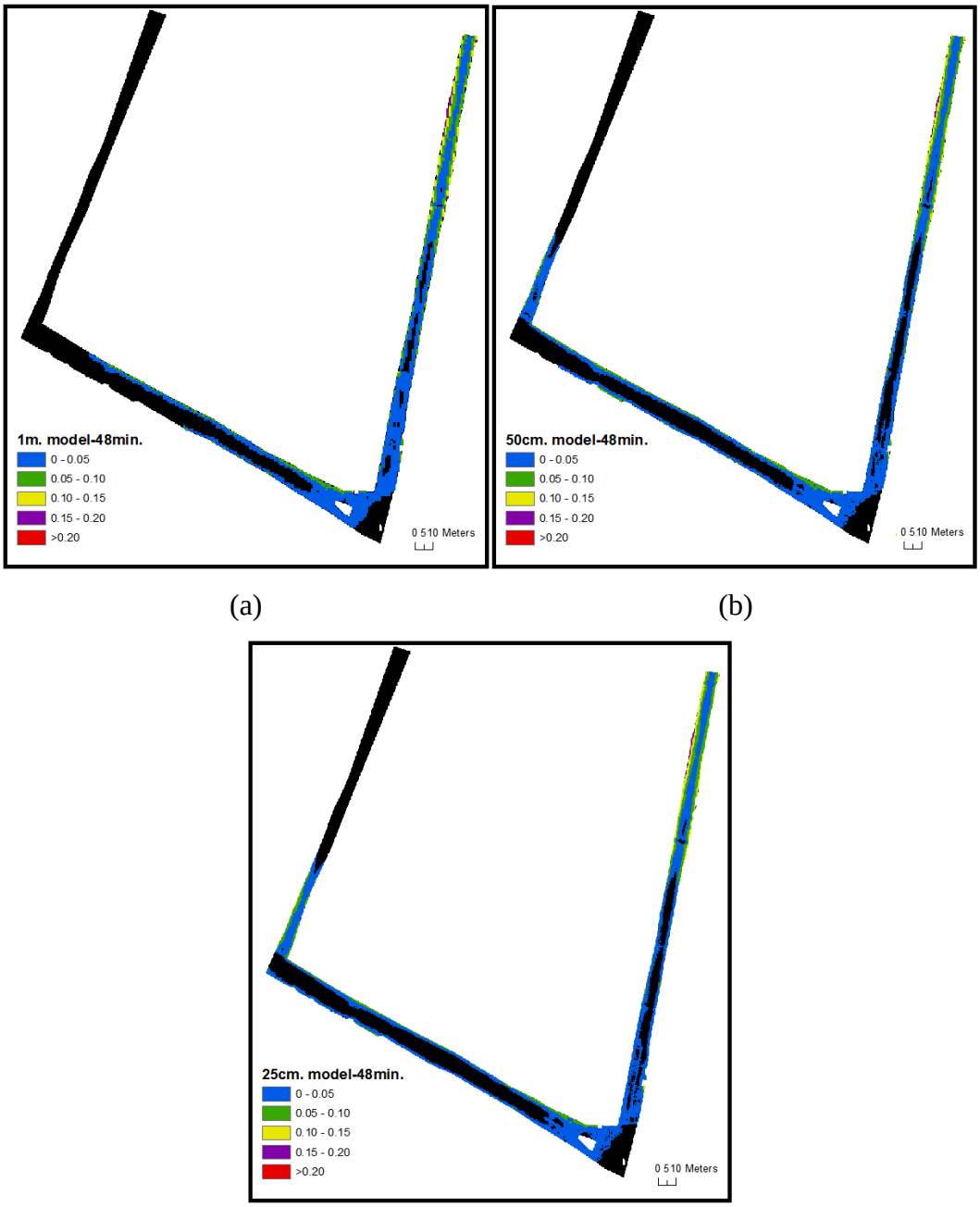


(a) (b)

(c)

**Figure 5-11** Inundation Extents of models having (a) 1 m spatial resolution, (b) 50 cm spatial resolution and (c) 25 cm spatial resolution at t=48 min.

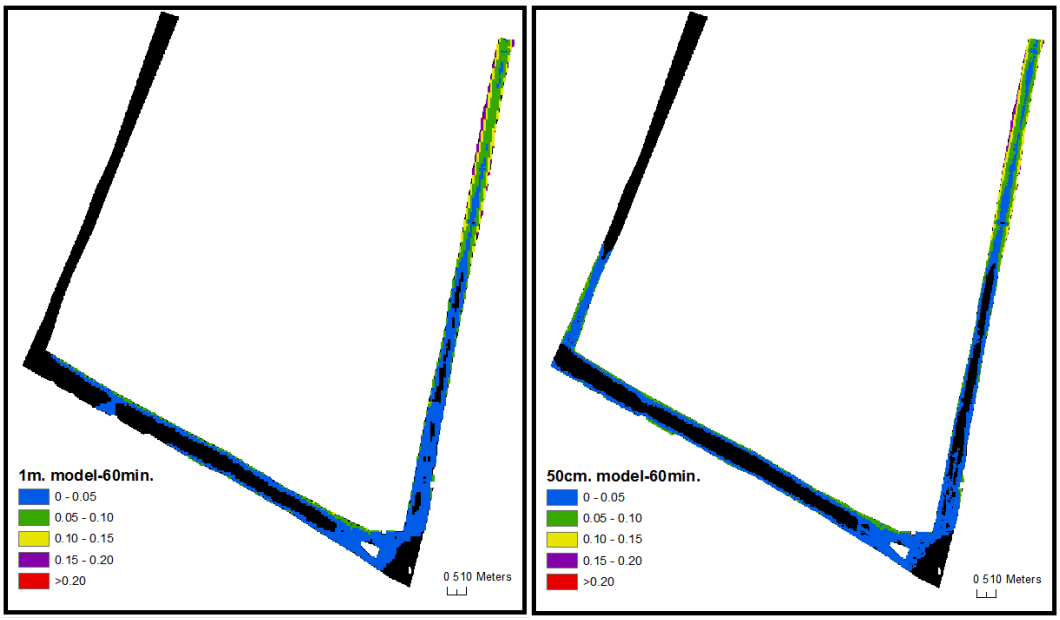


(a) (b)

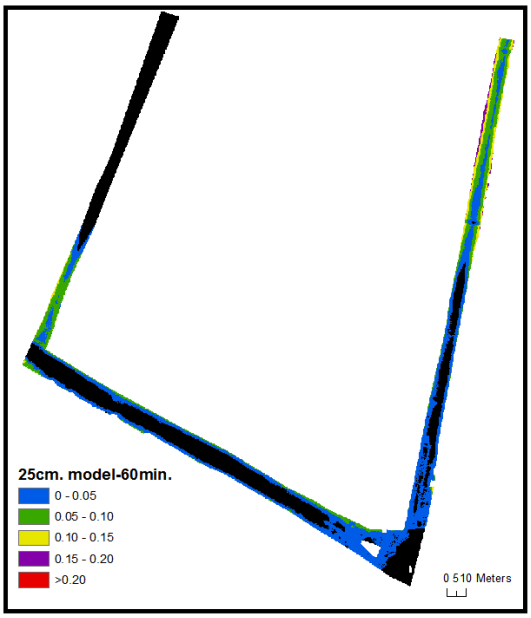


(c)

**Figure 5-12** Inundation Extents of models having (a) 1 m spatial resolution, (b) 50 cm spatial resolution and (c) 25 cm spatial resolution at t=60 min.

Initially (t=0 min), map area is empty and water just started to fill the domain at inflow control point in south-eastern corner of the DEM. At time t=6 min, the flow of water is divided into two parts – the first one is heading toward north-eastern part of the street (main) and second one is moving in north-western direction of the street (tributary). As simulation progresses, at time t=30 min the body of water is flowing in two directions and it can be clearly seen that the flow is heading through the edges leaving the central portion of the road dry. This behavior is expected and can be explained by the curved geometry of a road. Finally, at time t=60 min the main body of water has reached the boundary of the DEM and has flooded upper part of the main street. Meanwhile, other fraction of water body continues flowing within tributary street through road edges.

In terms of inundation extents, considerable differences can be noticed. Starting from t=18 min, for 25 cm model flow is propagating more rapidly in both directions (main and tributary streets) through road channels edges that are formed by more detailed road geometry in comparison to 50 cm and 1 m resolution models (boundaries at road edges serve as road curbs because maximum flow depth does not exceed 20 cm). It should also be noted that by time t=30 min, flow in 25 cm model has reached the third street (perpendicular to tributary street) while flow in 50 cm model has almost reached to the intersection of the two streets and 1 m model has only covered half the distance of tributary street. But eventually, at time interval t=48 min it can be seen that water in 50 cm model has reached the third street. Lastly, at t= 60 min, 25 cm and 50 cm models show reasonably identical behavior while 1 m model has still not reached third street instead accumulating higher amount of water within the main street.

Another way to present the differences between the models is shown in Figure 5-13 and Figure 5-14 where models were compared both graphically and numerically at time interval t=60 min. As mentioned before, significant variations between 25 cm and 1 m models can be distinguished whereas 25 cm and 50 cm models display

quite identical results. As far as numerical difference is concerned, 25 cm model is subtracted from 50 cm model and it can be immediately noticed that there is a difference, although less than 5 cm, in the third street and can be explained by more rapid propagation through small channels of 25 cm model, thus higher volume of water is accumulated in that area. Between 25 cm and 1 m models, there is the same variation of flow depths in the third street, however that difference is higher and lies between 5 and 10 centimeters. Also, it can be seen that higher flow depth (not exceeding 5 cm) is accumulated at the main street in 1 m model. This may be because of water being unable to flow toward tributary street due to lack of hydraulic connectivity (as in the 25 cm model), instead flows toward main street and ponds in that area.

To study differences between simulations outputs more thoroughly, 4 control points within the domain were chosen (Figure 5-7). Points 1 and 3 are located in the beginning of the main and tributary streets respectively so that it would be possible to trace flow depths and velocities nearby inflow control points. Point 2, meanwhile, is located at the end of the main street so that ponding in this area can be numerically evaluated. Finally, point 4 is located in the beginning of the third street. Flow depth variation throughout simulations at four control points of 3 resolution models are shown in Figure 5-15.

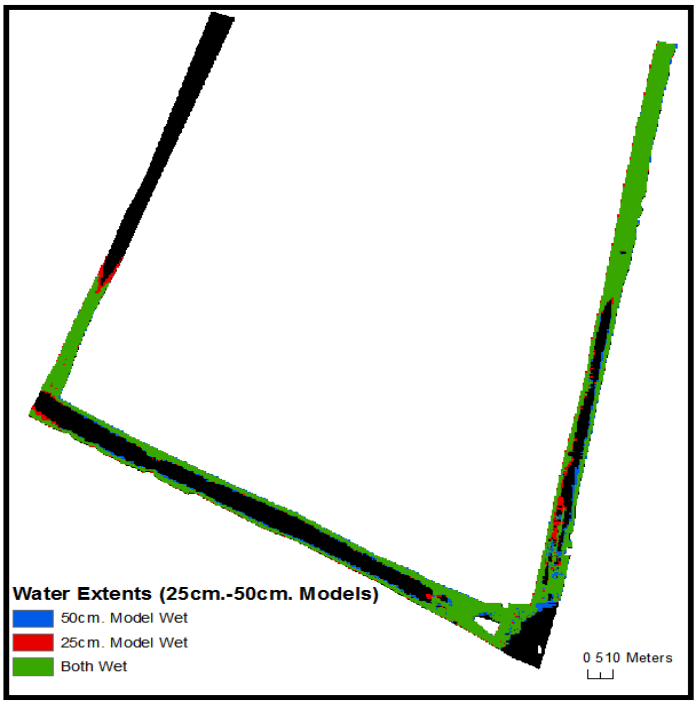


(a)

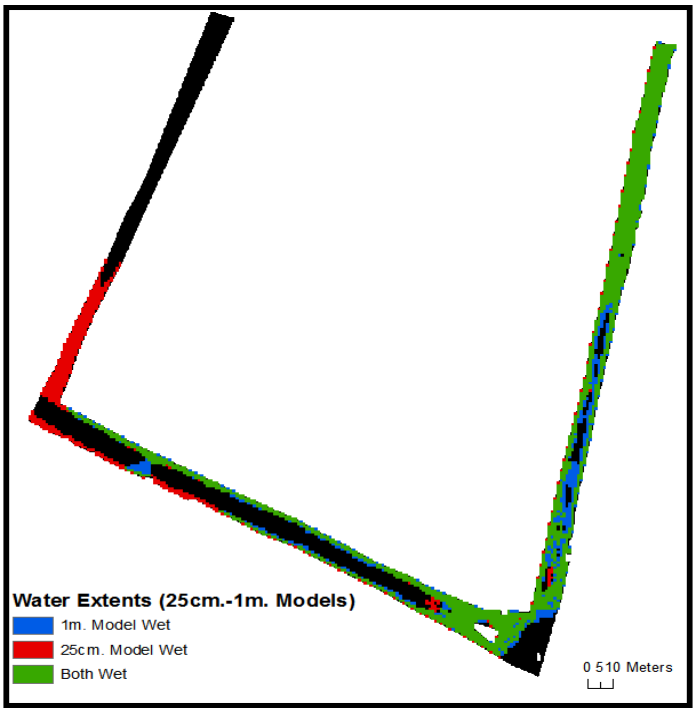


(b)

**Figure 5-13** Graphical representation of the differences in terms of inundation extents between (a) 25 cm and 50 cm and (b) 25 m and 1 m models at t=60 min.

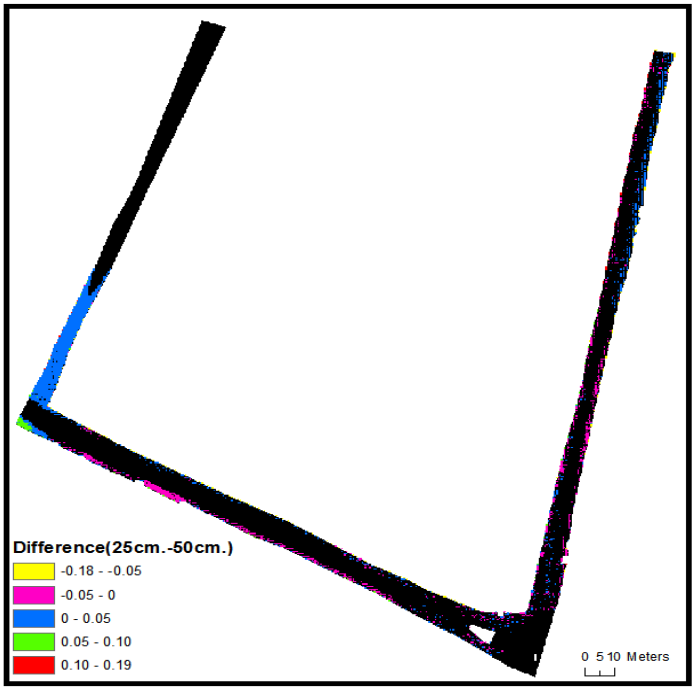


(a)

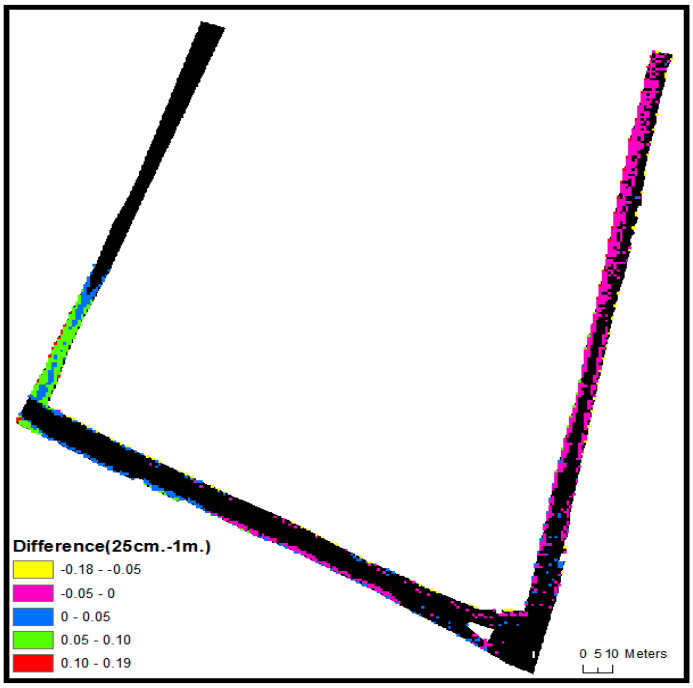


(b)

**Figure 5-14** Numerical subtraction of flow depths of (a) 25 and 50 cm and (b) 25 and 1 m models at t=60 min.

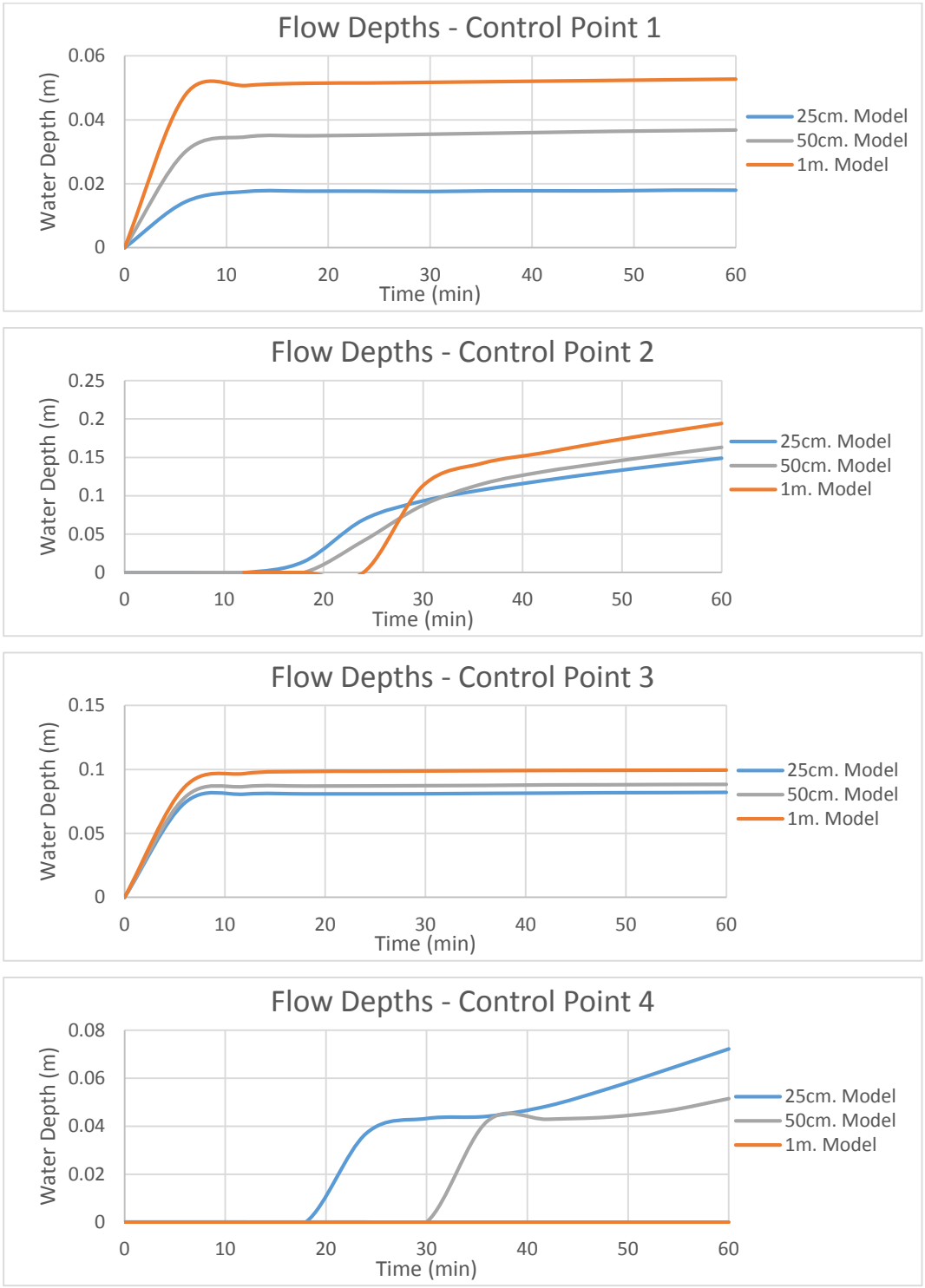


**Figure 5-15** Flow Depth Outputs at 4 control points of 25 cm, 50 cm and 1 m models through simulation time

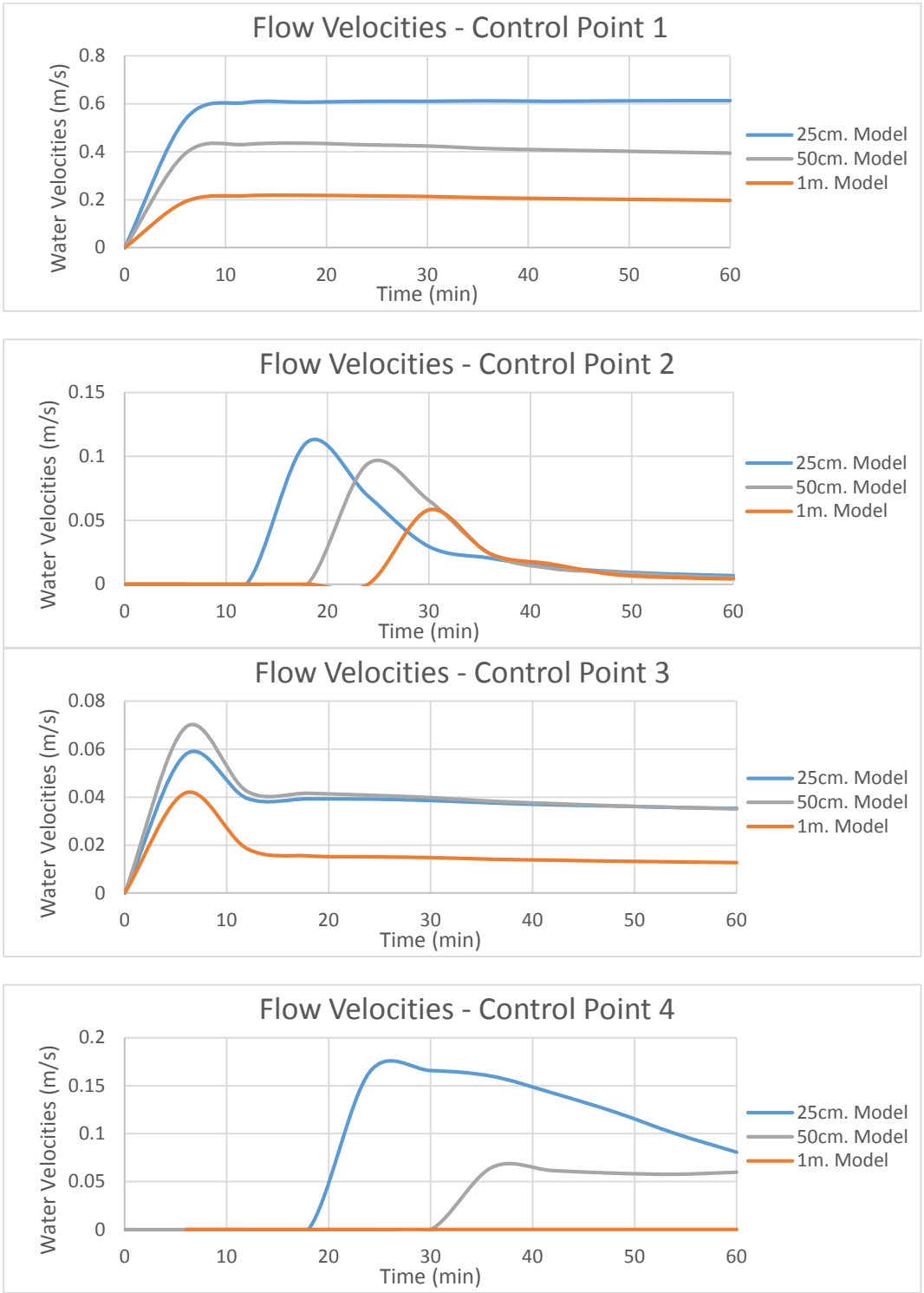


**Figure 5-16** Flow Velocity Outputs at 4 control points of 25 cm, 50 cm and 1 m models through simulation time

Flow depths at points 1 and 3 display similar behavior in a sense that maximum depths are reached at about the same time and that coarser models accumulate higher amounts of water. Also, difference in terms of peak depths can be particularly distinguished at point 1 where maximum flow depth in 1 m model is 5.27 cm while in 25 cm model - only 1.8 cm. At control point 2, expectedly flow in 25 cm model arrives fastest at about 12 minute while the slowest is the flow in 1 m model arriving at 30 minute but predicting higher peak depth (19.4 cm as opposed to 14.9 cm). Finally, it may be observed that water wave at 1 m model has not yet reached control point 4 after one hour of simulation. Meanwhile, between 25 cm and 50 cm models almost identical behavior may be seen but with a time delay of twelve minutes. Differences between models in terms of velocities can also be studied in Figure 5-16. Confirming previous findings, as resolution increases velocities within models also increase which is clearly shown at all four control points. Since flood wave more rapidly propagates in higher resolution models due to higher velocities, it is possible to assume that inundation extents will be higher for these models.

The effect of DEM resolution on flood wave inundation is shown in Figure 5-17 and Figure 5-18. As it is anticipated, 10 cm model predicts higher propagation than of 1 m model throughout whole 1 hour simulation. However, it is worth noting that toward the end of simulation 10 cm and 50 cm models show almost identical behavior. This can be explained by the fact that wave front of 10 cm model reaches the third street first but as simulation progressed 50 cm model caught up.

Three sections were also taken (Figure 5-19) for all three resolution models to compare flow depths at time t=60 min taking into account DEM elevation (Figure 5-20 to Figure 5-22). Looking at all three sections, it can be seen that as the resolution increases the detailing of topography becomes more evident, thus affecting the shallow water flow. In particular, there is a small channel on the left-hand side of sections 2 and 3 that water passes through.

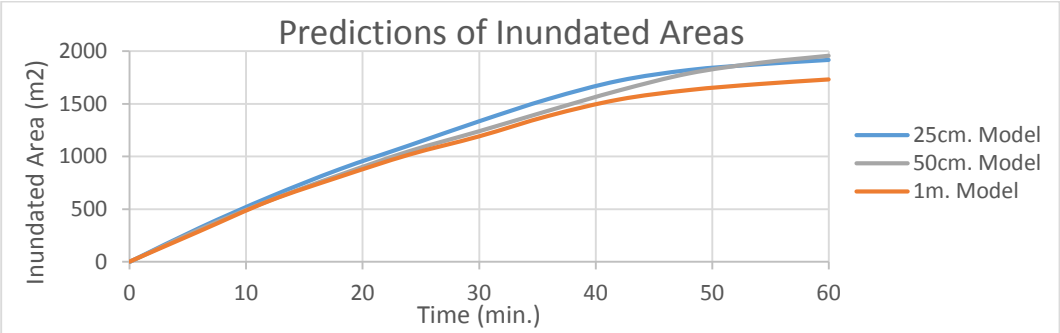


**Figure 5-17** Prediction of Inundation Areas of 25 cm, 50 cm and 1 m models through simulation time

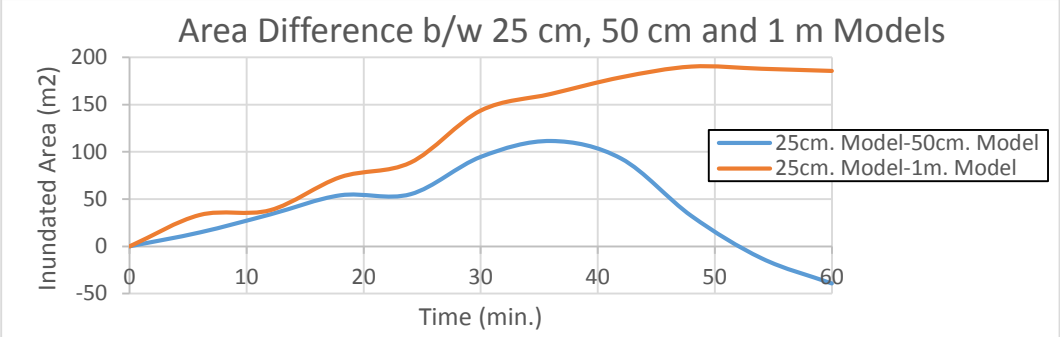


**Figure 5-18** Numerical Difference of Inundation Areas of 25 cm, 50 cm and 1 m models through simulation time

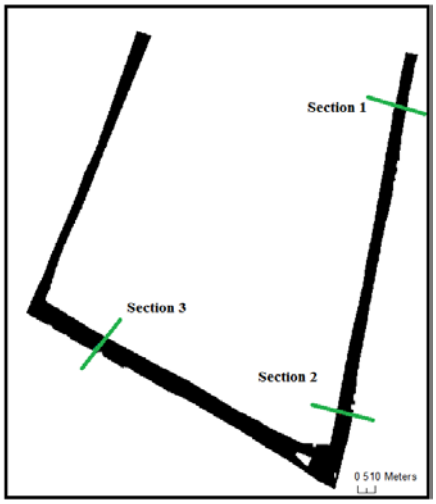


**Figure 5-19** Three sections taken to compare water elevations at t=60 min.

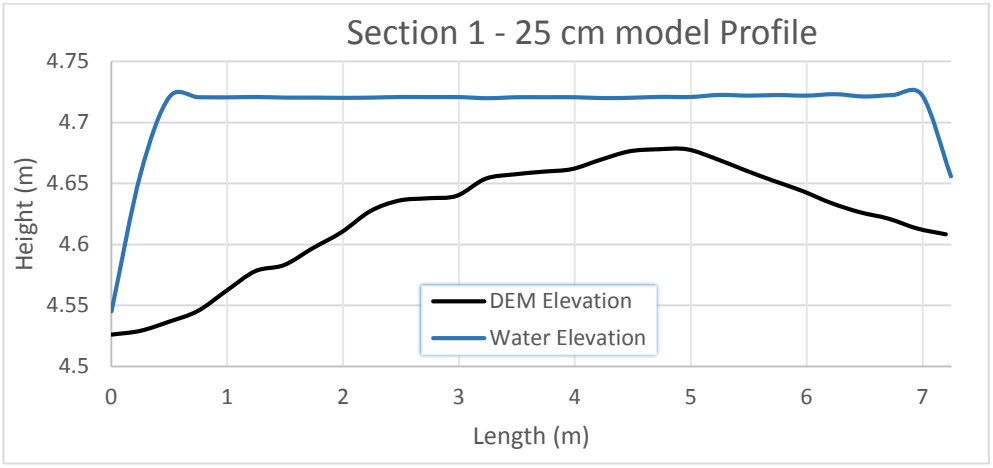


(a)

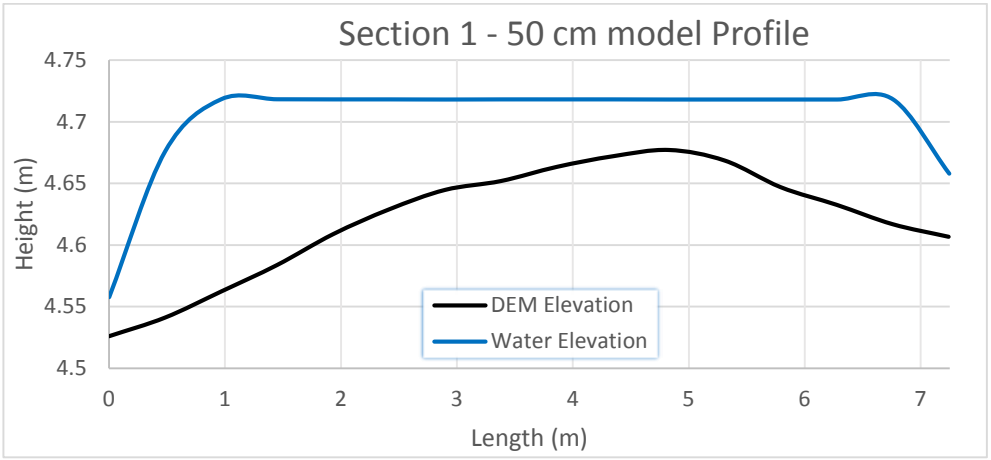


(b)

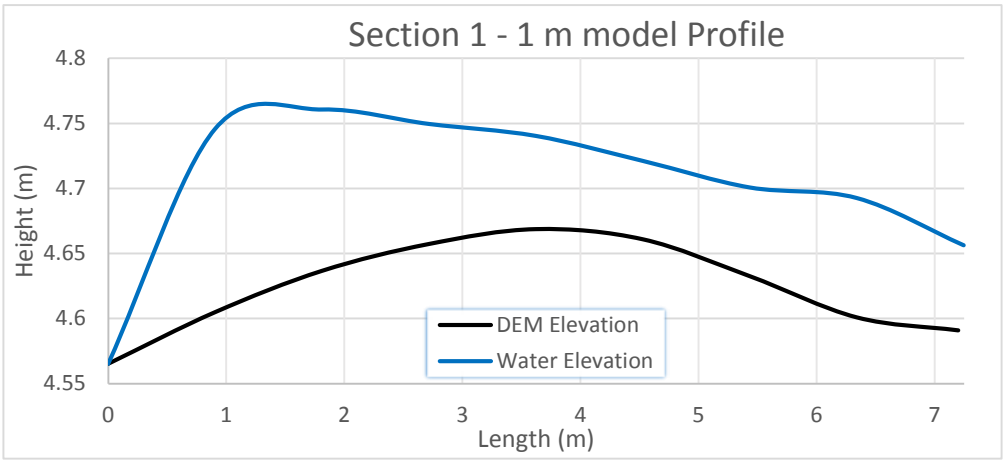


(c)

**Figure 5-20** Section 1 Profiles of Water Elevations of (a) 25 cm model, (b) 50 cm model and (c) 1 m model at t=60 min.

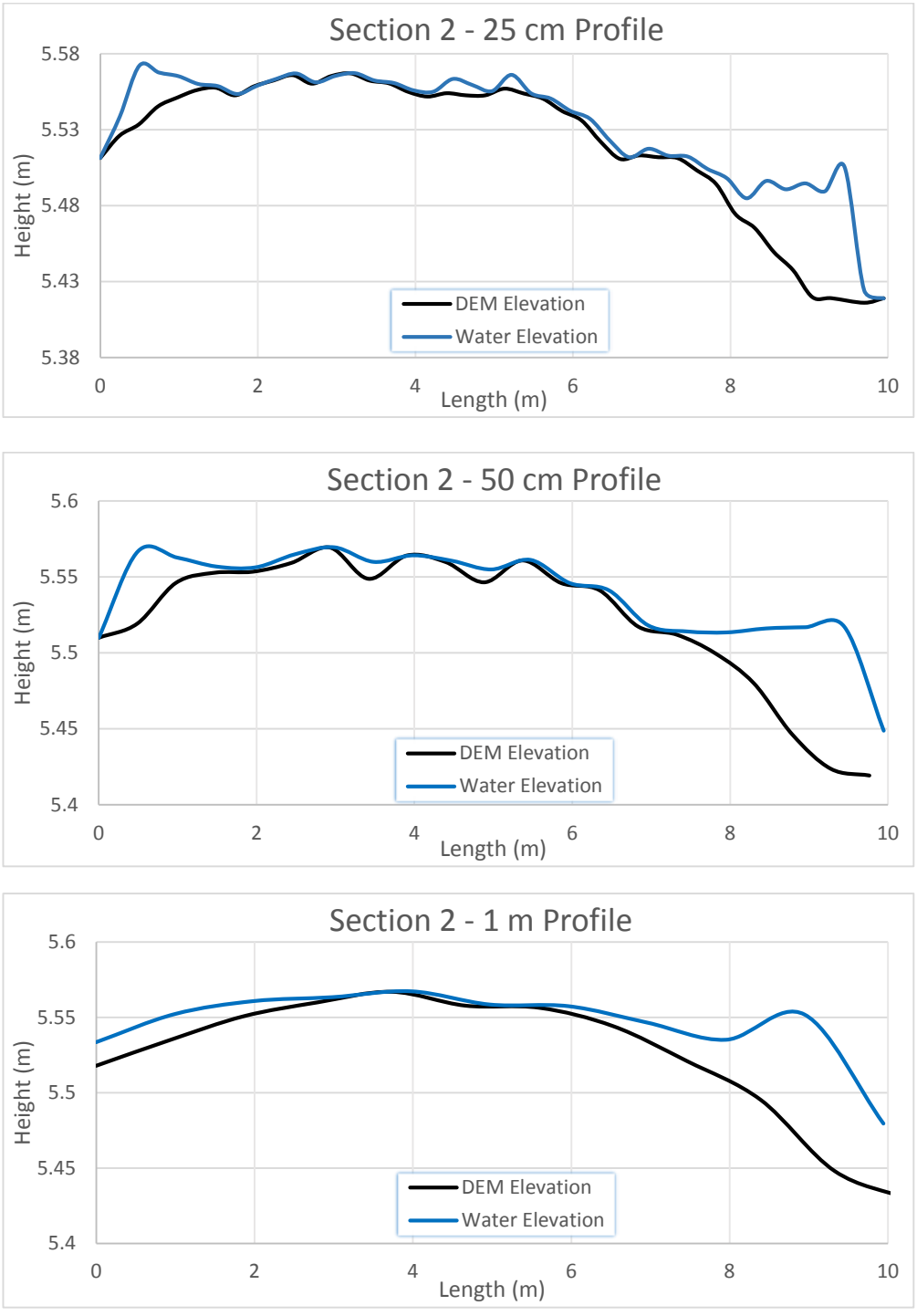


**Figure 5-21** Section 2 Profiles of Water Elevations of (a) 25 cm model, (b) 50 cm model and (c) 1 m model at t=60 min.

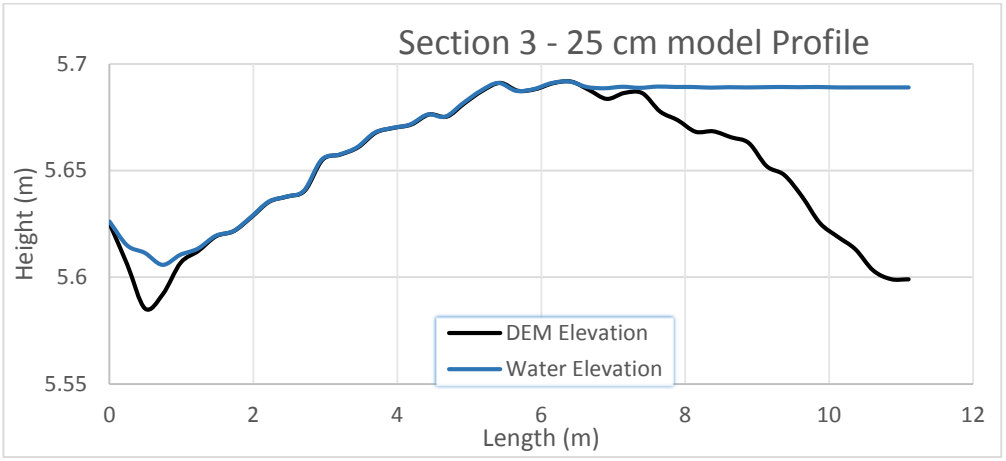


(a)

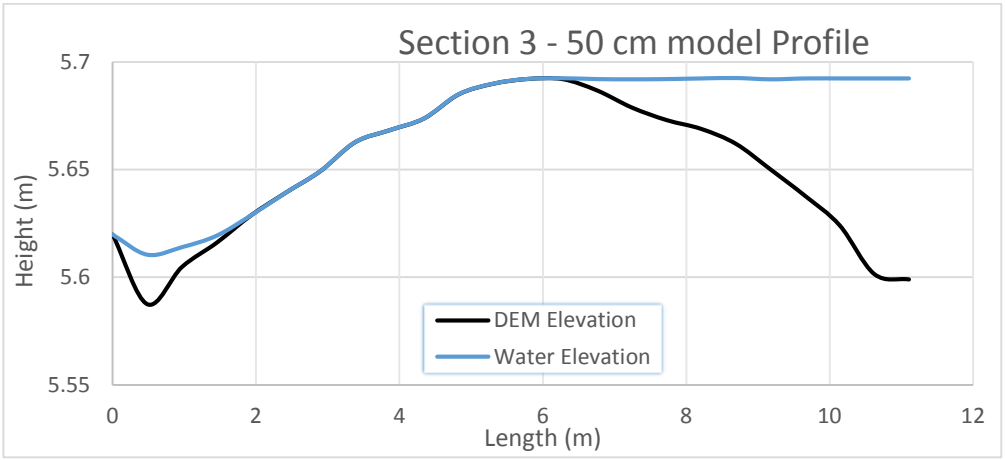


(b)

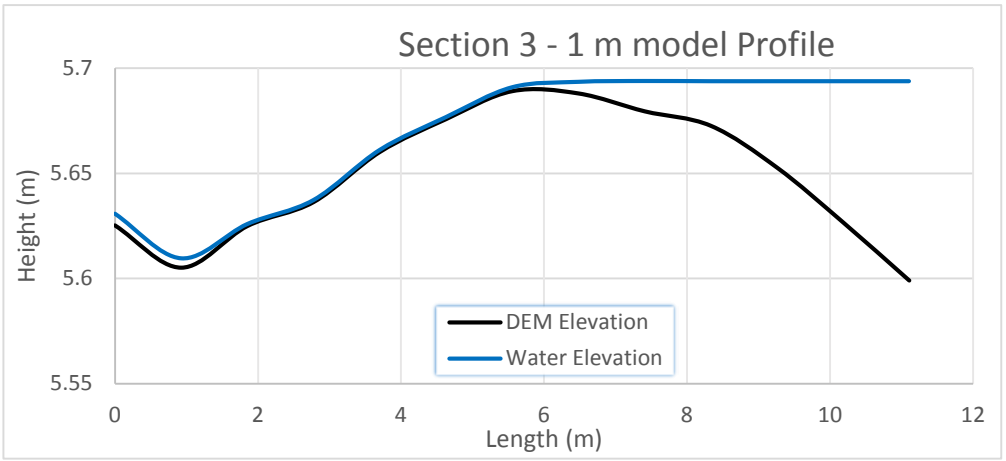


(c)

**Figure 5-22** Section 3 Profiles of Water Elevations of (a) 25 cm model, (b) 50 cm model and (c) 1 m model at t=60 min.

The impact of varying resolution (10 cm model being chosen as a benchmark) on simulation results were also evaluated using statistical measures. Firstly, RMSD of flow depths and velocities can be studied in Figure 5-23 and Figure 5-24. It can be immediately noticed that 1 m model show higher RMSD of depth (with maximum reaching up to 5 cm) and velocity (maximum difference of 0.22 m/s) throughout whole simulation time as opposed to 50 cm model (maximum of 2 cm for depth and 0.17 m/s for velocity). Secondly, Fit Statistic was compared for both of the models in terms of inundation extents (Figure 5-25). The same tendency can be observed meaning that lower resolution model display lower $F^2$ measure during simulation time.

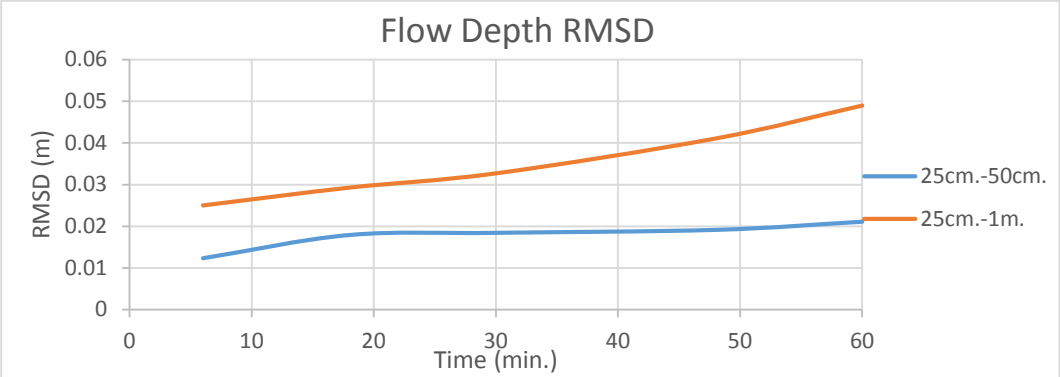


**Figure 5-23** RMSD of Flow Depths between 25 cm, 50 cm and 1 m models through simulation time

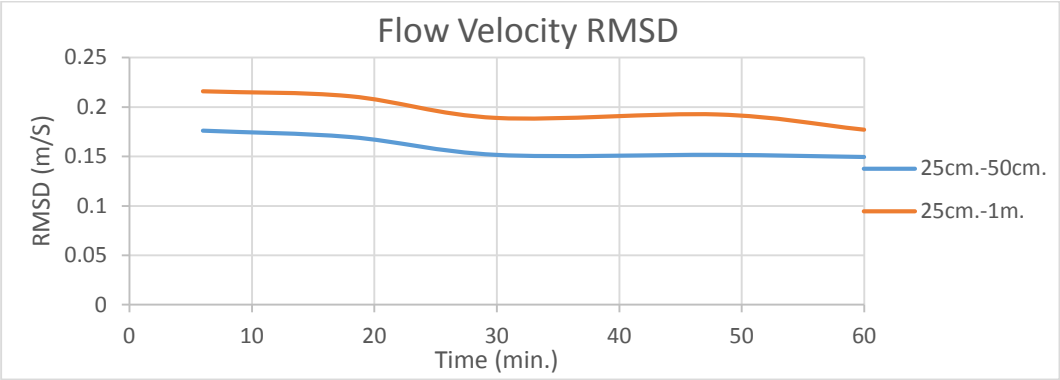


**Figure 5-24** RMSD of Flow Velocities between 25 cm, 50 cm and 1 m models through simulation time

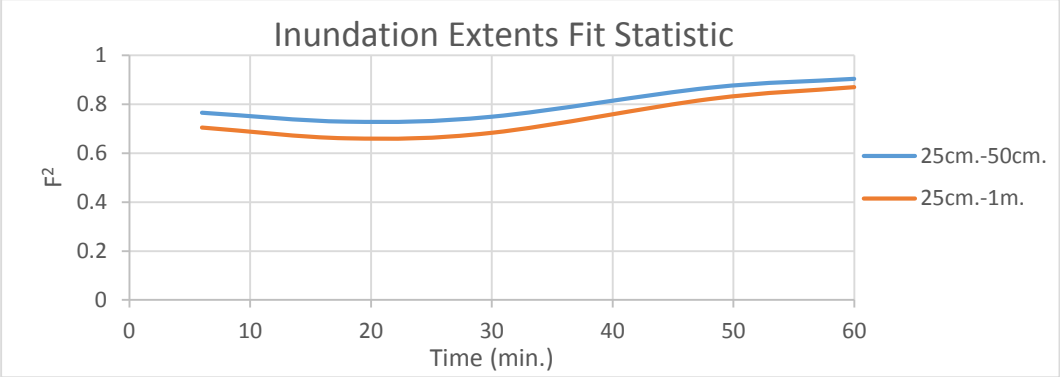


**Figure 5-25** Fit Statistic for Flow Depths between 25 cm, 50 cm and 1 m models through simulation time

### 5.2.2 Varying Roughness Study

In this section, a brief study was conducted on 25 cm resolution model to analyze differences between four cases representing various terrain roughness conditions. Figure 5-26 shows simulation outputs at the end of simulation at t=60 min. The only significant discrepancy that can be distinguished by looking at these figures is that as flow resistance decreases, higher depths are ponded within the third street due to faster progression of the flow.

In terms of difference between inundation areas (Figure 5-27 and Figure 5-28), although the variation is very small, it can be observed that initially models with lower roughness spread faster within the domain but toward the end of simulation higher roughness models inundate slightly larger area of the DEM. This difference can be seen in Figure 5-29, where models with higher roughness having less inertia to move forward instead propagate in a lateral direction (a “shot” was taken very close to an intersection of tributary and third street at time interval t=60 min).

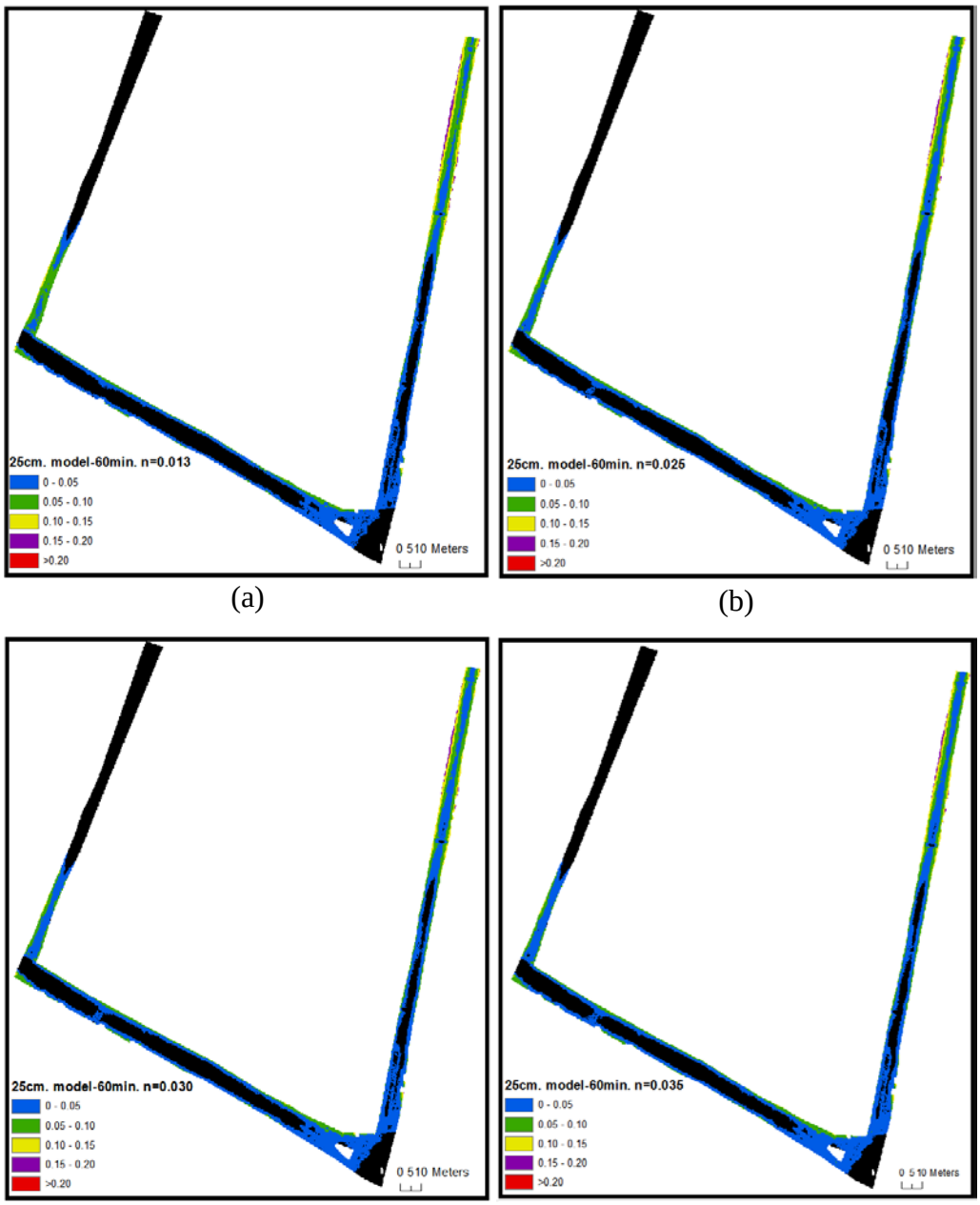


**Figure 5-26** Inundation Extents of simulation results of 25 cm model where (a) n=0.013, (b) n=0.025, (c) n=0.030 and (d) n=0.035 at t=60 min.

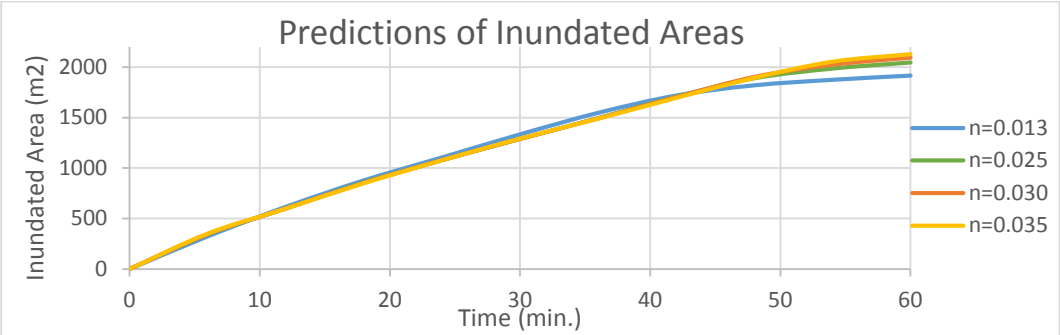


**Figure 5-27** Prediction of Flood Inundation Areas through simulation time of 4 models with different roughness conditions

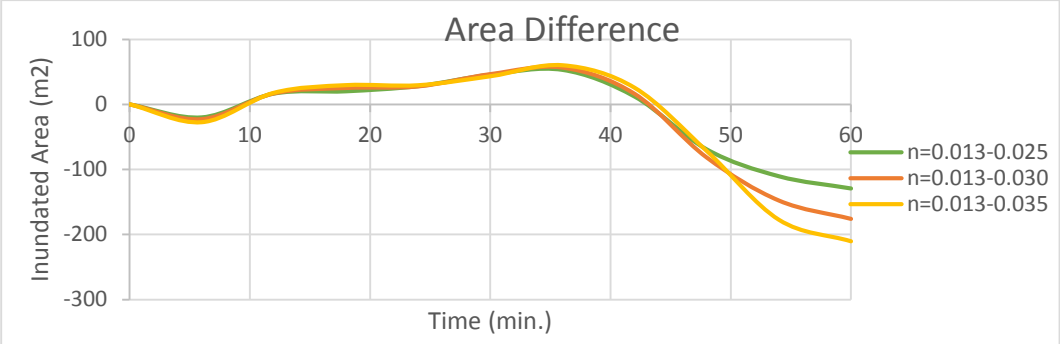


**Figure 5-28** Numerical Difference of Inundation Areas through simulation time of 4 models with different roughness conditions

Variation of flow depths and velocities at 4 control points are shown in Figure 5-30 and Figure 5-31. As a general trend, expectedly flow depths are lower, velocities are higher and flood wave propagates more rapidly as the roughness of the model decreases. It is interesting to note that maximum flow depths for control points 2 and 4 are higher in model output with n=0.013 and that is because the front wave had reached those points faster.

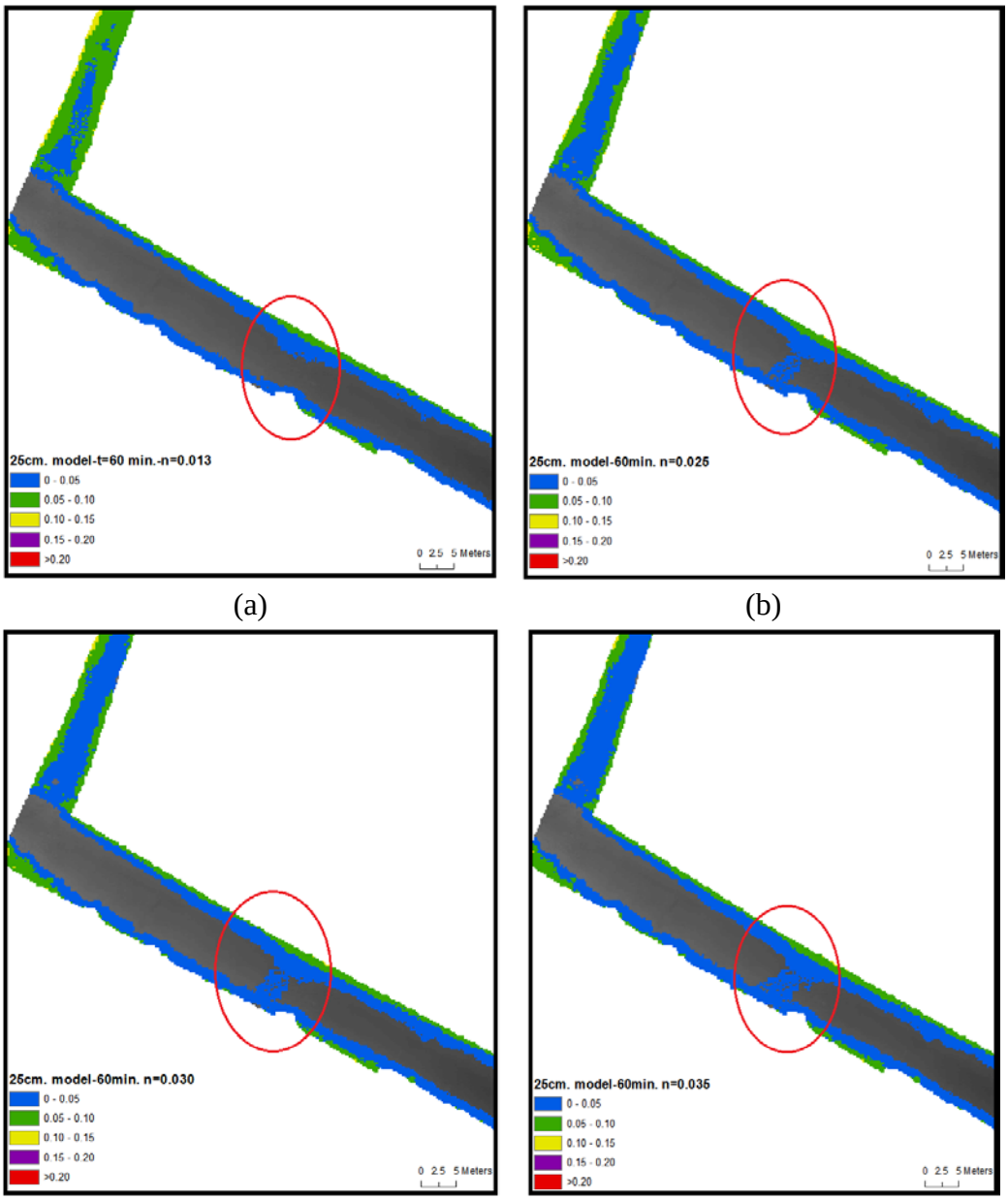


**Figure 5-29** Variation of inundation extents for simulation outputs of models where (a) n=0.013, (b) n=0.025, (c) n=0.030 and (d) n=0.035 at t=60 min.

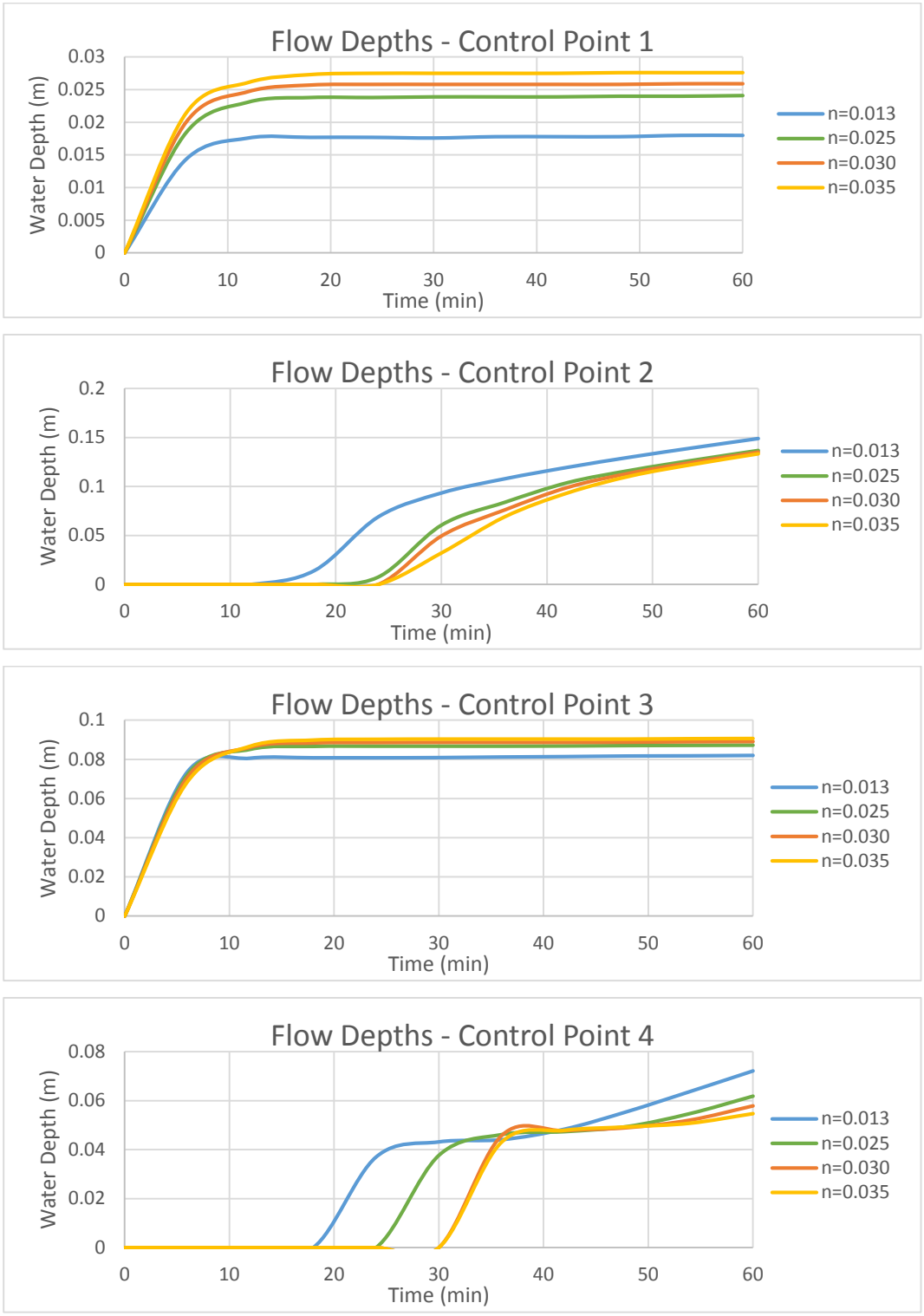


**Figure 5-30** Flow Depth Outputs at 4 control points through simulation time of 4 models with different roughness conditions

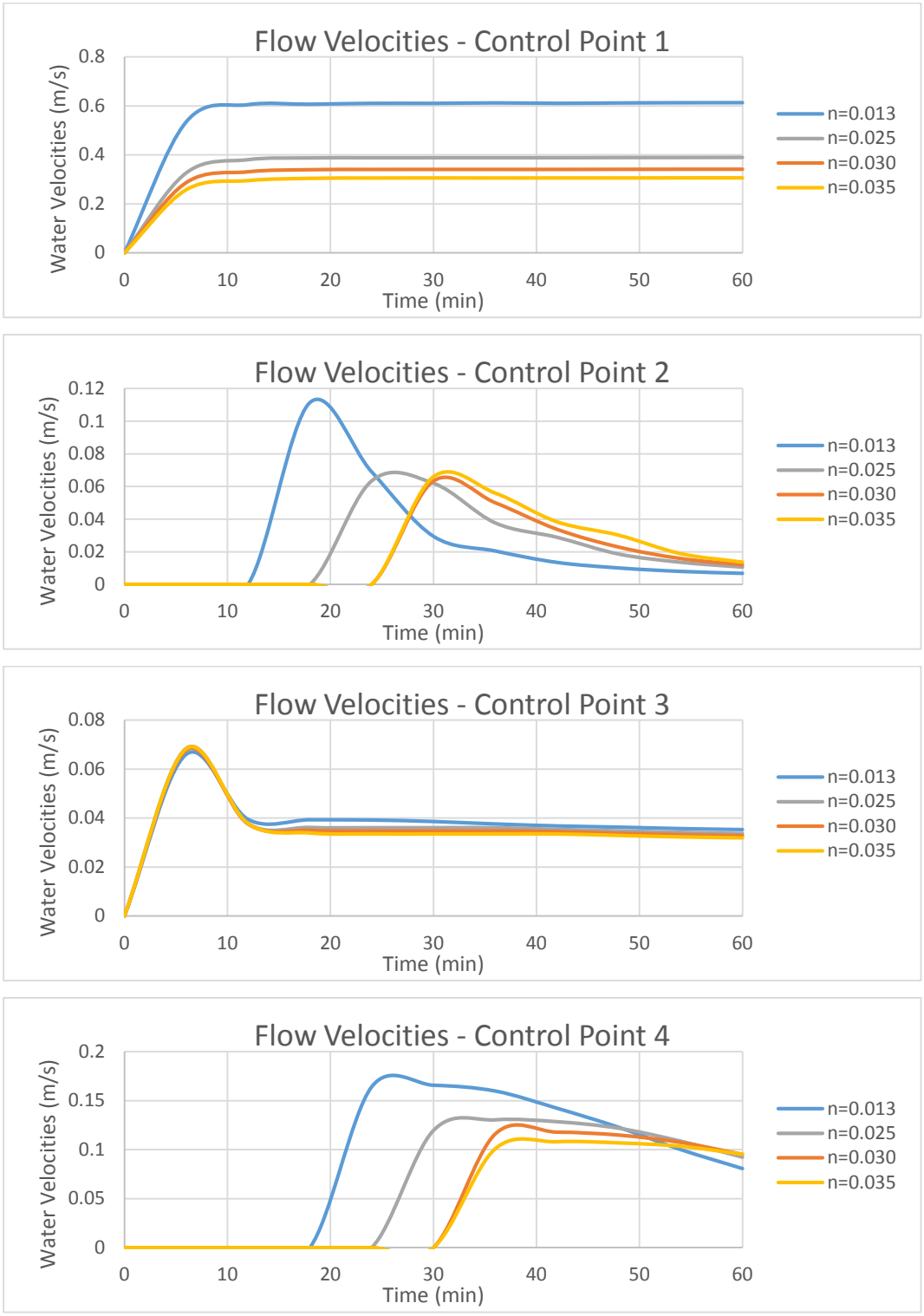


**Figure 5-31** Flow Velocity Outputs at 4 control points through simulation time of 4 models with different roughness conditions

Finally, taking a "n=0.013 model" as a benchmark RMSD of flow depths and velocities was calculated and shown in Figure 5-32 and Figure 5-33. As can be seen in these figures, higher roughness leads to higher variation between models with maximum difference of RMSD for depths is 3 cm and 0.03 m/s for velocities. Also, the $F^2$ statistic can also be studied in Figure 5-34 and the same conclusion can be drawn - there is a difference in terms of flood extents, although not very significant.

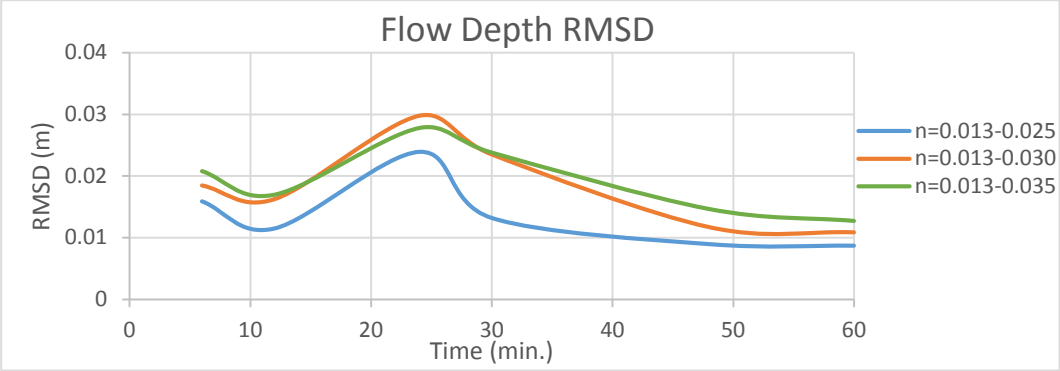


**Figure 5-32** RMSD for Flow Depths through simulation time of 4 models with different roughness conditions

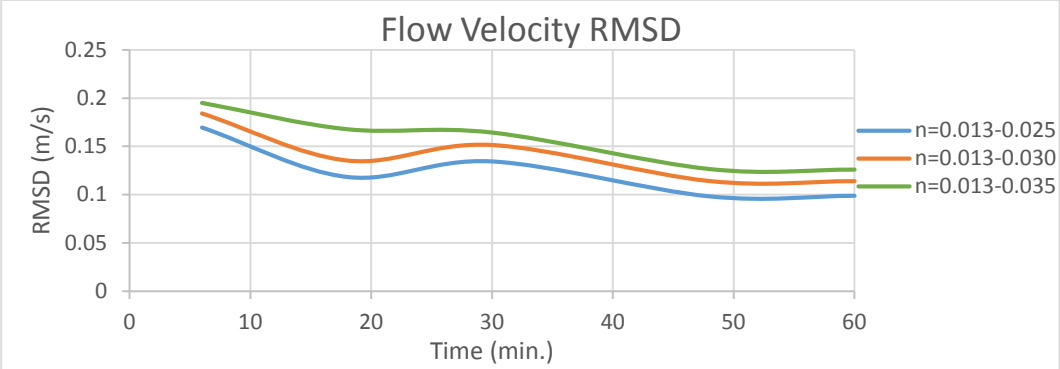


**Figure 5-33** RMSD for Flow Velocities through simulation time of 4 models with different roughness conditions

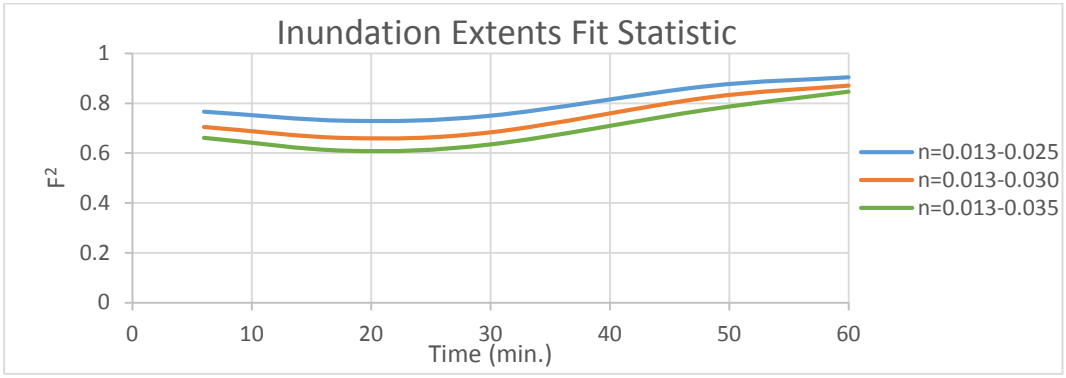


**Figure 5-34** Fit Statistic for Flow Depth through simulation time of 4 models with different roughness conditions

# CHAPTER 6

# DISCUSSION OF RESULTS AND CONCLUSIONS

## 6.1 Results of Lisflood-FP solvers evaluation

Four numerical solvers as a part of the Lisflood-FP flood inundation model were evaluated taking advantage of 1/1000 topographical DEM obtained from surveying of Terme town of Samsun Province obtained by DSI in 2013. Flow depths, velocities and inundation extents were analyzed to understand how varying complexity of shallow water equations representation in numerical schemes may affect model outputs. Two diffusive solvers – Flow-limited and Adaptive numerical schemes, both neglecting local and convective acceleration terms, only differ in handling of a time step among each other. The Acceleration model, meanwhile, neglects only convective acceleration term, hence only partially conserving momentum. The last model – Roe solver represents complete Saint-Venant formulation and includes all the terms of shallow water equations.

Both diffusive and Acceleration solvers show similar results of flow depths and inundation extents in all time intervals of simulation. It was shown that the difference of average depths across the domain did not exceed 1 cm (except for the 2 ponding areas where largest difference was 7 cm) and maximum RMSD was found to be just 2 cm in the last time interval. However, there were significant discrepancies among these models in comparison to Roe solver – the maximum depth difference was located in ponding areas reaching up to 25 cm and maximum RMSD for Roe and Acceleration solvers was found to be 9 cm. In terms of inundation extents, the trend continued as Roe solver vastly over predicted flooded

areas by almost 35% compared to Acceleration solver. It is unclear to what extent such different behavior is attributed to the numerical scheme as Roe solver is the most complex among the four but it was evident that Roe solver was influenced by numerical instabilities to a certain degree and overestimated volume of water in the domain by almost 5%.

### 6.2 Results of Lisflood-FP simplified inertial solver and Mike 21 model evaluation

Lisflood-FP and Mike 21 flood models were also studied using 1 m 1/1000 topographical DEM obtained by DSI in 2013. Flow water depths, velocities as well as inundation extent outputs of the two models were compared. It was shown that there is a general resemblance in terms of flow depths where differences did not exceed 5 cm for the majority of the domain at last time interval and maximum RMSD of depth not exceeding 4 cm during simulation time. However, for the areas of ponding, Lisflood-FP generates larger depths with differences reaching up to 20 cm. This may be explained by the fact that as inertia is only partially conserved, flow is overestimated in a region of higher flow depths because flux is more dependent on gravity and friction (Bates et al., 2010). Such variation of flow depths between the models in these areas cannot be ignored and shall be considered real and systematic (Sampson et al., 2012). The variation of peak velocities at four control points did not exceed 10% except for the area of high slope gradients exceeding 10%. The assumption is that numerical instability of Lisflood-FP model might have caused such differences in velocities due to limited representation of momentum terms in Saint-Venant equations (ignoring convective acceleration). In terms of inundation extents, Mike 21 predicted higher inundated area during simulation time with difference of ~10% for final time interval. Eddy viscosities were not considered in momentum equation while using Mike 21 model because they are not calibration parameters and their effects cannot be analyzed in this benchmarking studies.

## 6.3 Results of scale and roughness effects evaluation

This part of study was performed to evaluate resolution and roughness effects on two-dimensional urban flood modeling in Terme town, Samsun using simplified inertial solver within Lisflood-FP software. In terms of resolution, a terrestrial LIDAR raster models with scale of 25 cm, 50 cm and 1 m and n=0.013 representing asphalt roughness conditions were compared to analyze difference between flow depths and velocities, inundation extents, and other statistical measures.

The results indicate that increasing resolution of the DEM introduces more detailed representation of the topography such as sloping alignment of a road. This, in turn, results in development of small channels within road section allowing water to be conveyed faster through these channels, thus significantly affecting behavior of flow propagation. It was shown that there are noticeable differences between three models in terms of flow depths and velocities. As the simulation started, due to more rapid flow of fine resolution models lower depths in ponding areas and higher velocities at four representative control points were observed. Between 25 cm and 50 cm models, generally the depth variation did not exceed 5 cm. On the other hand, deviation among 25 cm and 1 m models was found to be more prominent due to differences in depths reaching up to 10 cm at certain regions. The same tendency was observed when comparing these models in terms of RMSD (considering 0.25 cm model as a benchmark) – maximum difference at the end of simulation time for 50 cm model was 2 cm and 5 cm for 1 m model. Meanwhile, maximum RMSD for flow velocities at the start of the simulation was found to be 0.18 m/s for 50 cm model and 0.22 m/s for 1 m model but that difference was gradually decreasing as simulation progressed.

The sensitivity analysis was also performed to understand how varying roughness conditions affect hydraulic model outputs. The 25 cm resolution model and four different roughness parameters that may be used in two-dimensional flood

modeling were chosen to compare flow depths, velocities and inundation extents. As expected, the model correctly predicted sensitivity to friction as models with smaller roughness had shown higher velocities observed at control points but flow depths vary due to more rapid propagation of flow – at ponding areas they are smaller, but in control points located further away from the inflow point, they display higher values due to earlier arrival times. Finally, in terms of inundation extents the difference between the models was almost negligible throughout whole simulation time.

## 6.4 Conclusion

First of all, a small discussion regarding applicability of the four solvers to accurately predict urban flood inundation must be made. In this part of the study, significant differences between simulation outputs of Roe solver compared to other three numerical schemes were presented. This may be explained by the fact that Lisflood-FP user manual suggests that only few scenarios were tested for Roe solver, thus it may not provide accurate results compared to other widely used hydraulic models. Conversely, the simulation outputs of more simple solvers provided consistent results. However, Flow-limited solver had to be manually calibrated to produce meaningful results which may not always be possible to accomplish during simulation of real flood events. In fact, the above-mentioned manual does not advise using the scheme due to its poor accuracy. Also, even though time step of Adaptive solver was automatically chosen by the scheme, its computational time would not allow to perform urban flood modeling studies. Consequently, for this study area only Acceleration solver combines both numeral accuracy and computational efficiency with assumption that the flow in simulations is subcritical and gradually varied in time.

Secondly, analysis of Lisflood-FP and Mike 21 numerical schemes was performed and it is safe to assume that for practical applications both flood inundation

numerical models may predict similar results of flow depths, velocities and inundation extents for gradually varied flows as well as DEMs with elevation gradients not exceeding 10%. According to Néelz and Pender (2013), local acceleration model is appropriate to be used in decision making of catchment flood management planning and flood risk assessment as well as predicting reasonably accurate assessment of velocities. The same conclusion was drawn when this numerical scheme was compared to Mike 21 model in this study.

Finally, it was shown that varying resolution and roughness significantly impacts the necessary outputs implemented in urban flood hydraulic modeling such as flow flood depths, velocities and inundation extents using simplified inertial model of Lisflood-FP software. Consequently, it is advantageous to perform such studies using fine scale digital elevation models based on terrestrial LIDAR surveys and realistic surface roughness conditions based on land use. Terrestrial LIDAR data is a good source to obtain high resolution DEM. However, this study is the first one where terrestrial LIDAR data is used in hydraulic modeling. It should be mentioned that careful attention must be paid in processing techniques of raw LIDAR point cloud data to eliminate inadequate topographic features that may result in instability problems of hydraulic modeling studies. Using high frequency LIDAR instruments produce more points which is difficult to eliminate in post-processing analysis. Therefore, 400 kHz LIDAR instrument may not be a good alternative for obtaining DEMs to be used in flood hydraulic modeling.

The Lisflood-FP simplified inertial solver provided reasonably accurate results dealing with gradually varied flows. However, when adverse slopes within DEM coupled with fine spatial resolution and very low surface roughness conditions are introduced into the model, numerical instability became so apparent that further analysis was proved to be meaningless. Therefore, future work should rely on further development of the model to improve numerical stability when dealing with such conditions.

Likewise, the use of Lisflood-FP Roe solver in flood inundation studies led to inconclusive results since, albeit small, the model also encountered numerical instability issues. Consequently, additional research as well as validating studies should be performed on this solver in the future. It would be particularly beneficial to develop this numerical scheme due to its handling of supercritical flows and shock capturing capabilities, although at a higher computational cost when compared to Lisflood-FP Acceleration solver.

The sensitivity of flood propagation on DEM varying resolution was shown in this study. Therefore, further use of terrestrial LIDAR scanning technology in flood inundation studies should be encouraged possibly leading to less sophisticated and easier to implement processing techniques of LIDAR raw point cloud data.

## REFERENCES


Bates, P. D., & De Roo, A. P. (2000). A simple raster-based model for flood inundation simulation. *Journal of Hydrology, 236*, 54–77.

Bates, P. D., Horritt, M. S., & Fewtrell, T. J. (2010). A simple inertial formulation of the shallow water equations for efficient two-dimensional flood inundation modelling. *Journal of Hydrology, 387*, 33–45.

Bates, P., Trigg, M., & Dabrowa, A. (2013). *Lisflood-FP user Manual.* School of Geographical Sciences, University of Bristol.

Brufau, P., Garcia-Navarro, P., & Vazquez-Cendon, M. E. (2004). Zero mass error using unsteady wetting–drying conditions in shallow flows over dry irregular topography. *International Journal for Numerical Methods in Fluids, 45*, 1047–1082.

Chow, V. (1959). *Open Channel Hydraulics.* New York: McGraw-Hill.

de Almeida, G. A., Bates, P., Freer, J. E., & Souvignet, M. (2012). Improving the stability of a simple formulation of the shallow water equations for 2-D flood modeling. *Water Resources Research, Vol. 48*, W05528. doi:10.1029/2011WR011570

de Almeida, G. A., & Bates, P. (2013). Applicability of the local inertial approximation of the shallow water equations to flood modeling. *Water Resources Research, 49*, 4833–4844. doi:10.1002/wrcr.20366

DHI. (2007). *Mike 21 Flow Model: Hydrodynamic module - Scientific Documentation.* DHI Water & Environment.

European Parliament. (2007). *Directive 2007/60/EC of the European Parliament and of the Council of 23 October 2007 on the assessment and management of flood risks.* Official Journal of the European Union.

Fewtrell, T. J., Duncan, A., Sampson, C. C., Neal, J. C., & Bates, P. D. (2011). Benchmarking urban flood models of varying complexity and scale using

high resolution terrestrial LiDAR data. *Physics and Chemistry of the Earth, 36*, 281–291.

Gilles, D., & Moore, M. (2010). *Review of Hydraulic Flood Modeling Software used in Belgium, The Netherlands, and The United Kingdom.* International Perspectives in Water Resource Management, IIHR – Hydroscience & Engineering, University of Iowa.

Gruen, A., Baltsavias, E. P., & Henricsson, O. (1997). *Automatic extraction of man-made objects from aerial and space images (II).* Basel: Birkhauser Verlag.

Guinot, V. (2003). *Godunov-type Schemes: an Introduction for Engineers.* ELSEVIER SCIENCE B.V.

Hunter, N. M., Horritt, M. S., Bates, P. D., Wilson, M. D., & Werner, M. G. (2005). An adaptive time step solution for raster-based storage cell modelling of floodplain inundation. *Advances in Water Resources, 28*, 975–991.

Hunter, N. M., Bates, P. D., Horritt, M. S., & Wilson, M. D. (2007). Simple spatially-distributed models for predicting flood inundation: A review. *Geomorphology*(90), 208-225.

Hunter, N. M., Bates, P. D., Neelz, S., Pender, G., Villanueva, I., Wright, N. G., . . . Mason, D. C. (2008). Benchmarking 2D hydraulic models for urban flooding. *Proceedings of the Institution of Civil Engineers - Water Management 161*(WMI), 13-30. doi:10.1680/wama.2008.161.1.13

Marks, K., & Bates, P. (2000). Integration of high-resolution topographic data with floodplain flow models. *Hydrological Processes, 14*, 2109-2122.

Neal, J., Villanueva, I., Wright, N., Willis, T., Fewtrell, T., & Bates, P. (2011). How much physical complexity is needed to model flood inundation? *Hydrological Processes, 26*, 2264–2282. doi:10.1002/hyp.8339

Néelz, S., & Pender, G. (2009). *Desktop review of 2D hydraulic modelling packages.* Bristol: Environment Agency, SC080035/SR.

Néelz, S., & Pender, G. (2013). *Benchmarking the latest generation of 2D hydraulic modelling packages.* Bristol: Environment Agency, SC120002.

Ozdemir, H., Sampson, C. C., de Almeida, G. A., & Bates, P. D. (2013). Evaluating scale and roughness effects in urban flood modelling using terrestrial LIDAR data. *Hydrology and Earth System Sciences, 17*, 4015-4030. doi:10.5194/hess-17-4015-2013

Priestnall, G., Jaafar, J., & Duncan, A. (2000). Extracting urban features from LiDAR digital surface models. *Computers, Environment and Urban Systems, 24*, 65-78.

Sampson, C. C., Fewtrell, T. J., Duncan, A., Shaad, K., Horritt, M. S., & Bates, P. D. (2012). Use of terrestrial laser scanning data to drive decimetric resolution urban inundation models. *Advances in Water Resources, 41*, 1-17.

UNISDR. (2002). *Guidelines for reducing flood losses.* United Nations Publications.

Villanueva, I., & Wright, N. G. (2006). Linking Riemann and storage cell models for flood prediction. *Proceedings of the Institution of Civil Engineers - Water Management 159*(WMI), 27-33.

Werner, M. G., Hunter, N. M., & Bates, P. D. (2005). Identifiability of distributed floodplain roughness values in flood extent estimation. *Journal of Hydrology, 314*, 139–157.